RESEARCH MEMORANDUM

for the

Bureau of Aeronautics, Navy Department

DYNAMIC RESPONSE OF CONTROL SERVO SYSTEM INSTALLED IN NAES-EQUIPPED SB2C-5 AIRPLANE (BUAER NO. 83135)

By Louis H. Smaus and Elwood C. Stewart

Ames Aeronautical Laboratory
Moffett Field, Calif.

NATIONAL ADVISORY COMMITTEE
FOR AERONAUTICS
WASHINGTON
Oct. 5, 1950

TABLE OF CONTENTS

NATIONAL ADVISORY COMMITTEE FOR AERONAUTICS

RESEARCH MEMORANDUM

for the

Bureau of Aeronautics, Navy Department

DYNAMIC RESPONSE OF CONTROL SERVO SYSTEM INSTALLED IN NAES-EQUIPPED SB2C-5 AIRPLANE (BUAER NO. 83135)

By Louis H. Smaus and Elwood C. Stewart

SUMMARY

Dynamic-response measurements for various conditions of displacement and rate signal input, sensitivity setting, and simulated hinge moment were made of the three control-surface servo systems of an NAES-equipped remote-controlled airplane while on the ground. The basic components of the servo systems are those of the General Electric Company type G-1 autopilot using electrical signal sources, solenoid-operated valves, and hydraulic pistons. The test procedures and difficulties are discussed. Both frequency and transient-response data are presented and comparisons are made. The constants describing the servo system, the undamped natural frequency and the damping ratio, are determined by several methods. The response of the system with the addition of airframe rate signal is calculated. The transfer function of the elevator surface, linkage, and cable system is obtained. The agreement between various methods of measurement and calculation is considered very good. The data are complete enough and in such form that they may be used directly with the frequency-response data of an airplane to predict the stability of the autopilot-airplane combination.

INTRODUCTION

A radio-remote-controlled SB2C-5 airplane, BuAer No. 83135, has been loaned by the Bureau of Aeronautics, Navy Department, to the Ames Aeronautical Laboratory of the NACA for an intensive evaluation of the control system. The radio-control and stabilization equipment was developed and installed by the Naval Air Experimental Station, Philadelphia, Pa.

The airplane is stabilized by an automatic pilot sensitive to airplane attitude and rate of change of attitude. Command signals

transmitted to the airplane by radio act to introduce voltages into the servo signal circuits to cause the airplane, through the automatic pilot, to assume the desired attitudes. For satisfactory performance under remote control, the servo systems of the autopilot must provide stable control of the airplane for all flight conditions and maneuvers including take-off and landing.

In evaluating the performance and stability of the system, it has been planned to determine the responses of the autopilot and of the airplane separately, to combine them mathematically, and to compare the result with the measured response of the autopilot-airplane combination. This report is concerned with the detailed measurements and calculations for the autopilot system only, with the airplane on the ground.

Static measurements of the various autopilot components were first made to obtain their values for use in later calculations and to determine the linear operating range of the system.

Frequency and transient-response measurements for various conditions of input signal amplitude, sensitivity setting, and hinge moment were then made and the effect of the control surface, linkage, and cable system, hereinafter referred to as the linkage system, was determined. The effect of airframe rate signal, in addition to the displacement signal, also was experimentally determined.

From these data it was then possible to make numerous calculations which either simplified the test procedure, afforded a check of the results, or defined the system in terms of constants. Where these calculations are not covered in servo literature, the necessary equations are fully derived in the text. In all cases the application of servo theory to a practical case is clearly shown.

The value of error voltage at which the servo-system operation becomes nonlinear was determined from the static measurements. A method for calculating the error voltage as a function of frequency for a given input signal amplitude is given. Thus, it was possible to utilize an input signal for which the servo remained in the linear range of operation, which is a necessary requirement for linear theory calculations. No attempt is made in this report to analyze effects of nonlinearity.

The open-loop transfer function of the servo was determined and it was found that the system is closely represented by a second-order differential equation. Thus, it may be defined in terms of two constants, the undamped natural frequency and the damping ratio. Methods are given for the determination of these constants from which the equation of the system is written. This not only affords a useful method of system analysis but, since the equation represents values of a practical and existing servo, it is also useful for theoretical studies of airframe-autopilot stability. Comparisons of the frequency-response curves are

made for (1) the theoretical second-order system, (2) the system as installed in the airplane, and (3) the bench setup in which control-surface linkage is absent. A useful formula for determining the frequency response for any desired value of sensitivity from the measured response at a particular sensitivity setting is given.

A method is developed for calculating the frequency responses with various amounts of airframe rate signal from the measured response of the system with sine-wave input and from the dynamic response of the rate gyro.

Finally, the frequency response of the control-surface linkage system was determined. Thus, the response of the surface to the servo-system input signal may be calculated directly from the basic servo-system response.

SYMBOLS

(Refer to fig. 1.)

A vector transfer function, output over input

A_a vector transfer function of amplifier

A_m vector transfer function of servo valve and actuator

A_{r_m} vector transfer function of rate gyro for maximum excitation

e base for natural logarithm system (2.718 . . .)

f frequency, cycles per second

I algebraic sum of servo-transfer-valve currents

j $\sqrt{-1}$

k_a amplifier-static-gain constant, milliamperes per volt

k_f follow-up constant, volts per inch of servo displacement for full excitation

k_g gyro constant, volts per degree

k_m servo-valve and actuator-static-gain constant, inches per second per milliampere

k_r rate-gyro constant, volts per cycle per second per degree oscillation

k_v amplifier-servo-velocity constant, $second^{-1}$

K_c linkage-system constant, surface deflection per unit servo travel, degrees per inch

M peak-amplitude ratio of frequency response

P_a attenuation of amplifier attenuator, dimensionless

P_f attenuation of follow-up voltage, percent (actual sensitivity)

P_r rate attenuation, percent (actual rate)

R general symbol for dimensionless amplitude ratio; absence of subscript denotes amplitude ratio of servo response $\left(\frac{v_f}{v_i}\right)$

R_{fr} amplitude ratio of servo response with the addition of input rate signal

T time constant of servo system

v_e error signal of servo system, input to amplifier attenuator, volts

v_{er} error signal of servo system with addition of rate signal, volts

v_f follow-up selsyn output modified by sensitivity setting, volts

v_{fr} follow-up selsyn output modified by sensitivity setting with addition of rate signal, volts

v_g displacement-gyro output, volts

v_i test input signal, volts

v_r rate-gyro output modified by rate setting, volts

δ control-surface deflection, degrees

δ_s servo displacement, inches

ϵ_e phase angle of v_e relative to v_i, degrees

ϵ_f phase angle of v_f relative to v_i, degrees

ϵ_{fr} phase angle of v_{fr} relative to v_i, degrees

ϵ_r phase angle of rate gyro, v_r relative to v_i, degrees

ζ damping ratio

θ angle of pitch, degrees

ω angular frequency, radians per second

ω_b angular frequency at which the break between -6 and -12 decibel per octave slopes occurs on an open-loop frequency-response plot

ω_M angular frequency of peak-amplitude ratio, M

ω_n undamped natural angular frequency

ω_t angular frequency of transient oscillations

DESCRIPTION OF SYSTEM

The components of the servo system are basically those of the General Electric Company type G-1 autopilot consisting of electrically driven displacement and rate gyros, selsyn-type pickoffs to provide 400-cycle signals, a three-channel electronic amplifier, solenoid-operated valves, and hydraulic piston servos operated at 160 pounds per square inch. The maximum output force available at this pressure is about 250 pounds. The servos are attached to the control-surface cables at points quite far removed from the surfaces themselves. A block diagram of one channel of the system (less remote control and trim components) is shown in figure 1.

The signal circuit is shown schematically in figure 2. The amplifier delivers a balanced output current to the two coils of the control-valve solenoid under static operation. Changes of input signal vary the ratio of current in the two coils causing the valve stem to move proportionally in one direction or the other. The follow-up selsyn is attached directly to the servo output shaft and its excitation is varied by means of a potentiometer labeled "Sensitivity" and graduated from 0 to 100. High sensitivity (high-scale reading) implies a large excitation voltage and a resultant small surface and servo movement to cancel out any given gyro-input voltage.

A signal derived from airplane rate of pitch, roll, or yaw by means of a rate gyro is available in the appropriate channel. A

potentiometer labeled "Rate" controls the amount of rate signal used and is graduated from 0 to 100, defining the percent of excitation voltage used on the pickoff (a transducer which produces an electrical signal proportional to a mechanical movement).

The "Speed" and "Trim" signals shown in figure 2 were not used in these tests.

CALIBRATION OF SYSTEM COMPONENTS

Displacement Gyros

The vertical (pitch and roll) and directional (yaw) displacement gyros were calibrated in terms of volt output from the selsyn pickoffs per degree displacement. The gyros were mounted on rotatable tables which could be set within 0.1°. The voltage was read with a Ballantine vacuum-tube voltmeter. As was to be expected, readings much below 1° were meaningless due to the presence of a quadrature voltage. It is to be noted that this quadrature voltage has little effect on the operation of the servo since the amplifier is responsive only to signals in phase or 180° out of phase with the primary 400-cycles-per-second supply.

It was particularly difficult to obtain good data from the pitch pickoff of the vertical gyro because of small random oscillations of the gyro in pitch and electrical noise apparently originating in the gyro motor. The measurements of the gyro in pitch were made with a 0.5 microfarad condenser across the output as is normally used in the NAES system for phase correction.

It is well to note at this point that the gyro constants, as well as all other pickoff constants, are materially affected by the value of condensers placed across their output. These condensers are usually added after the autopilot installation has been made in order to correct the phase of the 400-cps voltage and therefore are usually neglected in the initial design of the system. In the case of the pitch-gyro pickoff, the added condenser approximately doubled the output voltage. Hence it is very important that the final calibration of pickoffs be made in the system as installed in the airplane with all components connected for normal operation.

Over the ranges tested the output voltage varied linearly with displacement. The ranges covered for pitch, roll, and yaw axes were, respectively, ±30°, ±16°, and ±9°. Values of the gyro constants are as follows:

Pitch	–	0.51 volt per degree
Roll	–	.56 volt per degree
Yaw	–	.50 volt per degree

Rate Gyros

Dynamic measurements.– The frequency responses for the rate gyros were determined by oscillating the gyros sinusoidally on a table driven by a relatively long crank arm and a variable-speed transmission. This mechanical apparatus is shown in figure 3. An input of $\pm 1^\circ$ was used up to a frequency of 2 cps, the region of primary interest. Slightly beyond 2 cps, for this input, the gyro gimbal hit its mechanical stops. The resonant frequency of the oscillating table was found to be around 13 cps so that its effect at 2 cps was negligible. The amplitude measurements were made by comparing the peak of the modulated 400-cps selsyn pickoff voltage on an oscilloscope to that from a constant 400-cps voltage source. The phase was found from an oscillograph record of the modulated 400-cps voltage output, the zero phase reference coming from a contactor, mounted on the oscillating table, which provided a mark on the oscillograph record when the table was at zero position.

The frequency-response data for the rate gyros are presented in figures 4(a), (b), and (c). The phase angle of only the pitch-rate gyro was measured and it should be noted that this angle was not quite 90°. Since the gyros are slightly unsymmetrical, two amplitude curves are given for the two directions of motion.

The frequency response of a rate gyro over a wider range is of some interest and is shown in figure 5 for the roll-rate gyro. This curve was obtained with the rocking table apparatus using a very small input amplitude of the order of approximately 0.1°. The gyro is extremely underdamped and has its resonant frequency at 4.5 cps. It will be noted that the response does not fall off as sharply as might be expected at 5 cps and above. This phenomenon was caused by the effect of the table resonance mentioned previously.

Steady-state measurements.– The pitch- and roll-rate gyros were also calibrated on a rotating table with variable-speed selections. The output-voltage characteristics are shown in figures 6(a) and (b). A slight difference in absolute output will be noted for opposite directions of rotation although the slopes, which are the only concern here, are very nearly alike. In addition, the calibrations are not perfectly straight lines.

Obviously, it is possible to predict the frequency response from the steady-state data, neglecting the effect of resonance. This was done, taking into account the nonlinear steady-state curves by using the steady-state calibration value corresponding to the peak rate of pitch at each frequency considered. The peak rate of pitch was used since the peak value of voltage was measured in determining the frequency response experimentally. The nonlinearity of the steady-state calibration means that the output voltage will not be exactly sinusoidal and that the calculated frequency response will not be quite linear. Agreement of experimental and calculated results is shown in figures 4(a) and (b) and is fairly good up to the higher frequencies where resonance effects occur.

Amplifier Gain

The amplifier gain for each of the three channels was determined by reading the differences between output currents to the valve solenoids for various input voltages. Plots for the three channels are shown in figure 7. For each channel the slope of the linear portion of the curve represents the gain of the amplifier, the average value of which is, to two significant figures, 350 milliamperes per volt. The linear range of the amplifier is of paramount interest. Inspection of these curves shows that the amplifier is linear within 10 percent over a range of approximately ±0.10 volt. The above values apply when the amplifier gain control is set at maximum. In general, the system is operated with the gain at minimum which introduces an attenuation factor of 0.29. Thus, with minimum gain setting, an input signal of ±0.35 volt may be used without exceeding the linear range of the amplifier. As will be seen from the next paragraph, the amplifier is the first element to saturate and thus becomes the limiting component of the servo system with respect to linearity.

Servo Gain

The gain of the valve-servo combination was obtained in terms of the servo speed versus solenoid unbalance current. The speed was determined by recording, on a Brush oscillograph, the output of a pick-off attached to the servo piston shaft. Pen position on the oscillograph was calibrated against servo position. Unbalance currents were applied to the solenoids and the servo allowed to assume a steady speed. A plot of the results is shown in figure 8. The gain is linear over the maximum available range of unbalance currents from 0 to 50 milliamperes and has a value of 0.050 inch per second per milliampere. The maximum available stroke of the piston is approximately ±2 inches.

Sensitivity and Rate Potentiometers

The sensitivity (follow-up) and rate potentiometers in the adjustment unit on the SB2C-5 airplane were calibrated by measuring the output voltage as a function of dial setting for 112 volts excitation. The voltage values were reduced to percentages of full excitation and defined as actual sensitivities or rates. The relationship of dial setting to actual sensitivity is shown in figure 9 for the sensitivity potentiometers. As can be seen, this relationship is not linear over the range considered. The rate potentiometers were somewhat more linear and their calibrations are shown in figure 10. The sensitivities and rates which will be referred to throughout this report are the actual values, that is, percent of full excitation (112 volts) rather than dial settings.

The relationship between the follow-up selsyn output voltage for full excitation and the servo motion is defined as k_f and was found to be 14.0 volts per inch. The linkage system constant k_c expressed as the static ratio of surface deflection to servo displacement for each of the channels was found to be

Elevator – 15.6° per inch

Aileron – 13.7° (total) per inch

Rudder – 14.7° per inch

FREQUENCY-RESPONSE CHARACTERISTICS OF CONTROL SERVO SYSTEM

Frequency-Response Measurements Using a Sinusoidal-Voltage Input

Equipment.– For frequency-response tests of the servo system a 400-cps signal voltage, the amplitude of which varied sinusoidally, was introduced in series with the follow-up selsyn and the amplifier input with the remaining signal sources shorted out. This is equivalent to breaking (and electrically grounding) the system at point (a) in figure 2. With this connection, the closed-loop response is obtained.

The sine-wave signal generator consisted of a precision autosyn driven by a constant-speed motor through a ball-disc variable-speed drive mechanism. A cam-operated switch was provided and adjusted to make contact at a point of zero autosyn output voltage once every cycle to serve as a phase reference mark.

Selsyn pickoffs of the type used in the autopilot were mounted on the servo piston shaft (in tandem with the follow-up selsyn) at point (a) of figure 1 and at the control surface, point (b) of figure 1. The 400-cps output voltage of each selsyn pickoff was rectified by a bridge circuit comprised of two IN48 germanium diodes and two resistors, passed through a low-pass filter and fed to a Brush direct-current amplifier and oscillograph. It was found necessary, for recording purposes, to replace the Holtzer-Cabot 400-cycle, 3-phase, 750-VA inverter used in the SB2C-5 airplane with one having better wave form. A Leland inverter of the same rating was used. This change of inverters had negligible effect on the frequency response of the autopilot although, when an inverter with still poorer wave form was used, the servo response was observed to be definitely sluggish by comparison.

The device used to simulate hinge moment consisted of a lever acting on a rod in torsion. A 3/8-inch steel rod was rigidly clamped at one end. At another point along the rod, depending on the load to be simulated, one end of the lever arm was clamped. Ball-bearing supports were then moved to either side of the lever arm to support the rod. The other end of the lever arm was coupled to the control surface through a connecting rod in such a manner that the latter was essentially at right angles to both the lever arm and the chord of the control surface, thus minimizing any nonlinearity between rod and control-surface deflection. This resulted in a smooth and linear relation between load and surface deflection with negligible increase in inertia of the control system and with no dead spot at zero loading. A photograph of the apparatus is shown in figure 11.

Accuracy of data.- The accuracy of amplitude measurements is dependent on both the pickoff circuit and the recording circuit. For the first factor, the servo and surface-position pickoffs, in combination with their rectifiers and filters, were calibrated in terms of surface position. The filter direct-current output, in volts, was read with a Rhodes potentiometer voltmeter (accuracy of 1/4 percent) while the surface position was measured with a bubble protractor to within 0.1°. Linearity within 1 percent was obtained over the working range, which was limited to small angles of pickoff rotation (several degrees of surface deflection). Tests made of the Brush amplifier and oscillograph showed an accuracy of ±2 percent in amplitude for 90 percent of the readings; this figure includes effects of gain change and drift in the oscillograph amplifier and resolution of the oscillograph trace. Thus, an over-all accuracy of the pickoff and oscillograph combination better than ±3 percent was achieved for the amplitude measurements.

The accuracy of phase measurements cannot be stated in simple percentage terms since it depends on several factors, such as oscillograph-paper speed, sine-wave frequency, and the magnitude of the phase angle. It is possible to set the phase reference marker in the sine-wave generator to within ±1°. There is a possible error of ±2° at the lowest frequencies, which diminishes to less than ±1° at 1 cps and above as a

result of choosing the zero amplitude line which determines the zero point on the output sine wave to be compared with the phase marker. Finally, there is an error due to the limiting accuracy with which it is possible to measure. It was found to be best expressed as approximately ±2° per cycle per second up to a frequency of nearly 1 cps. Beyond this frequency, because of change in paper speed and increasing phase-lag angle, the percent error in phase-angle measurement rapidly decreases. Thus, at 0.1 cps the maximum total error in phase angle might be ±3° and at 1.0 cps, ±4.0°.

It is difficult to assess the accuracy with which large quantities of data are read, but the possibility of errors resulting from this process must be considered in the final accuracy. Many of the above errors, however, including those incurred in reading the data, are of a random nature and hence the accuracy of the curves, which have been faired through experimental points, should be reasonably close to the values given above. The general accuracy of data is shown by the small dispersion of experimental points in several of the frequency-response curves.

Electrical and mechanical difficulties.- Numerous minor difficulties were encountered in determining the autopilot response. In general, the over-all performance was not greatly affected by these troubles but measurements and analysis were made difficult. Some of these troubles are mentioned here to indicate the sort of factors that must be reckoned with in order to be certain that the desired performance is being obtained. Poor wave form of a 400-cycle inverter has already been mentioned.

It was found that the amplifier performance was materially affected by the tubes used. Random selection of tubes produced, in some cases, large unbalance currents in the amplifier output. While the trim voltage could be adjusted to compensate for the unbalance, the system was no longer operating in the linear range for one direction of motion. It was thus necessary to try several tubes to achieve an approximately balanced output. This condition could cause serious difficulty if the system were operated at close to maximum sensitivity in order to obtain optimum performance, as will be shown later.

A small amount of play exists in the lever mechanism connecting the follow-up selsyn in the elevator auto-trim follow-up box to the servo piston. When the mechanism was replaced by a single lever with no apparent play, it was found that the system could be operated at a higher gain (sensitivity setting) than previously without incurring steady oscillation. However, there was negligible difference in the frequency response at practical sensitivity settings.

A similar condition was encountered with respect to warm-up time of the system. The sensitivity could be set progressively higher without oscillation with the passing of time up to several hours. Again,

however, the difference in the transient and frequency response at practical sensitivities was negligible after a brief warm-up time of, say, 30 minutes.

A serious trouble that proved very difficult to find, due to the small motions involved, was encountered in the aileron system. With a sine-wave signal input to the servo system, the aileron surface produced a flat-topped sine-wave output. It was found that a flat spot had been worn on the aileron torque tube where the servo-driven horn was attached resulting in appreciable backlash. That section of the torque tube was replaced, completely eliminating the trouble.

The rudder output was a badly distorted sine wave. The trouble was due mainly to the rudder-servo horn linkage and mounting. The deck to which the horn was attached was strengthened and the whole assembly tightened. The performance was improved but not to the extent desired. Some of the remaining difficulty is due to the flexibility of the linkage system and to the eccentric connection of the servo piston shaft to the horn, but it was not considered justified in this instance to make this or other possible improvements.

Measurement of gearing factor.- For each frequency-response run, the static values of servo and surface output motions were determined for the given input electrical signal. The factor relating these quantities is termed the gearing factor and is given in inches per volt and degrees per volt for servo and surface, respectively. The results of these measurements are graphed in figures 12(a), (b), and (c) for the elevator, aileron, and rudder channels, respectively. Consideration of figure 1 indicates that the gearing factor is inversely proportional to the actual sensitivity, which is borne out in the curves presented.

It may be seen from the plots that the elevator and rudder-surface gearing factors in particular are considerably reduced when the surfaces are subjected to loads simulating hinge moments. Quantitative values of load for the maximum-load condition are given later. Measurements of the servo gearing factors under load were not made, but study of additional data not presented indicated that most of the difference is due to the linkage systems. It is important that the change in gearing factors under load be taken into consideration when determining gearings for the autopilot-airframe combination.

Frequency response curves.- The frequency-response data presented in the following sections are shown in the form of phase angles and nondimensional amplitude ratios plotted against frequency. The phase angle is the angle by which the output wave lags (or leads) the input wave, being negative for lagging angles and positive for leading angles. The amplitude ratio is the ratio of servo or surface amplitude at any given frequency to the respective amplitude at zero frequency for a constant amplitude sine-wave input signal. Thus, it is a dimensionless

quantity and must be multiplied by the gearing factor, which is dependent on sensitivity setting, in order to determine the actual output magnitude. Thus, the actual output magnitude of either servo or surface is the product of the amplitude ratio, the gearing given in figure 12, and the input voltage.

Bench tests.- One channel of the servo system was set up on a bench in the laboratory, partly to become familiar with the system before testing it in the airplane and partly to compare the response under laboratory conditions with that obtained when installed in the airplane. Control-surface inertia and hinge moment were not simulated.

It was found that the amplifier output currents were somewhat unequal for zero input signal so that a balancing circuit was added in one of the cathode circuits to bring the currents to balance. This was done only on the bench tests since trim potentiometers accomplish the same result in the airplane.

Frequency-response runs of the servo output were made for a large range of sensitivities and input voltages. These data will not be presented separately, but typical runs will be shown in comparison with the airplane ground-test runs later in the report.

Elevator-system ground tests.- The elevator system was very thoroughly investigated in the airplane on the ground in order to determine the relative importance of several variables. The three variables under investigation were (1) sensitivity, (2) surface loading, and (3) input signal magnitude. Frequency-response characteristics of the servo and elevator surface were measured for several values of sensitivity ranging from 24 to 63 percent for four different loadings, and for a number of input signals ranging between 0.115 and 1.56 volts. Data are presented in figures 13 to 16, inclusive, and grouped in a manner to show the effects of the variables. The analysis of the system based on these curves is presented later.

For measuring the effects of sensitivity and loading, the input signal used was of a low enough value not to cause any saturation of the amplifier. The effect of saturation is covered under the section on variation of input.

1. Effect of sensitivity.- Figures 13(a) and (b) show the servo and surface responses, respectively, to a sine-wave input signal to the servo system for actual sensitivities of 24, 33, 42, 52, and 63 percent. The input signal was ±0.115 volt, corresponding to approximately ±1/4° of pitch, and the surface was not loaded. A sensitivity of 76 percent was found to be slightly unstable at certain frequencies and is not shown. It may be noticed that, while there is a large change in response at the high frequencies as between different sensitivity settings, there is an almost negligible change below 1 cps. Such difference as does exist is

in favor of the highest sensitivity setting because of the slightly improved response (reduced amplitude ratio and phase lag) in the latter region.

If figures 13(a) and (b) are compared, it may be noted that the surface frequency response is quite different from the servo response. This difference, the effect of elasticity in the cable connection between servo and surface, is more clearly shown in figures 14(a), (b), and (c) where the servo and surface responses are plotted together on the same graph for each of three sentitivities, namely, 24, 42, and 63 percent. Again it is seen that the differences are quite small below 1 cps, but rapidly increase at higher frequencies.

The effect of the elevator-control-cable resonance near 5 cps is shown on both servo and surface response curves. The effect on the surface response is very great compared to the effect on the servo response which exhibits only a slight leveling off in the amplitude curve and a peak in the phase curve. These effects will be discussed in detail later.

2. Effect of surface loading.- Frequency-response runs were made for several values of simulated-surface hinge moment in addition to the no-load runs. The maximum load used was 20 foot-pounds per degree elevator deflection corresponding roughly to an airspeed of 200 knots on the SB2C-5 airplane. Since the differences between various loadings are not great, figures 15(a), (b), (c), and (d) compare only the no-load and maximum-load conditions for servo and surface at sensitivities of 24 and 42 percent at an input of ±0.115 volt. While the difference in amplitude ratio and phase lag is not very great under the two loading conditions, it may warrant consideration in applying the data, depending on the frequency range of interest. It may be noticed that the servo response for the loaded case does not exhibit the peaking of phase and leveling of amplitude at high frequencies as in the no-load case. For the surface-response curves the application of load causes an increase in the frequency at which the elevator-control-cable system affects the amplitude and phase.

The data for figures 15(a), (b), (c), and (d) were taken at a later time than the runs presented in figures 13(a) and (b). The no-load servo responses were nearly identical for the two sets of curves, but it should be noted that the surface responses were somewhat different because the tension of the elevator-control cable had been altered between these two tests.

3. Effect of input-voltage magnitude.- Figures 16(a), (b), (c), and (d) show the effect on the frequency response of a variation of input voltage of ±0.20, 0.39, 0.78, and 1.56 volts for sensitivities of 26 and 56 percent at no load. These inputs correspond to approximately ±3/8°, 3/4°, 1-1/2°, and 3° of gyro displacement.

Figures 16(e) and (f) show the effect under maximum load and at a sensitivity of 41 percent. This particular range of inputs was chosen to study the effects of saturation. Partial plots of the calculated error voltage, or input to the amplifier, are also shown on the curves for the servo response only to indicate the frequency at which the system departs from linearity by 10 percent due to partial saturation of the amplifier.

It would be expected that the responses for different inputs should be essentially the same in the region where the system remains in the linear operating range; that is, where the input to the gain control of the amplifier does not materially exceed 0.35 volt, and should not differ appreciably until the error voltage has considerably exceeded the nonlinear level. This is borne out by the curves presented. Thus, for practical purposes involving calculations for airframe-autopilot stability, the limit of error voltage may be extended somewhat.

It may be noticed that the values of sensitivity and input signal used in this investigation are different from those values in the two preceding sections. This was due to an apparent change in gain of the system for these tests. When the data were first checked it was found that the responses of these runs did not agree with those of similar runs taken for other investigations. Analysis of the data by comparing the amplitude and phase responses, the frequencies of the amplitude ratio peaks, and the calculated open-loop responses revealed that the difference between the responses in all cases corresponded to an increase in gain for the condition of these runs by a factor of about 1.7. This gain change was traced to the forward gain circuit (composed of amplifier-gain potentiometer, amplifier, and servo) since the gain of the feedback circuit (composed of the follow-up unit and sensitivity potentiometer) was found to be identical in all tests. The source of the trouble was due very probably to the amplifier-gain control having been accidentally displaced from its normal minimum position. For comparison purposes, however, it is necessary that the forward gain be identical in all tests. The response for the system in which the gain potentiometer was not at its minimum value is identical to that of the system with a minimum-gain setting and a 1.7 factor increase in values of sensitivity, input-signal amplitude, and error voltage. This correction has been applied to the values given in figure 16.

Aileron-system ground tests.- After an examination of the elevator data it was found that such a complete coverage of the three variables, sensitivity, loading, and input, was not necessary for the aileron and rudder channels. Three sensitivity settings were considered to be sufficient to cover the range of interest. Because of the small effects found in the elevator channel, it was decided to simulate only two load conditions. An input-signal value was chosen which did not cause

saturation below 2 cps (the region of interest for the autopilot–airplane combination). This was determined by brief tests and calculation of the error voltage at 2 cps. The calculation of error voltage is described in the Analysis section of this report. An additional input of very large magnitude was also investigated. Since the principal region of interest lies in the frequency spectrum below 2 cps, many of the aileron runs are plotted only out to that frequency.

1. Effect of sensitivity.– The responses of the aileron channel for sensitivities of 26, 44, and 65 percent are shown in figures 17(a) and (b) for the servo and the surface, respectively. The input signal used was ±0.275 volt corresponding to ±1/2° of roll. As was the case with the elevator channel, there is little difference in results between sensitivities below 1 cps, but such difference as there is favors the highest sensitivity setting because of its slightly reduced amplitude ratio and phase lag. In contrast with the elevator data already presented, effects of the aileron linkage system on the servo and surface responses are minor over the frequency range tested (up to 10 cps).

2. Effect of loading.– The effects of surface loading are shown in figures 18(a) and (b) for servo and surface at a sensitivity setting of 44 percent and an input of ±0.275 volt. While two values of loading were tested, only the maximum-load condition is compared to the no-load data since there is little effect from the load. This maximum load was taken as 12 foot-pounds per degree aileron deflection corresponding roughly to an airspeed of 200 knots in the SB2C-5 airplane. Up to a frequency of 2 cps, which is the upper limit of the loaded curves, the difference between no load and maximum load may be seen to be negligible. The effect was no greater at other sensitivities.

3. Effect of input-voltage magnitude.– As was stated previously, it was possible to choose an input voltage that would not saturate the system in the region below 2 cps; this value was taken as 0.275 volt, or approximately 1/2°. To show the effect of a large signal which does saturate the system at low frequencies an amplitude of 1.65 volts, or approximately 3°, was used. The responses under these two input conditions are compared in figure 19 for servo and surface with no load. The error voltage is also plotted in this figure to indicate the frequency at which the system becomes nonlinear. The effect of magnitude of input signal with maximum hinge moment was essentially the same as with no load and is not presented since it has been shown that the addition of load has negligible effect up to 2 cps.

Rudder-system ground tests.– As has been discussed previously, the rudder response was quite distorted from a pure sine wave, thus making analysis of the data difficult. Only part of the data taken are presented here.

In general, the same conclusions as were reached on the elevator and aileron channels regarding effects of sensitivity, load, and input magnitude are valid for the rudder channel. Again, the signal amplitude chosen, ±0.25 volt, corresponding to about ±1/2°, did not cause saturation of the system in the region below 2 cps.

1. Effect of sensitivity.- The responses for sensitivity settings of 24, 42, and 62 percent are shown in figures 20(a) and (b) for servo and surface, respectively, at an input of ±0.25 volt. The response of the rudder surface at a sensitivity of 62 percent was so badly distorted that it was not considered worth-while to evaluate the data. It may be noted that the effects of the rudder-linkage system are very pronounced.

2. Effect of load.- The responses under maximum load are compared with the no-load data in figures 21(a) and (b) for the servo and surface at an input of ±0.25 volt. The maximum load was taken as 19 foot-pounds per degree rudder deflection, again corresponding to an airspeed of 200 knots. The effect of load is moderate on the servo response, but is very pronounced on the surface response above a frequency of 1 cps.

3. Effect of input-voltage magnitude.- The servo response for a large signal input, 1.0 volt or 2°, is compared with that for ±0.25 volt input in figure 22 at a sensitivity of 42 percent. Plots of the error voltage are also shown to indicate the frequency at which saturation occurs. The surface response for the large input signal was too distorted to evaluate the data.

Frequency-Response Measurements With Oscillating Vertical and Rate-Gyro Inputs

In order to determine experimentally the response of the system with both displacement and rate signals, it was necessary to oscillate mechanically the displacement and rate gyros instead of using a synthetic input signal. These gyros were mounted on the oscillating table apparatus previously described (fig. 3). The signal circuit was then the same as in the normal autopilot installation (fig. 2). Tests were made at actual rate settings of 8, 20, and 31 percent for the elevator and 7.2, 18, and 27 percent for the aileron channels which covered the range of practical settings used in flight.

The frequency range was restricted from 0.1 cps to 2 cps only for two reasons. The error voltage reached saturation before 2 cps for the lowest rate setting used (rate of 8). In addition, as has been pointed out before, the effect of the table resonance is negligible at 2 cps but becomes progressively worse for higher frequencies.

Pitch.- The first test was made with the vertical-gyro-elevator-channel pickoff fed through its two-phase transformer as the displacement input. With the oscillating table at a standstill, it was noted that the gyro output was quite unsteady, causing a jittery surface movement. An overhaul of the gyro showed that the damper used in the erection system was dirty. Cleaning this damper made a definite improvement in the gyro behavior. Nevertheless, when the test was tried again, the surface was still jittery. The difficulty appeared inherent in the electrical system and was traced to an electrical interaction between the gyro motor excitation and the servo system. Disconnecting this excitation (phase 3) stopped the jittering completely. The test could have been performed by opening the motor excitation each time before taking data except for excessive gyro drift with the power off. Therefore, the vertical gyro was reoriented by 90° and the aileron-channel pickoff was used in place of the elevator-channel pickoff. The surface response was then quite good and the previous interaction was absent.

Figures 23(a) and (b) show the resultant experimental responses for this test for actual rates of 8, 20, and 31 percent. The first thing to notice is the improvement in the phase-angle response which now shows lead instead of lag over most of the frequency range of interest. It will also be noticed that the amplitude ratio increases very rapidly both with increasing rate potentiometer setting and with frequency, tending to partially neutralize the beneficial effects of leading phase angle.

Roll.- No difficulties were experienced in the aileron-channel tests. The results are shown in figure 24 for actual rates of 7.2, 18, and 27 percent. The same comments as were made with reference to the pitch channel apply here as well.

Transient Response

In general, transient responses to a step input signal were recorded for all conditions for which frequency runs were made. The technique employed was to leave the sine-wave generator in a fixed position at the desired input voltage and to alternately short and unshort the input voltage to obtain both polarities of transients. A typical set of transients for the elevator-channel servo and surface is shown in figure 25 for actual sensitivities of 24, 42, and 63 percent each for an input step magnitude of 0.115 volt. Results and analysis of all transient tests are presented in a later section.

ANALYSIS OF DYNAMIC CHARACTERISTICS OF ELEVATOR CHANNEL

Autopilot Frequency and Transient Response With Displacement Signal

For purposes of calculations involving the autopilot, it is desirable to know the analytic expressions which represent the system response and to show how closely these expressions simulate the experimental tests. In this way servo performance is not only put into more compact form, but operation can be predicted for values of parameters not specifically tested. The desired expressions, therefore, will be derived in the following sections.

Calculation of error voltage.- In general, calculations from frequency-response data are based on linear relationships and the data must, therefore, be taken over the linear operating range of the system. As has been previously shown, an error voltage input to the attenuator of the servo amplifier in excess of 0.35 volt, with the amplifier set for minimum gain, caused the system to depart from linear operation. It becomes necessary, then, to calculate this error voltage to determine the frequency range of linear operation for each condition. This can be done by using the measured frequency response as follows:

With reference to figure 1, the basic input equation for the servo system alone (in which case $v_i = v_E$) is

$$v_e = v_i - v_f \tag{1}$$

where v_e and v_f are vector quantities with phase angles relative to the vector v_i.

The amplitude ratio and phase angle of the servo-system closed-loop response may be represented by R and ϵ_f, respectively. As previously defined, then, for a constant input signal

$$Re^{j\epsilon_f} = \frac{(\delta_s)_{f=f_1}}{(\delta_s)_{f=0}} \tag{2}$$

where δ_s is the servo motion.

This equation may be put into a more convenient form by two simplifying relationships. First, since the linear range of the pickoffs is never exceeded in these tests, $v_f = k_1\delta_s$ where k_1 is a constant. Second, at zero frequency the error voltage is negligible so that $(v_f)_{f=0} \approx v_i$. Therefore, equation (2) reduces to

$$Re^{j\epsilon_f} = \frac{(v_f)_{f=f_1}}{(v_f)_{f=0}} = \frac{(v_f)_{f=f_1}}{v_i}$$

or

$$v_f = v_i \, Re^{j\epsilon_f} \tag{3}$$

The phase angle ϵ_f is defined as positive when v_f leads v_i and negative when v_f lags v_i.

Then $$v_e = v_i - v_i \, Re^{j\epsilon_f}$$

$$= (v_i - v_i R \cos \epsilon_f) - j(v_i R \sin \epsilon_f) \tag{4}$$

and

$$v_e = v_i \sqrt{1+R^2 - 2R \cos \epsilon_f} \; e^{j\epsilon_e} \tag{5}$$

where

$$\epsilon_e = -\tan^{-1} \frac{R \sin \epsilon_f}{1-R \cos \epsilon_f} \tag{6}$$

Only the magnitude of v_e is of interest here. Inspection of equation (5) shows that for a given input signal the error voltage increases as the closed-loop response magnitude and phase angle increase. Thus, for the condition of displacement signal only, the error voltage will be small at very low frequencies and increase to a peak near the resonant frequency. Ultimately, at high frequencies where the response magnitude diminishes to zero, the error voltage approaches the input voltage.

The variation of the error voltage is plotted on some frequency-response curves; whereas on others where no plot is given it may be assumed that for the entire response the error voltage does not reach the limiting value for linearity.

Calculation of open-loop response.- The order of the differential equation which governs the response over the frequency range of interest may be determined from the open-loop characteristic which expresses the relationship between output and input with the loop opened, that is, with the follow-up voltage disconnected from the amplifier attenuator input. This is equivalent to the ratio of output to error v_f/v_e in the closed-loop case and hence may be calculated from the closed-loop frequency-response curves. It is generally not feasible to measure

the open-loop response directly. This is due to the large and impractical amplitudes at low frequencies and also because of inherent drift in an open-loop-type system. The method of calculation is given subsequently and must be confined to those frequency-response curves entirely in the linear range.

Referring to the preceding section and dividing equation (3) by equation (5) gives

$$\frac{v_f}{v_e} = \frac{Re^{j\epsilon_f}}{\sqrt{1+R^2 - 2R\cos\epsilon_f}\, e^{j\epsilon_e}}$$

which has an amplitude of

$$\left|\frac{v_f}{v_e}\right| = \frac{R}{\sqrt{1+R^2 - 2R\cos\epsilon_f}} \tag{7}$$

or, in decibels,

$$\left|\frac{v_f}{v_e}\right|_{db} = 20\log_{10}\frac{R}{\sqrt{1+R^2 - 2R\cos\epsilon_f}} \tag{8}$$

and a phase angle of $\epsilon_f - \epsilon_e$

From equations (4) and (5),

$$\epsilon_e = -\sin^{-1}\left(\frac{R}{\sqrt{1+R^2 - 2R\cos\epsilon_f}}\sin\epsilon_f\right) \tag{9}$$

Substituting equation (7) in (9) yields

$$\epsilon_e = -\sin^{-1}\left(\left|\frac{v_f}{v_e}\right|\sin\epsilon_f\right)$$

The phase angle of v_f/v_e is therefore

$$\text{Angle}\left(\frac{v_f}{v_e}\right) = \epsilon_f + \sin^{-1}\left(\left|\frac{v_f}{v_e}\right| \sin \epsilon_f\right) \qquad (10)$$

The elevator-channel, open-loop, frequency-response characteristic was calculated by means of equations (8) and (10) from the closed-loop frequency-response data of figure 13(a) for sensitivities of 24 and 42 percent. The open-loop response is plotted in figure 26. Slopes of -6 db and -12 db per octave represent, respectively, the effect of terms of the first and second order in the denominator of the transfer function (reference 1, p. 241). It may be seen from these curves that a second-order differential equation is obeyed fairly closely as shown by the quite definite slopes of -6 and -12 db per octave. On the basis of this analysis, second-order differential equations may be used satisfactorily for calculations.

The true position of the two slopes may be difficult to locate precisely for several reasons. At low frequencies the accuracy might be expected to be poor, since, as may be seen in equation (7), when $R \approx 1$ and $\cos \epsilon_f \approx 1$, v_f/v_e is extremely critical to small errors in R or ϵ_f. In addition, the slope falls off from the -6 value because the original closed-loop phase angle did not level off at zero angle, due to loading of the servo as described in a later section comparing experimental and theoretical responses. In equation (7), then, it may be seen that too large a phase angle ϵ_f would cause a falling off of the response v_f/v_e. At high frequencies, on the other hand, where $R << 1$, the accuracy may also be expected to be poor. As R approaches zero, log v_f/v_e (see equation (8)) becomes large negatively and a scatter of points may be observed because of the difficulty of measuring small values of R accurately. In addition, the reaction of the elevator-control system on the servo, which becomes appreciable at sensitivity settings above 42 percent, may cause a departure from the straight lines in a narrow frequency band around 5 cps.

It may be noted that the vertical spacing between the gain curves should equal the ratio of sensitivities expressed in decibels. This spacing should, therefore, be about 4.8 db which is reasonably close to the actual value of about 4 db.

Determination of servo system constants.- Since it has been determined that the servo system under study behaves as a second-order system, its characteristics can be defined for analytical purposes in terms of two constants ζ, the damping ratio, and ω_n, the undamped natural angular frequency. The actual numerical values can be determined in a number of ways which offer excellent checks against each other. Evaluations can be made from either the closed-loop frequency response, from the open-loop response, or from transient data. These methods follow with numerical values tabulated in table I.

1. Servo-system constants from closed-loop response.- Servo theory for a second-order equation (reference 1, p. 107) shows that the resonant angular frequency ω_M and the peak height M of the closed-loop response are given by

$$M = \frac{1}{2\zeta\sqrt{1-\zeta^2}} \tag{11}$$

$$\omega_M = \omega_n\sqrt{1-2\zeta^2} \tag{12}$$

from which the two unknowns ζ and ω_n may be calculated for given values of M and ω_M. Equations (11) and (12) were applied to the responses for sensitivities 24 through 63 percent shown in figure 13(a).

2. Servo-system constants from open-loop response.- It is also possible to find ζ and ω_n from the open-loop plots already discussed, in which case the values ultimately depend upon many points on the closed-loop frequency-response curve rather than upon the values at the point of peak response only. It can be shown (reference 2, p. 222) that the intersection of the -12 db per octave slope with the zero decibel line occurs at ω_n and that $\zeta = \omega_b/2\omega_n$ where ω_b is the frequency at which the break between the -6 and -12 db per octave slope occurs.

As has been pointed out, portions of the open-loop curve are subject to appreciable error so that the exact position of the two slopes is not easy to determine accurately. Hence, the system values determined from the open-loop curves might be expected to be inaccurate. The values for ζ in this case were not too consistent with those obtained by other methods although the ω_n values agreed satisfactorily.

3. Servo-system constants from transient response.- The constants of this system can also be determined quite simply from the transient step-input data. For $\zeta < 1$ it has been shown in servo literature (reference 1, pp. 48-51) that the basic transient equation is

$$\frac{v_e}{v_i}(t) = \frac{e^{-\zeta\omega_n t}}{\sqrt{1-\zeta^2}} \sin\left(\omega_n t\sqrt{1-\zeta^2} + \sigma\right) \tag{13}$$

where

$$= \tan^{-1}\frac{\sqrt{1-\zeta^2}}{\zeta} \tag{14}$$

Since

$$v_e(t) = v_i(t) - v_f(t)$$

then

$$\frac{v_f}{v_i}(t) = 1 - \frac{v_e}{v_i}(t)$$

$$\frac{v_f}{v_i}(t) = 1 - \frac{e^{-\zeta\omega_n t}}{\sqrt{1-\zeta^2}} \sin\left(\omega_n t\sqrt{1-\zeta^2} + \sigma\right) \qquad (15)$$

For illustrative purposes a transient sketch represented by equation (15) is shown as follows:

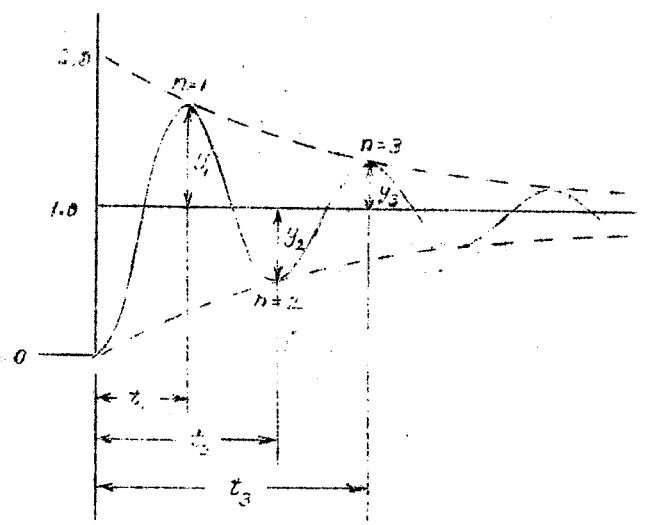

If the damping ratios are low enough so that the output transient consists of several oscillations, equation (15) can be used directly to evaluate ζ and ω_n since the frequency of the transient oscillations is

$$\omega_t = \omega_n \sqrt{1-\zeta^2}$$

and the exponential envelope is $e^{-\zeta\omega_n t}$. Direct measurement of ω_t and the determination of $\zeta\omega_n$ from points on the envelope curve at two different times is then sufficient to find the two unknowns.

Practical sensitivity settings, however, usually do not exhibit enough oscillations to permit direct measurement of ω_t or to accurately define the envelope. In such cases, ω_n and ω_t may be determined from the peak heights as long as at least one peak appears. For this purpose it will be necessary to find the times at which peaks of the oscillations occur by equating the derivative of equation (15) with respect to $\omega_n t$ to zero.

$$-\left[e^{\zeta\omega_n t}\cos\left(\omega_n t\sqrt{1-\zeta^2}+\sigma\right)-\frac{\zeta e^{-\zeta\omega_n t}}{\sqrt{1-\zeta^2}}\sin\left(\omega_n t\sqrt{1-\zeta^2}+\sigma\right)\right]=0$$

or

$$\cos\left(\omega_n t\sqrt{1-\zeta^2}+\sigma\right)=\frac{\zeta}{\sqrt{1-\zeta^2}}\sin\left(\omega_n t\sqrt{1-\zeta^2}+\sigma\right)$$

$$\tan\left(\omega_n t\sqrt{1-\zeta^2}+\sigma\right)=\frac{\sqrt{1-\zeta^2}}{\zeta} \tag{16}$$

Comparison of equations (16) and (14) indicates that

$$\omega_n t\sqrt{1-\zeta^2}=0,\ \pi,\ 2\pi,\ \ldots\ n\pi \tag{17}$$

for consecutive maxima and minima. At the values defined by equation (17), the response of equation (15) is

$$\frac{v_f}{v_i}(t,n)=1-\frac{e^{-\zeta\omega_n t}}{\sqrt{1-\zeta^2}}\sin(n\pi+\sigma) \tag{18}$$

For all values of n (including zero)

$$\sin(n\pi+\sigma)=(-1)^n\sin\sigma=(-1)^n\sin\left(\tan^{-1}\frac{\sqrt{1-\zeta^2}}{\zeta}\right)$$

$$=(-1)^n\sqrt{1-\zeta^2} \tag{19}$$

Therefore, equation (18) reduces to

$$\frac{v_f}{v_i}(t,n) = 1 - (-1)^n e^{-\zeta\omega_n t} \tag{20}$$

Equation (20) may be expressed in terms of only ζ by substituting for $\omega_n t$ from equation (17). Then, for the upper envelope of peaks defined by odd values of n,

$$\frac{v_f}{v_i}(n) = 1 + e^{-\frac{n\pi}{\sqrt{\frac{1}{\zeta^2}-1}}} = 1 + y_n \text{ (n odd)} \tag{21}$$

where

$$y_n = e^{-\frac{n\pi}{\sqrt{\frac{1}{\zeta^2}-1}}} \text{ (n odd)} \tag{22}$$

from which ζ can be solved as follows:

$$\ln y_n = -\frac{n\pi}{\sqrt{\frac{1}{\zeta^2}-1}}$$

$$\frac{1}{\zeta^2} = \frac{(n\pi)^2 + (\ln y_n)^2}{(\ln y_n)^2}$$

$$\zeta = \sqrt{\frac{(\ln y_n)^2}{(n\pi)^2 + (\ln y_n)^2}} \tag{23}$$

Thus ζ can be calculated from equation (23) by measuring y_n at a known-order peak. It must be remembered that in the previous transient sketch y_n is defined as the percentage of overshoot in terms of the final value since the final value is unity. Then the value of f_n can be found from equation (17) as

$$f_n = \frac{n}{2t_n\sqrt{1-\zeta^2}} \tag{24}$$

Thus ζ and f_n can be found by measuring y_n and t_n for a particular value of n and solving equations (23) and (24). Obviously this method is applicable to all sensitivity settings for which at least one output overshoot exists. It can be applied to successive peaks of the oscillations although each trial should give the same values. The spread in these values is indicated in table I.

In the actual analysis of the transients, several effects caused unexpected changes in transient response and they will be mentioned only briefly. First, opposite servo or surface deflections were found to define inconsistent ζ values, probably because of unequal loadings in these two directions. Second, the above inconsistency was negligible at low, but not at high, sensitivities. A study of the relationship defined by equation (23) shows that a small difference in overshoot for high damping ratios (low sensitivity) has negligible effect on the determination of ζ compared to that for low damping ratios where the effect is magnified. Third, the value of ζ as evaluated at successive peaks appears to decrease, probably because of blacklash.

4. Comparison of constants determined by various methods.- Table I shows the comparison of system constants as determined by the aforementioned methods. In addition, the values obtained from a "best fit" theoretical curve are shown. It is known from servo theory that ω_n is directly proportional to and ζ is inversely proportional to the square root of the over-all gain factor of the open loop. In this case the gain factor is proportional to P_f so that ideally ζ is inversely proportional to $\sqrt{P_f}$ and f_n is directly proportional to $\sqrt{P_f}$. On logarithmic plots these relationships are straight lines of slope 1/2. Therefore, log ζ and log f_n were plotted as a function of log P_f for the various methods used to evaluate ζ and f_n, and a straight line with the ideal slope 1/2 was then drawn to give the best fit of the experimental points. The best-fit values given in table I are points on these lines, the equations for which are

$$\zeta = \frac{0.242}{\sqrt{P_f}} \tag{25}$$

$$f_n = 4.71 \sqrt{P_f} \tag{26}$$

Comparison of constants from all methods and the best-fit theoretical values show good agreement up to perhaps a sensitivity of 52 percent. At higher sensitivities all the values for ζ, as calculated from experimental data, remain in quite good agreement but they indicate a definite departure from the theoretical $\sqrt{P_f}$

relationship. The methods which depend on the closed-loop frequency response cannot be used beyond a sensitivity of 63 percent because of saturation effects, but even at 63-percent sensitivity both transient and frequency-response methods indicate a change from the theoretical.

The departure at high sensitivities from theoretical behavior could be caused by either or both of two factors: the reaction of the elevator linkage on the servo response, and the backlash and friction in the piston, valve, and follow-up unit. Both factors cause a decrease in ζ below the theoretical value. The effect of the elevator-control reaction, which becomes important only at high sensitivities, will be presented in the section comparing bench and ground tests. The effect of backlash should be approximately the same at all sensitivities since the amplitude of mechanical motion at resonant frequency was of the same order of magnitude at all sensitivities, any increase in amplitude ratio at higher sensitivities being approximately offset by the reduced static deflection.

The natural undamped frequencies f_n, however, remain in fairly good and consistent agreement over the entire frequency range. Evidently the factors which cause a low value of ζ at high sensitivity either do not influence f_n to an appreciable extent or tend to compensate for each other.

Open-loop servo system transfer function.- The servo-system response under investigation can be expressed mathematically in terms of a second-order open-loop response equation, or transfer function, as

$$\frac{v_f}{v_e} = \frac{k_v}{j\omega(j\omega T + 1)} \tag{27}$$

where k_v represents the system gain and T the system time constant.

It will be shown that the constants k_v and T can be obtained from the constants ζ and ω_n which have been determined previously. The relationship comes from the equations given in reference 1, pages 45-49. It should be noticed that, since each term in these equations represents a force, the variables should be expressed in units of motion, such as inches; then, since the same constant may be chosen relating motion and voltage for both output and error, the basic equation may be expressed in terms of voltages as shown.

$$\frac{d^2v_f}{dt^2} + 2\zeta\omega_n \frac{dv_f}{dt} = \omega_n{}^2 v_e$$

Letting $d/dt = j\omega$, then

$$\frac{v_f}{v_e} = \frac{\omega_n^2}{(j\omega)^2 + 2\zeta\omega_n(j\omega)} = \frac{\frac{\omega_n}{2\zeta}}{j\omega\left(\frac{j\omega}{2\zeta\omega_n} + 1\right)} \tag{28}$$

Comparing equations (27) and (28) gives

$$k_v = \frac{\omega_n}{2\zeta} = \frac{\pi f_n}{\zeta} \tag{29}$$

and

$$T = \frac{1}{2\zeta\omega_n} = \frac{1}{4\pi\zeta f_n} \tag{30}$$

Substitution for values of ζ and f_n from equations (25) and (26) gives

$$k_v = 61 \ P_f \ \text{sec}^{-1}$$

$$T = 0.070 \text{ sec}$$

Theoretically the open-loop plot of figure 26 may also be used to calculate the constants of equation (27). In practice, however, T cannot be found by this method with any degree of accuracy. It may be easily demonstrated that the break frequency between the two asymptotes occurs when $\omega T = 1$ (reference 1, p. 238) from which T could be calculated, but as mentioned previously these asymptotes are not determined sufficiently accurately for this calculation.

The gain constant in equation (27) can be evaluated from the open-loop response by measuring the decibel gain from the curve at a known frequency and solving for k_v as

$$k_v = \left|\frac{v_f}{v_e}\right| \sqrt{(\omega^2 T)^2 + \omega^2} \tag{31}$$

Evaluation of equation (31) in terms of a general sensitivity gave

$$k_v = 74 \ P_f$$

A check may also be made on k_v using the static calibrations previously presented. Its value can be obtained from the relation

$$k_v = P_a k_a k_m k_f P_f \tag{32}$$

which has dimensions of sec^{-1}. The values of the first three factors were found previously to be

$$P_a = 0.29 \text{ for minimum gain}$$

$$k_a = 350 \text{ milliamperes per volt}$$

$$k_m = 0.05 \frac{\text{inch/second}}{\text{milliampere}}$$

$$k_f = 14.0 \text{ volts/inch}$$

Substituting these values in equation (32) gave a value of

$$k_v = 71.1 P_f$$

The resultant open-loop response for equation (27) for a minimum amplifier gain setting and based on the best-fit theoretical values would then be

$$\frac{v_f}{v_e} = \frac{61 P_f}{j\omega(j0.07\omega + 1)} \tag{33}$$

The complete range of k_v depends then upon actual sensitivity and the amplifier gain setting. At minimum gain ($P_a = 0.29$) and with a sensitivity of 24 percent ($P_f = 0.24$), $k_v = 15$ sec^{-1}. At a high sensitivity of 63 percent, $k_v = 38$ sec^{-1}.

Comparison of experimental and theoretical response curves.- For purposes of comparison, an ideal response for a second-order equation corresponding to the damping ratio and natural frequency calculated in table I has been plotted in figure 27 with the actual ground-test experimental curves for a sensitivity of 33 percent. These ideal curves may be calculated or taken from nondimensional curves given in many texts. Two ground runs taken at different times are presented to indicate the repeatability of the system. General agreement may be seen to be quite good.

Two definite effects should be noted, however. First, the reaction of the elevator-control-cable system on the servo response causes the experimental values to deviate appreciably from the theoretical at high frequencies. Second, the low-frequency phase shift for ground tests always approaches a constant value of 6° to 10°, as may be seen also in the curves previously presented. This merely means that 6° to 10° lag between input and follow-up voltage is required to produce a small error signal before the output will move. This minimum error voltage required to move the output is equal to the value of input voltage when the

output is zero, that is, $v_i \sin \epsilon_f$. For an input of ±0.115 volt and phase angle of 8°, this minimum voltage is 0.016 volt. Friction in the valve and piston is a probable source of this phenomenon.

Experimental response curves at other sensitivities have been compared to the theoretical responses with similar correlation as above. Agreement was found to depart at a sensitivity of 63 percent which would be expected because it has already been shown that the basic system constants ζ and ω_n do not obey the second-order equation theory at this and higher sensitivities.

Comparison of bench and ground tests.- In general, the comparison of ground and bench tests might be expected to show slight differences since a different set of servo-system components was used for the bench tests. In addition, in contrast to the ground tests, no control linkage system was attached to the servo during the bench tests. Figure 28(a) shows the comparison of bench and ground tests for a sensitivity of 24 percent. Several effects are readily apparent. The amplitude curves are slightly different, which could be caused by a slight difference in the gain factor. The dip of amplitude for the ground tests around 5 cps is the reaction of the elevator controls as mentioned previously. Purely on the basis of the comparative amplitude curves, the phase curve for ground tests should be nearly equal or slightly below that for bench tests in midfrequencies. However, the ground curves have the greater lag, which may be the effect of a greater loading of the servo in ground tests. Elevator-control reaction, again, causes the peaking effect around 5 cps on the phase curves which is absent in bench tests.

A very informative comparison is shown in figure 28(b) for the high sensitivity of 63 percent. As was pointed out in a previous section, the ground tests departed from theory at this sensitivity and this set of curves indicates several causes. Table I shows that the damping ratio ζ should be about 0.31, but that the value actually obtained for the ground tests was 0.17. Application of preceding methods to the bench-test data revealed that $\zeta = 0.31$, which is in agreement with the theoretical value. Thus the explanation of the departure from the theoretical value in ground tests at high sensitivities may be found in the difference between ground and bench tests. Two possible causes are differences in backlash of pistons, valves, or follow-up units, and the reaction of the elevator linkage system.

Backlash in the piston, valve, or follow-up unit has the effect of causing a more unstable system or reduced ζ. As mentioned previously in the transient section, there was some indication of backlash in valve or piston. Trouble with follow-up backlash in ground tests and improvements to minimize this have been mentioned under mechanical difficulties. The follow-up unit in bench tests was coupled directly to the servo shaft, thus avoiding linkages with consequent backlash.

The second possible cause of the difference, elevator-linkage reaction, would appear to be the more important. The oscillations of the elevator linkage impose mechanical loads back on the servo system which may affect the servo output or take up the backlash in the system. At low sensitivities, the natural frequency of the linkage system is much higher than that for the servo system so that reactions are negligible. Thus, at a sensitivity of 24 percent, table I shows that for the servo system f_n is equal to 2.3 cps, which should be compared to a resonant frequency of 4.8 cps for the linkage system as shown later. At high sensitivities, however, the natural frequency for the servo system approaches that for the control system and hence reactions are possible. At a sensitivity of 63 percent, f_n for the servo system equals 3.8, which is reasonably close to the value for the linkage system.

Calculation of frequency response for any value of sensitivity.- While frequency responses were obtained and presented for only a few different values of sensitivity, it is possible to obtain the response, within the linear range of operation, at any particular sensitivity by direct calculation from a known response. This method is useful for obtaining intermediate values that may be required for the desired airplane-autopilot response and for comparing two runs taken at different sensitivities. The method developed is shown subsequently and has the advantage that the primary closed-loop frequency-response data can be used directly to calculate the new frequency response at the new sensitivity. Thus it is not necessary to convert closed-loop to open-loop data, change the sensitivity, and then change back to the new closed-loop response as in the conventional method.

For the given sensitivity condition 1, servo theory shows that the closed-loop response or transfer function may be represented by

$$\frac{v_{f_1}}{v_i} = \frac{A_1}{1 + A_1} \tag{34}$$

where A_1 is the open-loop transfer function derived from the product of the individual component transfer functions $P_a A_a A_m k_f P_f$, for setting 1 of P_f. For the new desired gain condition 2,

$$\frac{v_{f_2}}{v_i} = \frac{A_2}{1 + A_2} \tag{35}$$

It is convenient to define A_R as

$$A_R = \frac{A_2}{A_1} = \frac{P_{f_2}}{P_{f_1}} \tag{36}$$

Substituting A_2 from equation (36) into equation (35), thus eliminating A_2,

$$\frac{v_{f_2}}{v_i} = \frac{A_R A_1}{1 + A_R A_1} \tag{37}$$

From equation (34),

$$\frac{v_{f_1}}{v_i} + \frac{v_{f_1}}{v_i} A_1 = A_1$$

$$A_1 = \frac{v_{f_1}/v_i}{1 - (v_{f_1}/v_i)}$$

which, when substituted into equation (37), gives

$$\frac{v_{f_2}}{v_i} = \frac{A_R(v_{f_1}/v_i)}{1 - (v_{f_1}/v_i) + A_R(v_{f_1}/v_i)} \tag{38}$$

The ratio $\frac{v_{f_1}}{v_i}$ is the complex vector $R_1 e^{j\epsilon_{f_1}}$.

Substituting this expression for $\frac{v_{f_1}}{v_i}$ in equation (38),

$$\frac{v_{f_2}}{v_i} = \frac{A_R R_1 e^{j\epsilon_{f_1}}}{1 - R_1 e^{j\epsilon_{f_1}} + A_R R_1 e^{j\epsilon_{f_1}}}$$

$$\frac{v_{f_2}}{v_i} = \frac{A_R R_1 e^{j\epsilon_{f_1}}}{1 + R_1(A_R - 1) \cos \epsilon_{f_1} + jR_1(A_R - 1) \sin \epsilon_{f_1}} \tag{39}$$

Separating into amplitude and phase components,

$$\frac{v_{f_2}}{v_i} = R_2 e^{j\epsilon_{f_2}}$$

$$= \frac{A_R R_1 e^{j\left(\epsilon_{f_1} - \tan^{-1}\frac{B}{A}\right)}}{\sqrt{\left[1 + R_1(A_R-1)\cos\epsilon_{f_1}\right]^2 + \left[R_1(A_R-1)\sin\epsilon_{f_1}\right]^2}} \tag{40}$$

where A and B are the real and imaginary parts, respectively, of the denominator of equation (39).

Autopilot Frequency Response With Displacement and Rate Signals

Calculation of response with rate.- Experimental data for the response with both displacement and rate signals have already been presented for a limited number of conditions. The response with rate signal may also be calculated using the frequency response of the servo system without rate signal and the frequency response of the rate gyro. Thus the response can be predicted for any other desired combination of sensitivity and rate not covered by the experimental data.

Let A represent the complex gain $P_a A_a A_m k_f P_f$ for the amplifier, servo, and follow-up unit. The closed-loop amplitude ratio can then be written as

$$\frac{v_{f_r}}{v_g} = \frac{Av_{er}}{v_g} \tag{41}$$

where v_{f_r} and v_{er} are the follow-up voltage and error voltage, respectively, with combination displacement and rate signal. The displacement gyro output v_g in this case corresponds to the input signal v_i.

The error voltage v_{er} may be expressed as

$$v_{er} = v_g + v_r - v_{f_r} \tag{42}$$

where v_r is the rate signal.

Substituting v_{er} from equation (42) into equation (41)

$$\frac{v_{f_r}}{v_g} = \frac{A(v_g + v_r - v_{f_r})}{v_g} = A + A\frac{v_r}{v_g} - A\frac{v_{f_r}}{v_g}$$

$$= \frac{A}{1+A}\left(1 + \frac{v_r}{v_g}\right) \tag{43}$$

For the situation with no rate, v_r/v_g is zero, and

$$\frac{v_f}{v_g} = \frac{A}{1+A} \tag{44}$$

Combining equations (43) and (44)

$$\frac{v_{f_r}}{v_g} = \frac{v_f}{v_g}\left(1 + \frac{v_r}{v_g}\right) \tag{45}$$

This gives the rate response v_{f_r}/v_g as a function of the no-rate response v_f/v_g and the amount of rate v_r. Expanding equation (45) then gives

$$\frac{v_{f_r}}{v_g} = Re^{j\epsilon_f} + R\left|\frac{v_r}{v_g}\right| e^{j(\epsilon_r+\epsilon_f)} = R\cos\epsilon_f + R\left|\frac{v_r}{v_g}\right|\cos(\epsilon_r+\epsilon_f) +$$

$$j\left[R\sin\epsilon_f + R\left|\frac{v_r}{v_g}\right|\sin(\epsilon_r + \epsilon_f)\right] \tag{46}$$

from which magnitude and phase are easily obtainable as shown in previous examples if v_r is known.

Determination of rate-gyro signal.- The rate-gyro output voltage and phase, as a function of frequency, were given in figure 4. The rate-gyro output voltage is essentially proportional to rate of change of angle. Thus, if the pitch rate gyro is assumed to be rocking with a motion,

$$\theta = \theta_{max}\sin\omega t$$

then

$$\frac{d\theta}{dt} = \omega\theta_{max} \cos \omega t$$

$$= 2\pi f\theta_{max} \cos \omega t \tag{47}$$

and

$$v_{r_m}(t) = k_r f\theta_{max} \cos \omega t \tag{48}$$

where v_{r_m} is the rate signal before modification by the rate potentiometer. The final rate signal after modification by the rate potentiometer is

$$v_r(t) = P_r k_r f\theta_{max} \cos \omega t$$

where P_r is the percentage rate used, or, in vector notation,

$$v_r = P_r k_r f\theta_{max} e^{j\epsilon_r} \tag{49}$$

From the dynamic response curves presented in figure 4(a), it can be seen that k_r is essentially a constant up to about 1.2 cps, above which resonance effects begin to appear. At frequencies above the range for which k_r is constant, values of $k_r f$ may be obtained conveniently from figure 4(a) for use in calculations. The phase angle ϵ_r was constant at 86° leading over the range tested up to 2 cps.

Values of v_r from equation (49) were used in equation (46), using values of $k_r f$ from figure 4(a).

Calculation of error voltage with rate signal.- Frequency responses with rate signal calculated by equation (46) assume linear servo characteristics. The calculated responses would be expected to agree with the experimentally determined responses only so long as the error voltage in the experimental runs did not exceed the linear range of the amplifier. The magnitude of the error voltage with a rate signal present can be calculated as follows:

For the case with rate signal, the basic error expression is given in equation (42). The value of displacement gyro voltage v_g, which corresponds here to the input signal, is known for a given run. The value of v_{f_r} is given by $R_{f_r} v_g e^{j\epsilon_{f_r}}$ where R_{f_r} and ϵ_{f_r} are the amplitude ratio and phase angle, respectively, of the output v_{f_r} with

respect to the input v_g when the vertical and rate gyros are oscillated simultaneously on the rocking table assembly. Substituting values of v_{f_r} from above and v_r from equation (49) in equation (42) gives

$$v_{er} = v_g - R_{f_r} v_g e^{j\epsilon_{f_r}} + P_r (k_r f)\theta e^{j\epsilon_r}$$

$$= [\, v_g - R_{f_r} v_g \cos \epsilon_{f_r} + P_r (k_r f)\theta \cos \epsilon_r] \; -$$

$$j\, [R_{f_r} v_g \sin \epsilon_{f_r} - P_r (k_r f)\theta \sin \epsilon_r \,] \qquad (50)$$

The plots of the magnitude of the error voltage given by equation (50) are shown in figure 23(a) for the three rates, 8, 20, and 31 percent. Agreement of experimental rate-response curves with theoretical curves can be expected only up to an error voltage, again, of 0.35 volt, above which saturation effects occur.

Comparison of calculated and measured responses.- The above calculations, of course, depend upon the no-rate response. Since the input signal for the rate tests is obtained from an oscillating gyro, whereas the no-rate tests were made with a synthetic input signal, it was desirable, before attempting any check between calculated and experimentally determined responses with rate, to first compare the responses for zero rate using the rocking table assembly with that using the sine-wave generator. Agreement was found to be fairly good over the range tested up to 2 cps so that this comparison is not shown.

By the use of the zero-rate response curve, then, the responses with rate were calculated from equation (46) for rates of 8, 20, and 31 percent, and are shown in figure 23(a) with the experimental results. The experimental and calculated responses are in very good agreement up to the nonlinear level of error voltage.

Elevator Control Cable Response

From data previously presented, it is possible to determine the elevator-linkage-system characteristics. The surface response curves in figure 14(a), for example, represent the output of the elevator linkage system; whereas its input is the servo output as shown in the same figure. Thus the transfer function for the elevator linkage system may be computed as the ratio of surface to servo response. This transfer-function amplitude and phase for the no-load condition is shown in figure 29(a); whereas 29(b) shows the amplitude plotted in decibels

against frequency. The equation for this type mechanical system is closely represented by a quadratic equation with dimensionless constants ζ and ω_n with the same meanings as defined for the servo system. The damping ratio ζ would appear to be less than 0.1 and f_n is about 4.8 cps; high frequencies approach a slope of 12 db per octave which is consistent with the second-power term of a quadratic factor. It is to be expected that this characteristic should vary with the surface loading so that the same procedure was applied to a set of maximum-load tests. The resultant effect, plotted in figure 29(c), shows the characteristic to be appreciably altered, its resonant frequency shifting to about 6.6 cps.

The known transfer function for the elevator-control linkage may be used to predict the surface response relative to amplifier input from the servo response for any desired combination of conditions, provided that reactions of the elevator-control linkage system do not appreciably alter the servo response. The surface response is then simply the product of the servo- and linkage-system responses.

The interaction of the elevator linkage system on the servo-response characteristic is appreciable at the higher sensitivities, particularly in the neighborhood of resonant frequency. (See fig. 28.) However, at the lower sensitivities and at the lower frequencies, even at 63-percent sensitivity, the interaction is not great and the above procedure for predicting surface response is valid.

The measured elevator linkage response applies, of course, only so long as the control-cable tension is unaltered.

ANALYSES OF AILERON AND RUDDER CHANNELS

A similar analysis of the aileron and rudder channels was not undertaken. A calculation of error voltage, as plotted on the corresponding frequency-response runs, showed the aileron runs to reach saturation on all sensitivities, thus making the methods of calculations, as discussed previously, invalid. For the prime purpose of these tests it was only necessary that the error voltage did not exceed the limiting value of 0.35 volt at frequencies below 2 cps. If an analysis similar to that made on the elevator channel were to be made on the aileron or rudder channels, the input signal would have to be made low enough to prevent the error voltage from reaching its limiting value at any frequency. The rudder-channel data, in addition, were not as smooth and consistent as in the case of the other channels because of the distorted response of the rudder.

CONCLUDING REMARKS

Frequency-response data of the servo system for various conditions of operation are presented in usable form, and the equation for the servo system with experimentally determined values is given. It is shown that the frequency response is somewhat better at high values of sensitivity because of slightly reduced phase lag and amplitude ratio at frequencies up to approximately 2 cps. The effect of large input signals is to reduce the amplitude ratio and materially increase the phase lag, as would be expected when the system becomes nonlinear due to saturation. The system response measured at the surface exhibits higher amplitude ratios and greater phase lags than at the servo output shaft due to resonance of the control-surface linkage system, but again the difference is not great at frequencies below 2 cps.

Of greater concern when considering the application of the autopilot to an airplane is the effect of the loading from the control-surface hinge moment. The servo-system frequency response is not greatly changed by the addition of load, but the actual output amplitude at the surface is materially reduced under these conditions, due principally to stretch in the control cable. This fact must be taken into account when determining the required gearing, or static ratio of autopilot output to input, for airframe-autopilot stability. While flexibility in the control linkage would generally be considered objectionable, it may be noted that it does have the beneficial effect of reducing the autopilot gearing at the higher airspeeds where the control effectiveness is high. This inherent reduction in gearing at high speeds should aid in maintaining stability of the autopilot-airplane combination over a wide speed range.

On the SB2C-5 airplane, the gearing in terms of control-surface deflection per degree of gyro inclination is changed by varying the sensitivity (follow-up) control. From the data which have been presented, it is obvious that changing the sensitivity alters the autopilot dynamic characteristics as well as the characteristics of the autopilot-airplane combination. The gearing could also be changed by providing adjustable excitation voltage for the displacement gyro. This arrangement would be more satisfactory as it would permit adjustment of the gearing independently of the servo-system response.

The optimum setting of sensitivity or gain of the servo system is determined in part by the response of the system to which it is coupled. It is known that the response of the SB2C-5 airframe to forced oscillations is negligible beyond 2 cps. While servo-system design usually calls for a peak-amplitude ratio in the neighborhood of 1.4, this criterion does not necessarily apply in this case. Larger peak values and correspondingly lower damping ratios are tolerable and even desirable when the natural frequency of the servo system is several times that of the short-period oscillation of the airframe because the higher peak

values are accompanied by less phase lag in the vicinity of the airframe natural frequency. Thus the sensitivity or gain of the servo system should be set as high as possible without danger of incurring instability.

The servo system in general is considered to be well-designed since there is a considerable range over which it is stable and the performance does not change greatly. The gyros, while probably adequate for the SB2C-5 airplane, are not considered suitable for higher performance aircraft due to gimbal friction and electrical noise. Also, mechanical tolerances would have to be held more closely for higher performance aircraft. For the same reason an amplifier should be obtained that is not materially affected by changing tubes.

The suitability of this system for controlling the SB2C-5 airplane in flight is the subject of further investigation.

Ames Aeronautical Laboratory,
National Advisory Committee for Aeronautics,
Moffett Field, Calif.

REFERENCES

1. Brown, Gordon S., and Cambell, Donald P.: Principles of Servomechanisms. John Wiley and Sons, Inc., New York, 1948.

2. Lauer, Henri, Lesnick, Robert, and Matson, Leslie E.: Servomechanism Fundamentals. McGraw-Hill Company, New York, 1947.

TABLE I.- SUMMARY OF CONSTANTS OF ELEVATOR-CHANNEL SERVO SYSTEM DETERMINED BY VARIOUS METHODS

Method \ Sensitivity	Damping ratio,					Undamped natural frequency, f_n				
	24	33	42	52	63	24	33	42	52	63
Closed-loop response	0.50	0.45	0.38	0.31	0.17	2.2	2.8	3.3	3.8 4.1	4.0 4.2
Open-loop response	.67	--	.55	--	--	2.3	--	2.9	--	--
Transient response										
Minimum values	.50	.42	.34	.31	.16	2.2	2.6	2.3	3.2	3.5
Maximum values	.52	.46	.36	.33	.17	2.3	2.9	2.9	3.8	4.1
Best-fit theoretical curve	.49	.42	.37	.33	.31	2.3	2.7	3.1	3.4	3.8

FIGURE LEGENDS

Figure 1.- Block diagram of one channel of autopilot.

Figure 2.- Schematic diagram of one channel of autopilot signal circuits.

Figure 3.- Ground test apparatus with oscillating table.

Figure 4.- Frequency response of rate gyros; $\pm 1^{\circ}$ input. (a) Pitch.

Figure 4.- Continued. (b) Roll.

Figure 4.- Concluded. (c) Yaw.

Figure 5.- Response characteristic of roll rate gyro.

Figure 6.- Calibration of rate gyros. (a) Pitch.

Figure 6.- Concluded. (b) Roll.

Figure 7.- Amplifier gain characteristics.

Figure 8.- Valve and servo-actuator gain characteristic.

Figure 9.- Calibration of sensitivity potentiometers.

Figure 10.- Calibration of rate potentiometers.

Figure 11.- Surface hinge-moment simulator.

Figure 12.- Autopilot gearing characteristics. (a) Elevator channel.

Figure 12.- Continued. (b) Aileron channel.

Figure 12.- Concluded. (c) Rudder channel.

Figure 13.- Effect of sensitivity on elevator-channel frequency response; no load; ±0.115 volt ($\approx \pm 1/4^{\circ}$) input. (a) Servo response.

Figure 13.- Concluded. (b) Surface response.

Figure 14.- Effect of elevator linkage system on elevator-channel frequency response for various sensitivities; no load; ±0.115 volt ($\approx \pm 1/4^{\circ}$) input. (a) Sensitivity, 24 percent.

Figure 14.- Continued. (b) Sensitivity, 42 percent.

Figure 14.- Concluded. (c) Sensitivity, 63 percent.

Figure 15.- Effect of load on elevator-channel frequency response; ±0.115 volt ($\approx \pm 1/4^{\circ}$) input. (a) Sensitivity, 24 percent; servo response.

Figure 15.- Continued. (b) Sensitivity, 24 percent; surface response.

Figure 15.- Continued. (c) Sensitivity, 42 percent; servo response.

Figure 15.- Concluded. (d) Sensitivity, 42 percent; surface response.

Figure 16.- Effect of input signal amplitude on elevator-channel frequency response. (a) Servo response; no load; sensitivity, 26 percent.

Figure 16.- Continued. (b) Surface response; no load; sensitivity, 26 percent.

Figure 16.- Continued. (c) Servo response; no load; sensitivity, 56 percent.

Figure 16.- Continued. (d) Surface response; no load; sensitivity, 56 percent.

Figure 16.- Continued. (e) Servo response; maximum load; sensitivity, 41 percent.

Figure 16.- Concluded. (f) Surface response; maximum load; sensitivity, 41 percent.

Figure 17.- Effect of sensitivity on aileron-channel frequency response; no load; ±0.275 volt ($\approx \pm 1/2^{\circ}$) input. (a) Servo response.

Figure 17.- Concluded. (b) Surface response.

Figure 18.- Effect of load on aileron-channel frequency response; ±0.275 volt ($\approx \pm 1/2^{\circ}$) input; sensitivity, 44 percent. (a) Servo response.

Figure 18.- Concluded. (b) Surface response.

Figure 19.- Effect of input signal amplitude on aileron-channel frequency response; sensitivity, 44 percent; no load.

Figure 20.- Effect of sensitivity on rudder-channel frequency response; no load; ±0.25 volt ($\approx \pm 1/2^{\circ}$) input. (a) Servo response.

Figure 20.- Concluded. (b) Surface response.

Figure 21.- Effect of load on rudder-channel frequency response; ±0.25 volt ($\approx \pm 1/2^{\circ}$) input; sensitivity, 41 percent. (a) Servo response.

Figure 21.- Concluded. (b) Surface response.

Figure 22.- Effect of input signal amplitude on rudder-channel frequency response; no load; sensitivity, 41 percent.

Figure 23.- Effect of rate signal on elevator-channel frequency response; ±0.115 volt (≈±1/4°) input; no load; sensitivity, 24 percent. (a) Servo response; experimental and calculated.

Figure 23.- Concluded. (b) Surface response; experimental only.

Figure 24.- Effect of rate signal on aileron-channel frequency response; experimental response; ±0.275 volt (≈±1/2°) input; no load; sensitivity, 44 percent.

Figure 25.- Transient response of elevator channel. (a) Sensitivity, 24 percent. (b) Sensitivity, 42 percent. (c) Sensitivity, 63 percent.

Figure 26.- Open-loop servo frequency response of elevator channel.

Figure 27.- Comparison of experimental ground tests and theoretical elevator-channel servo frequency response; sensitivity, 33 percent.

Figure 28.- Comparison of bench and ground tests of elevator-channel servo frequency response. (a) Sensitivity, 24 percent.

Figure 28.- Concluded. (b) Sensitivity, 63 percent.

Figure 29.- Transfer function of elevator control linkage. (a) No load.

Figure 29.- Continued. (b) Decibel amplitude ratio; no load.

Figure 29.- Concluded. (c) Maximum load.

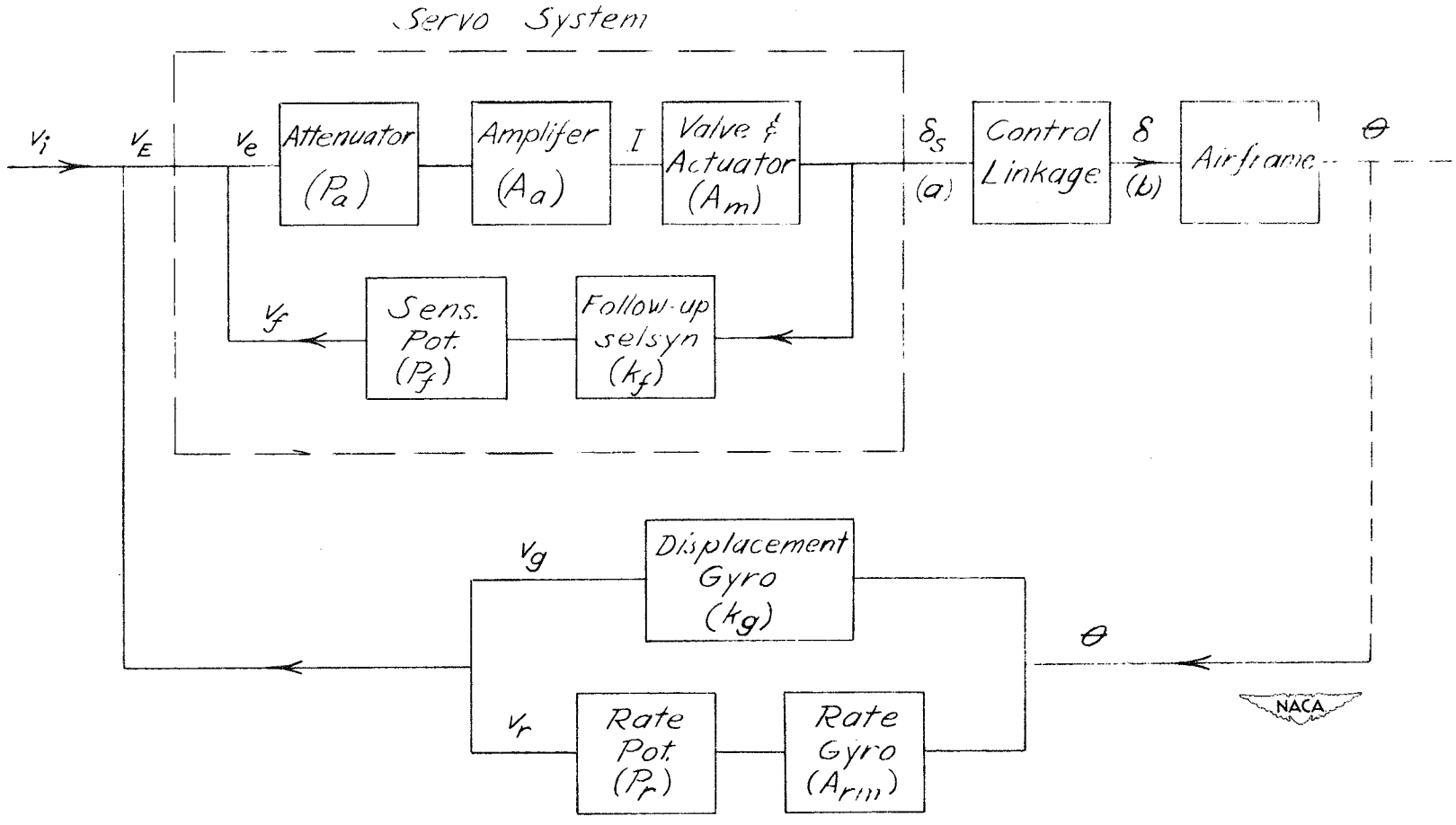

Figure 1.– Block diagram of one channel of autopilot.

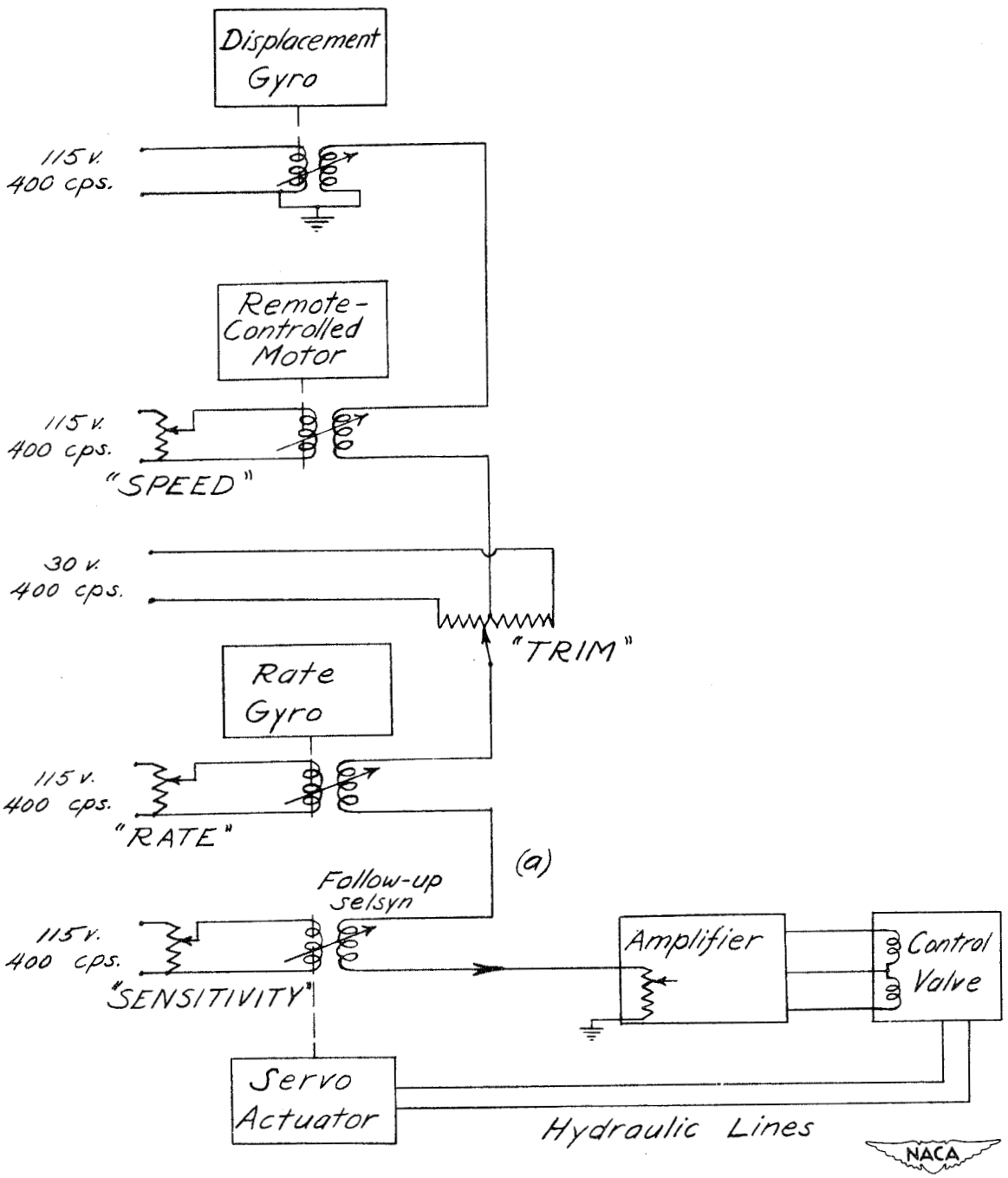

Figure 2.- Schematic diagram of one channel of autopilot signal circuits.

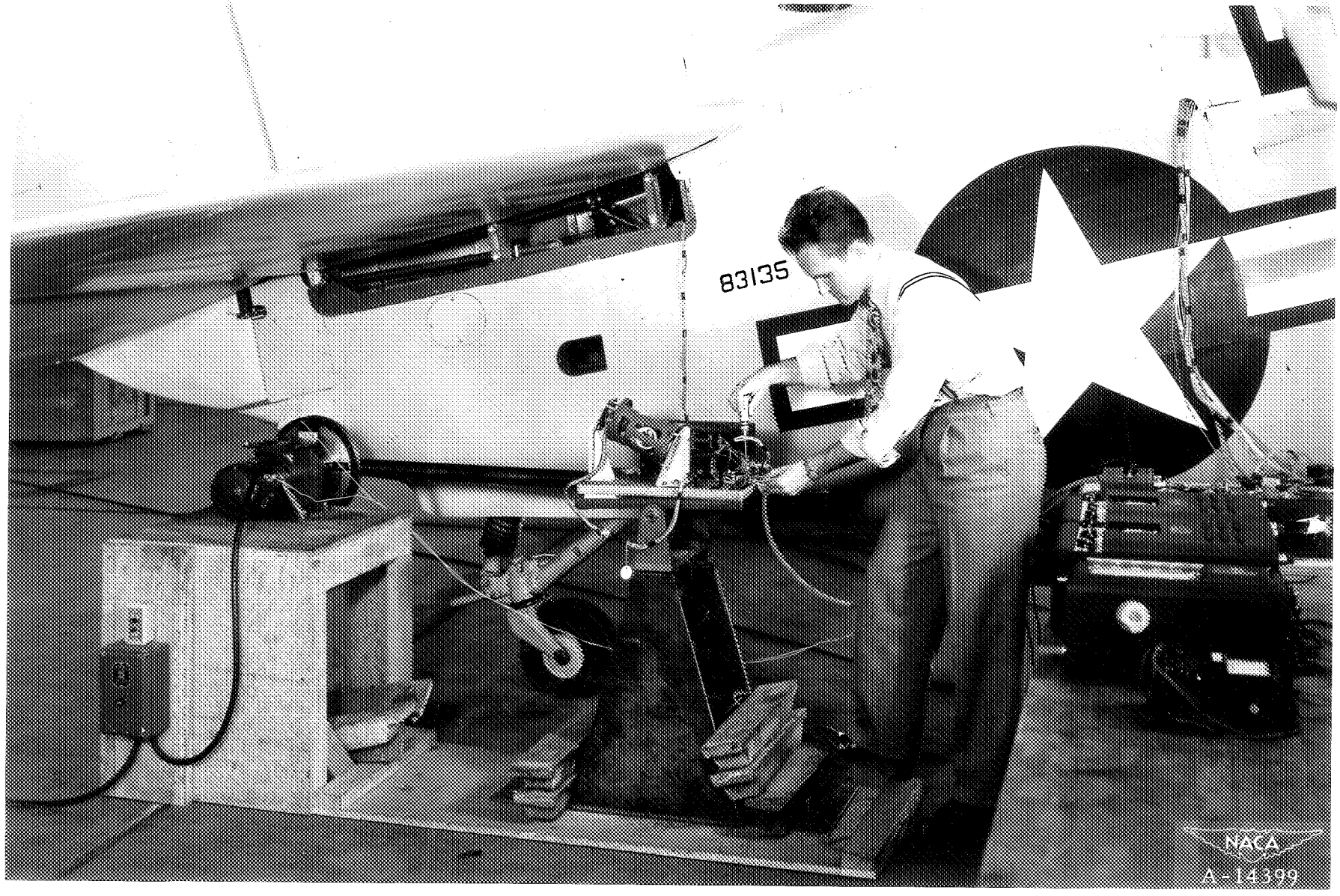

Figure 3.- Ground test apparatus with oscillating table.

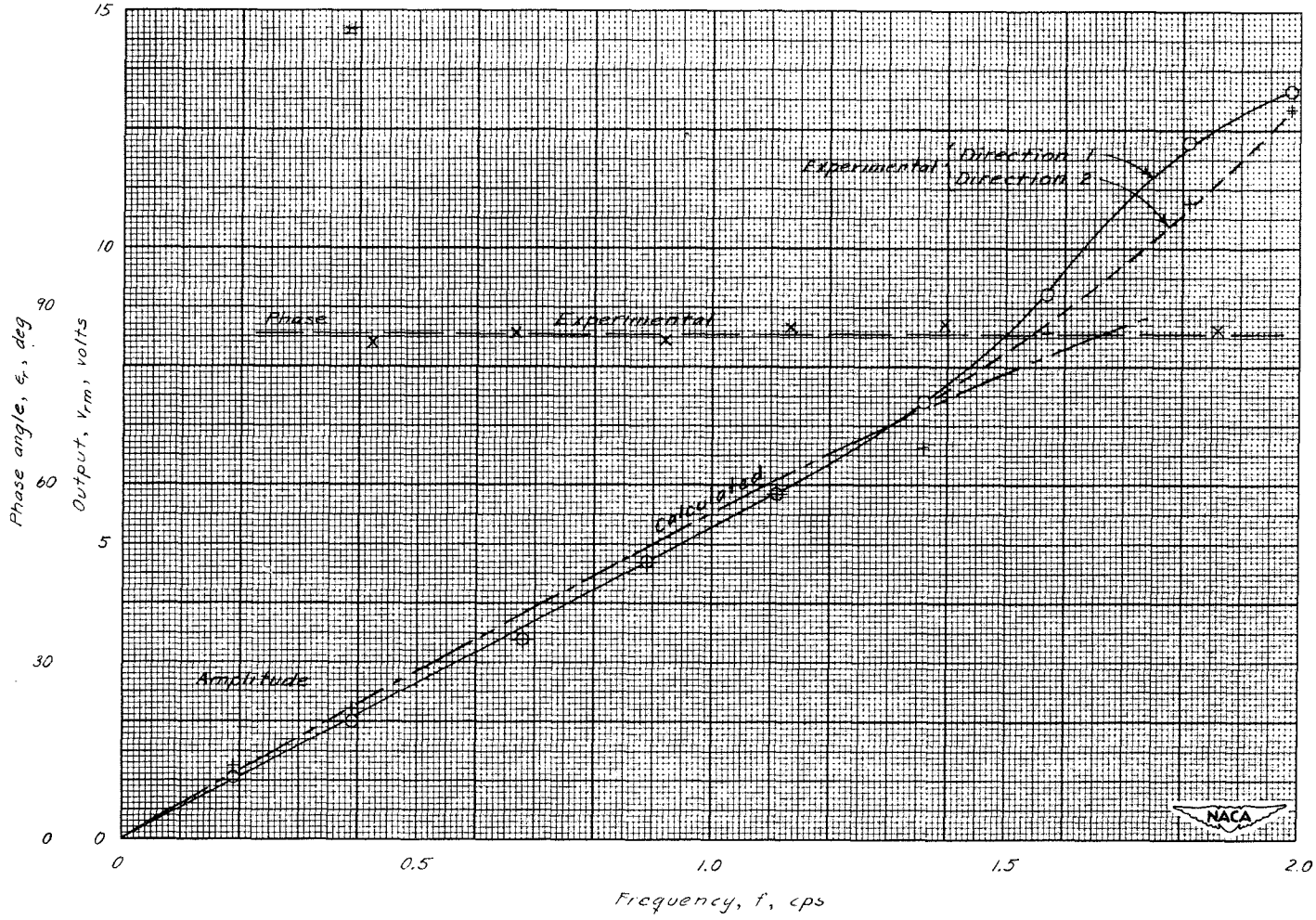

(a) Pitch.

Figure 4.– Frequency response of rate gyros; ±1° input.

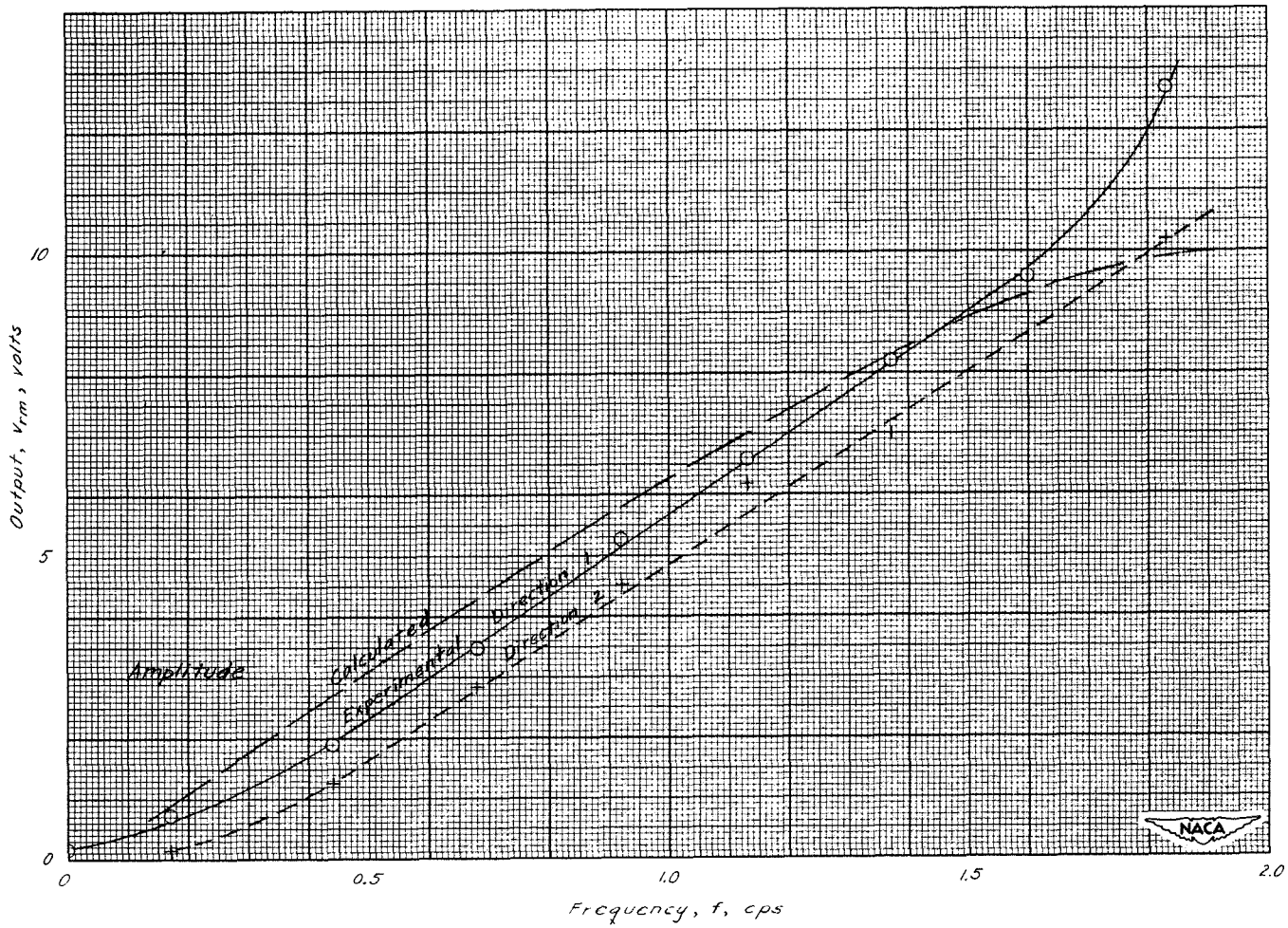

(b) Roll.

Figure 4.- Continued.

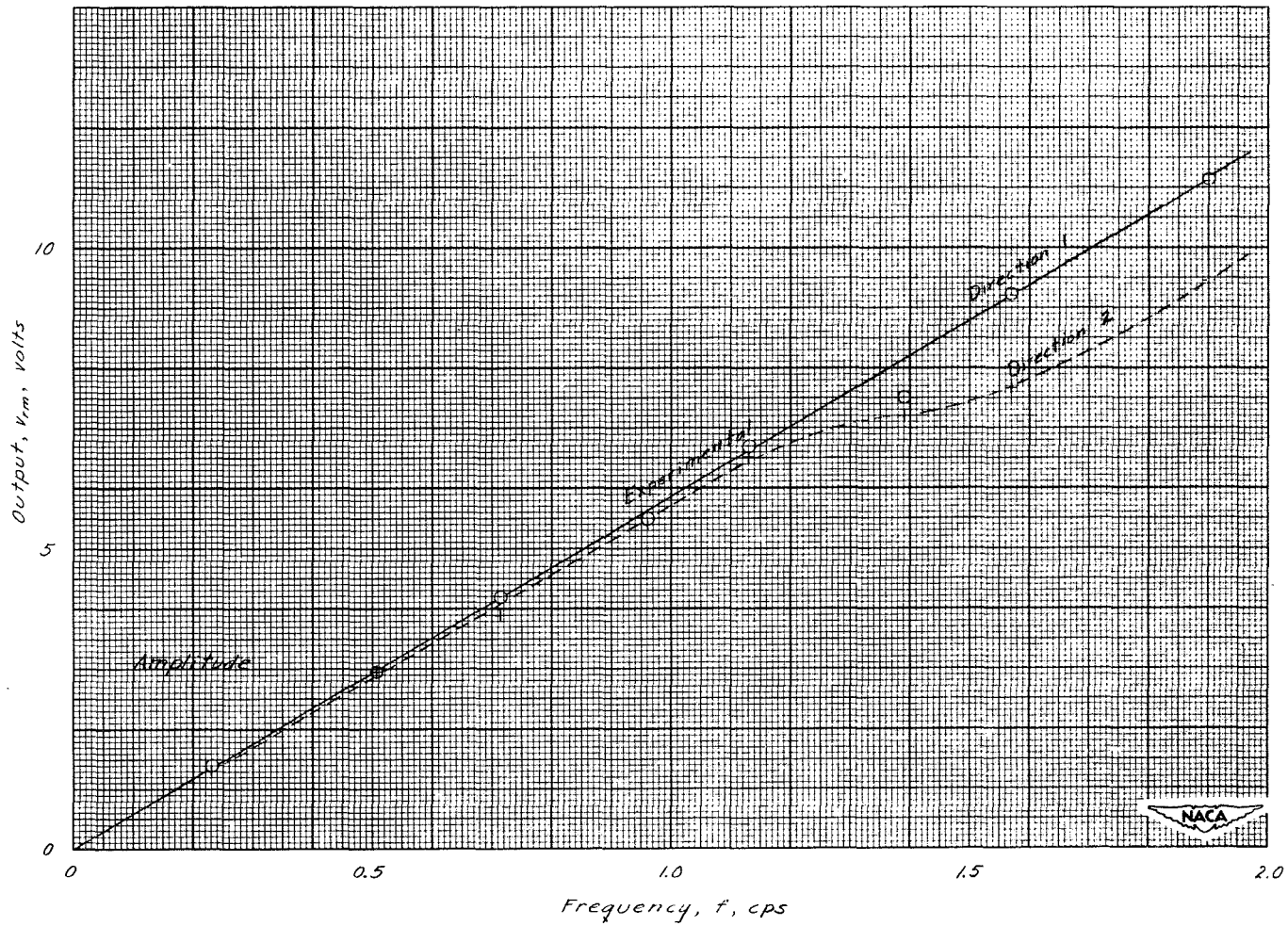

(c) Yaw.

Figure 4.- Concluded.

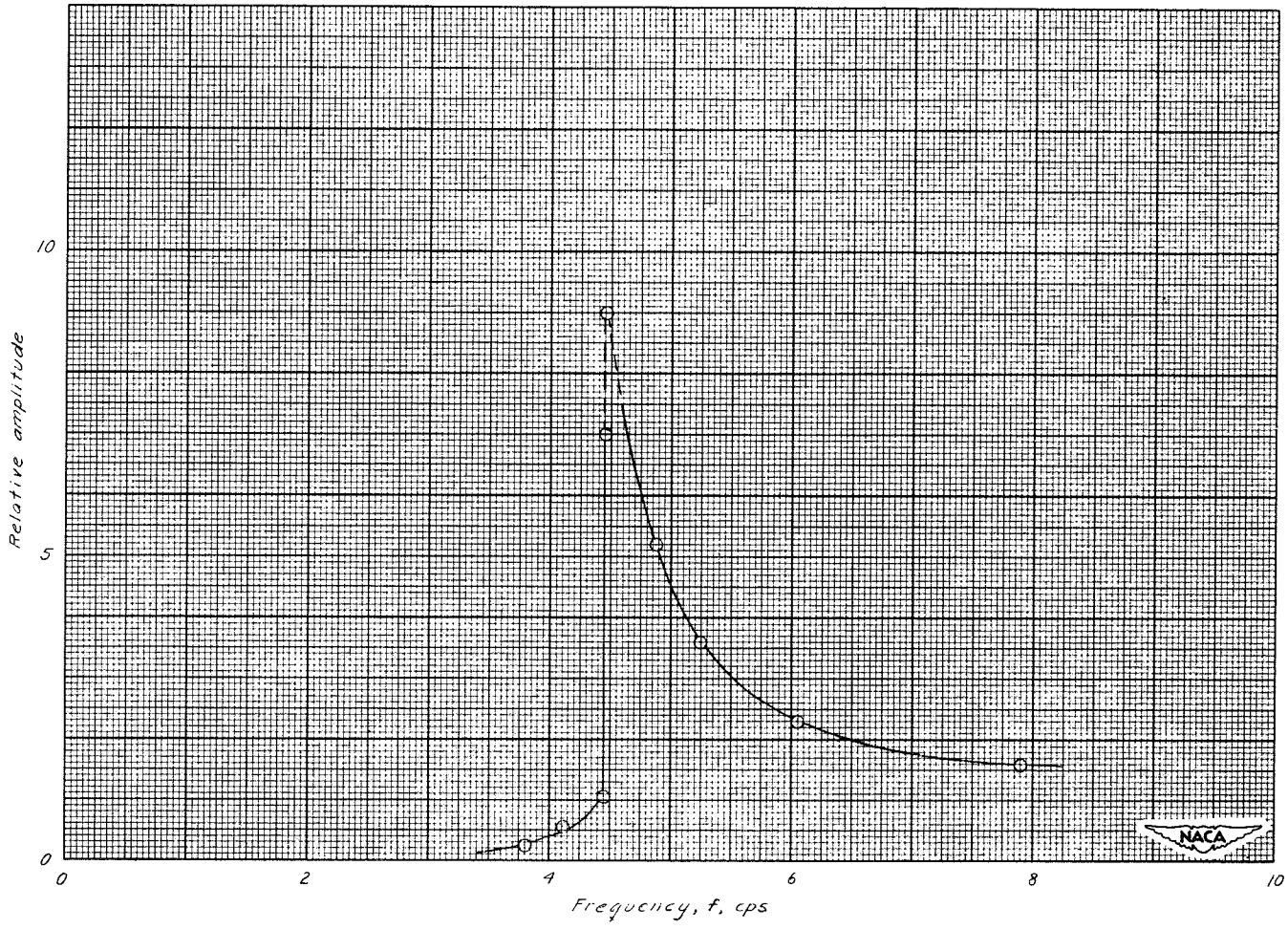

Figure 5.- Response characteristic of roll rate gyro.

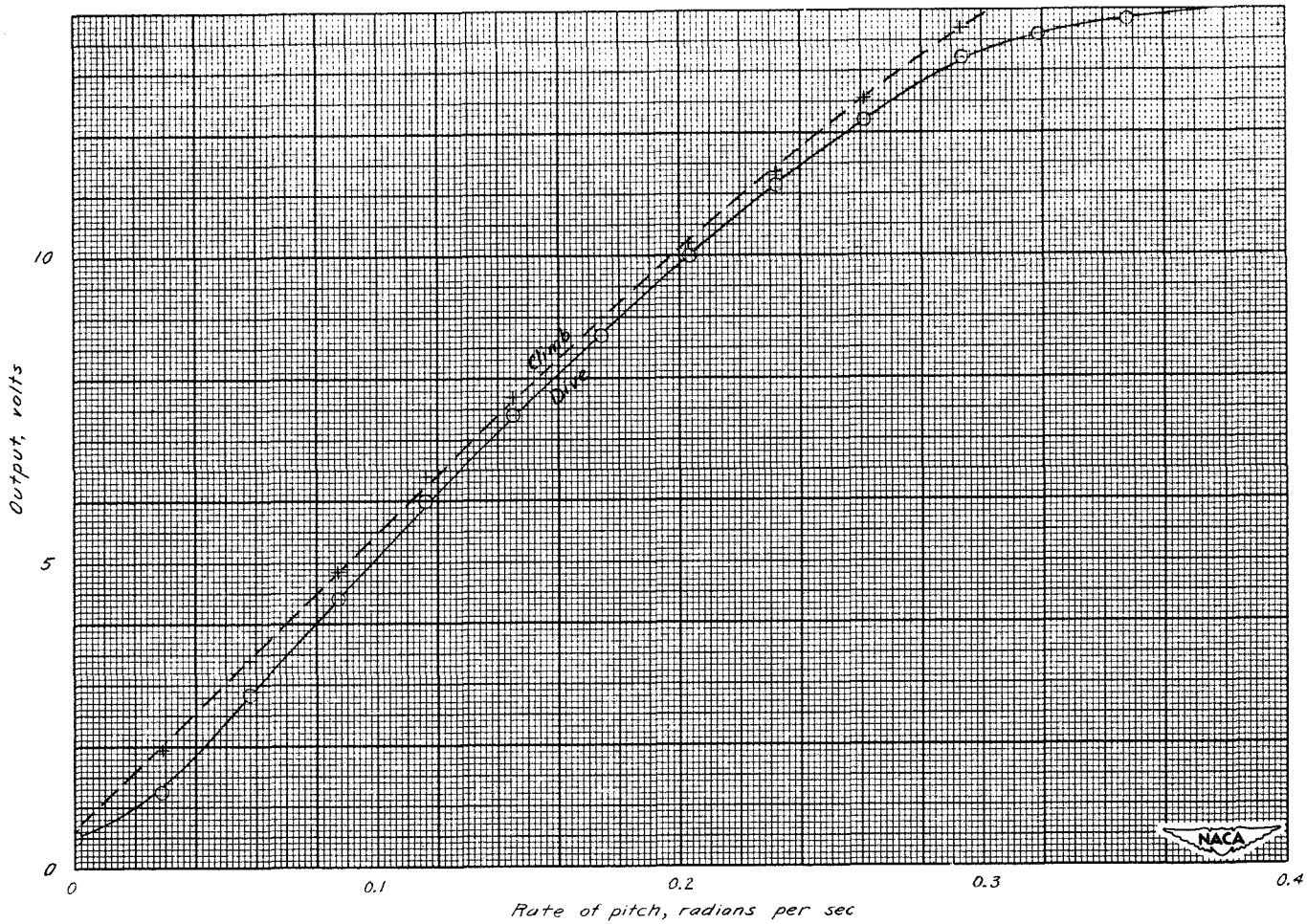

(a) Pitch.

Figure 6.- Calibration of rate gyros.

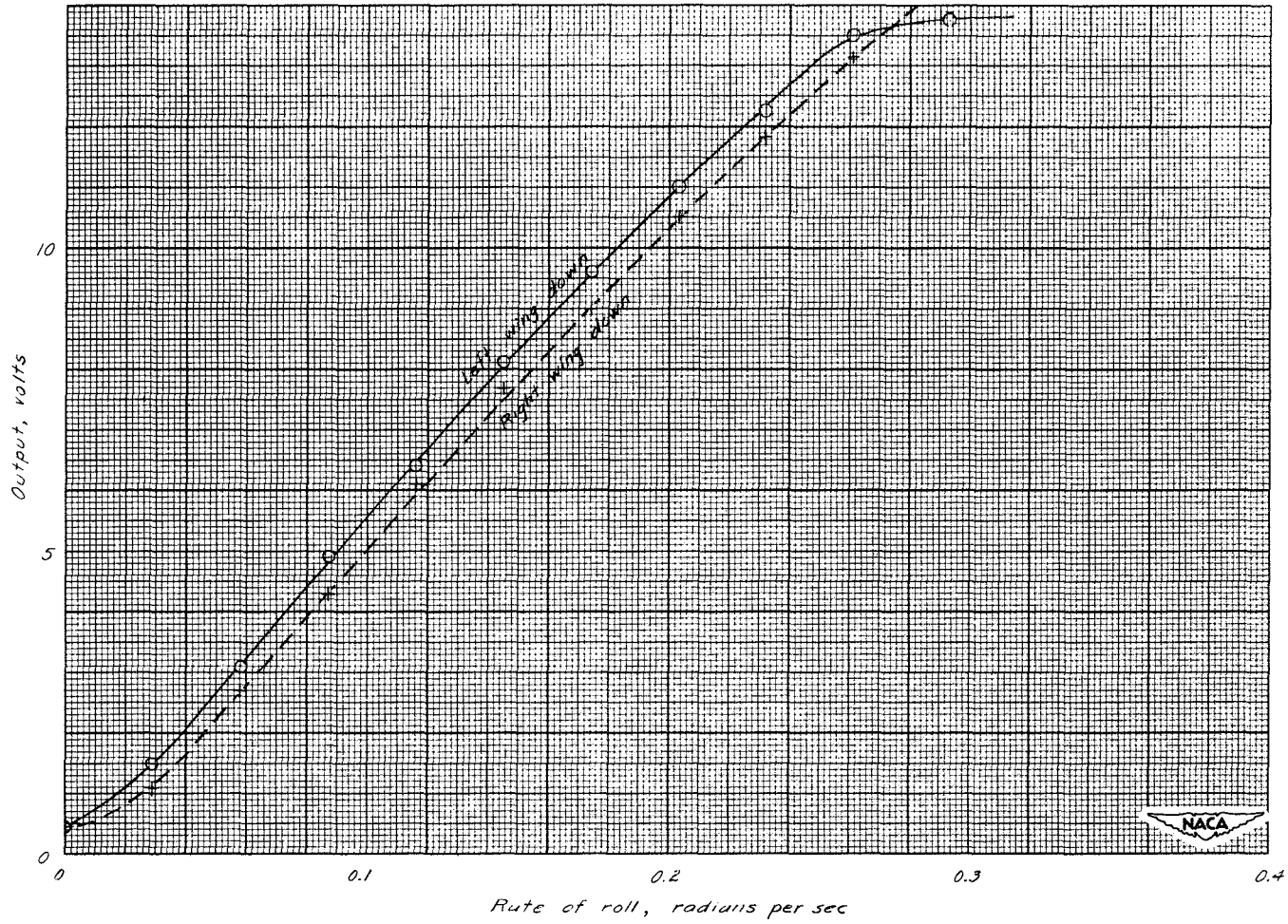

(b) Roll.

Figure 6.– Concluded.

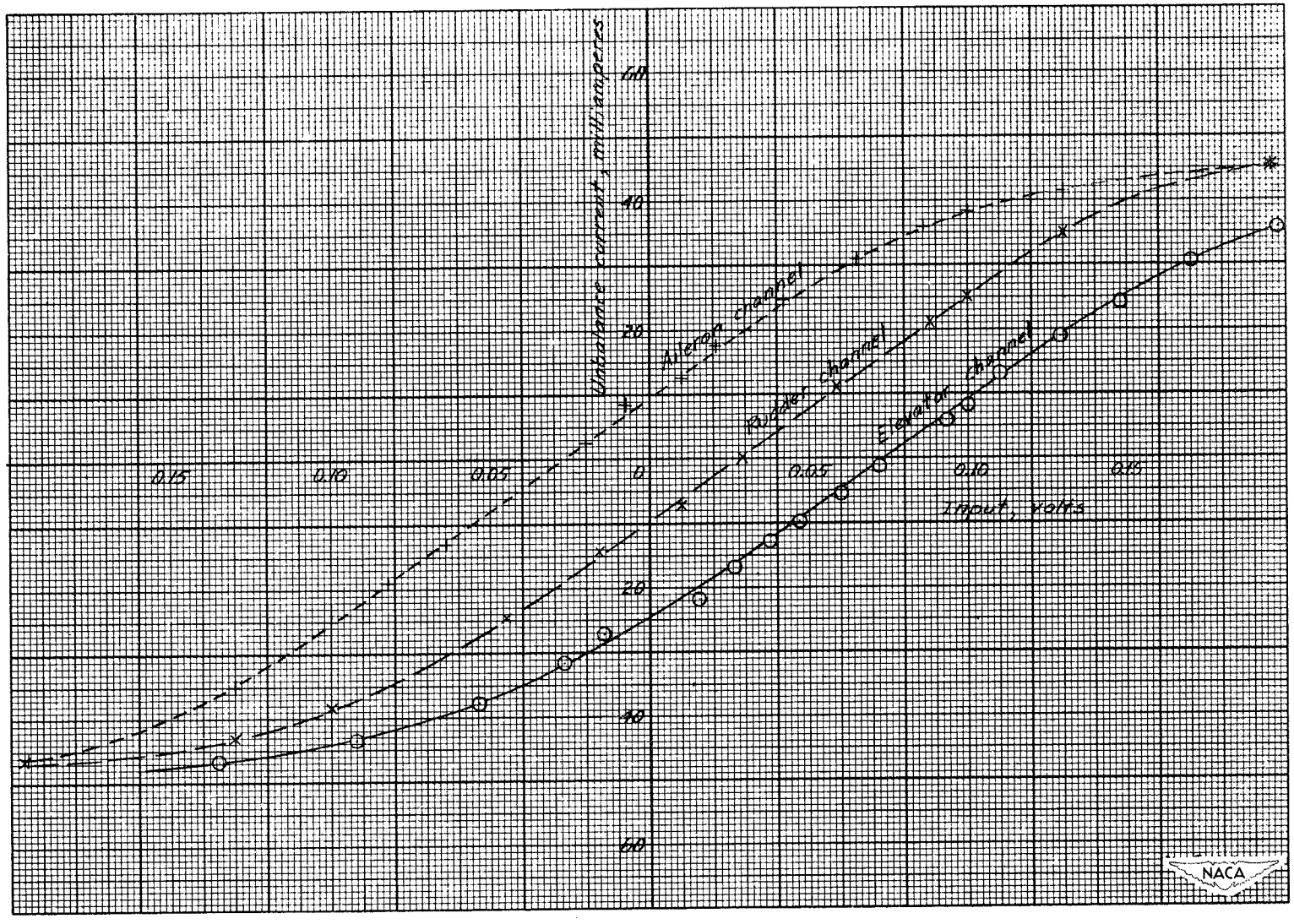

Figure 7.– Amplifier gain characteristics.

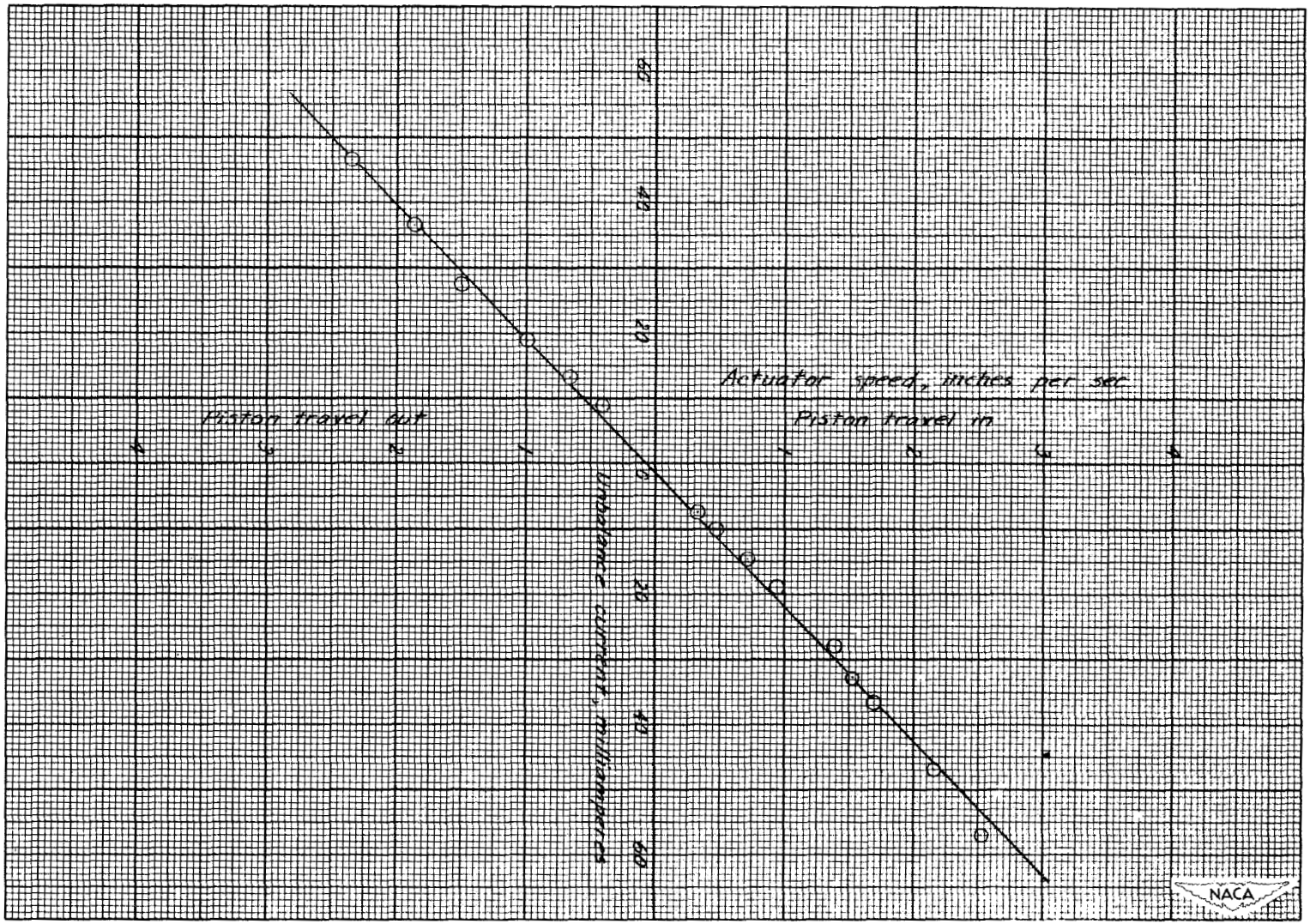

Figure 8.- Valve and servo-actuator gain characteristic.

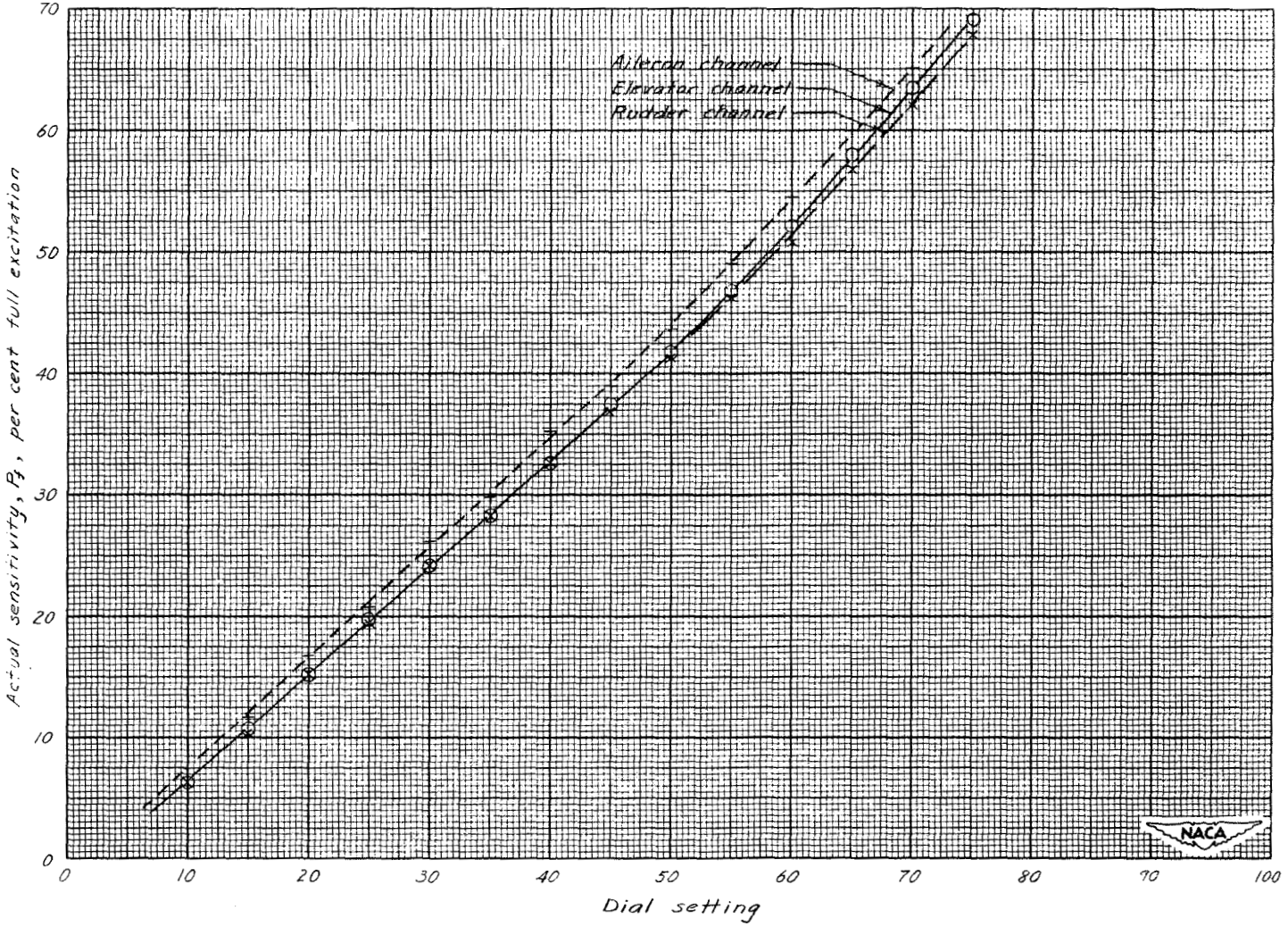

Figure 9.- Calibration of sensitivity potentiometers.

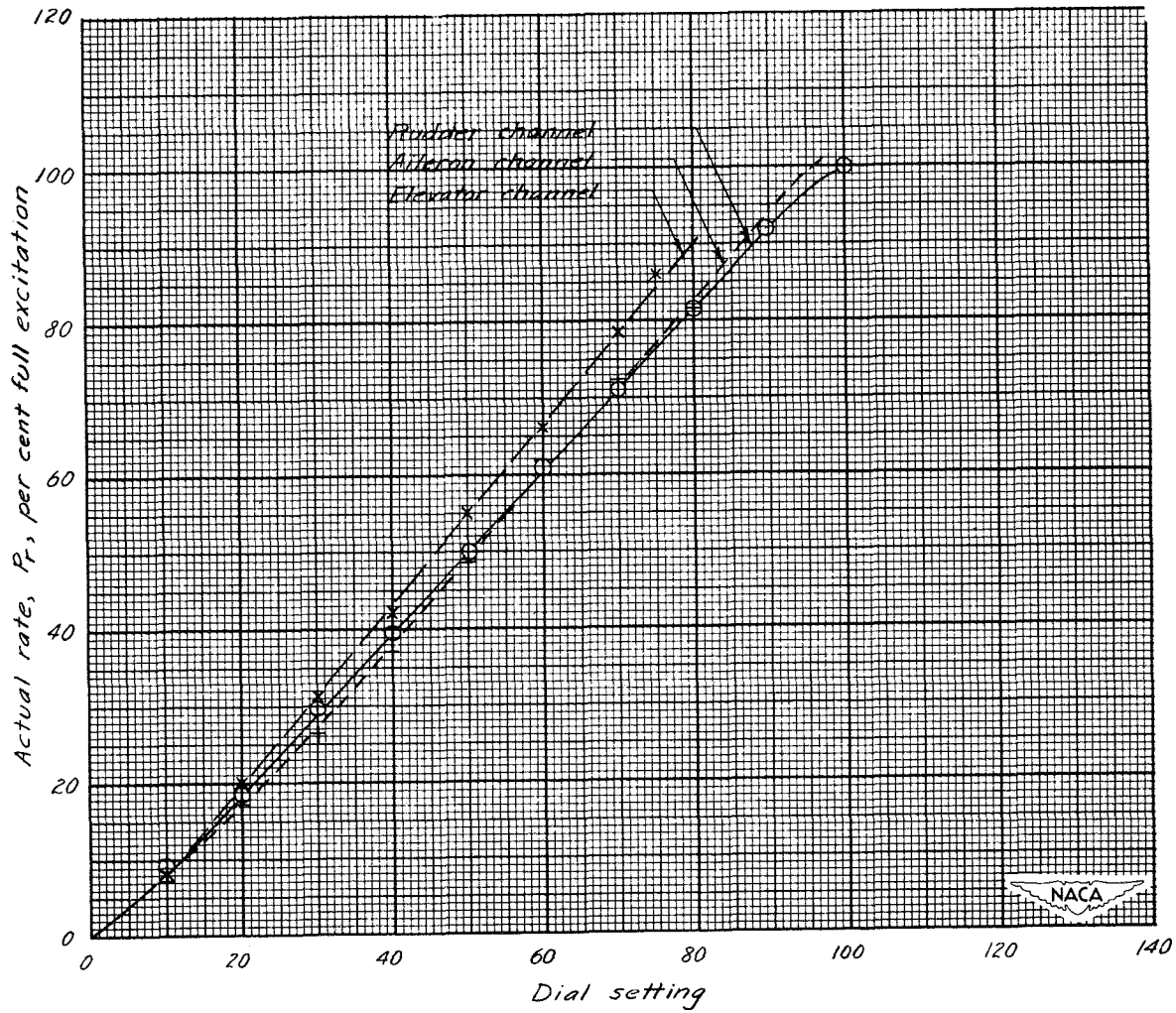

Figure 10.- Calibration of rate potentiometers.

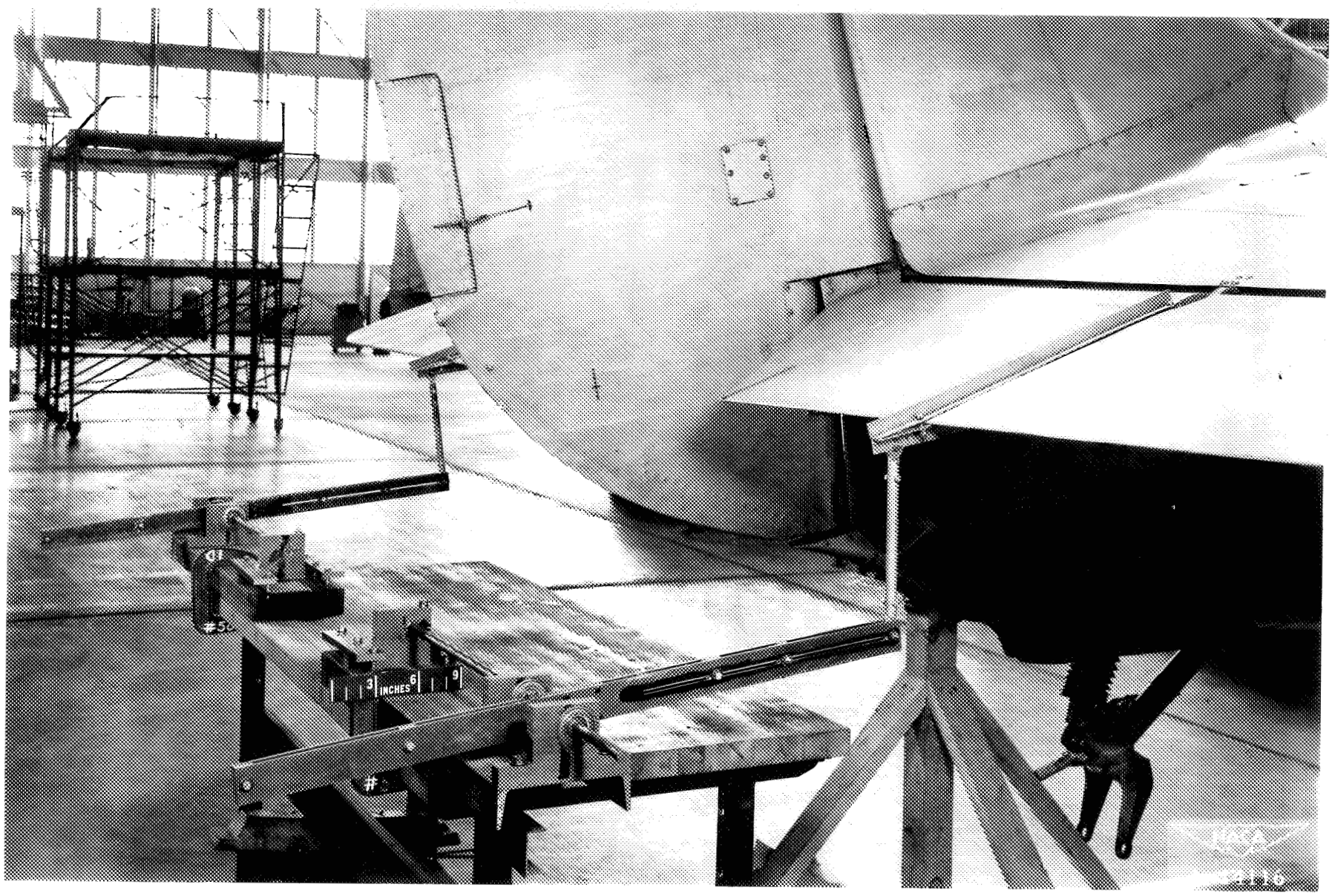

Figure 11.- Surface hinge-moment simulator.

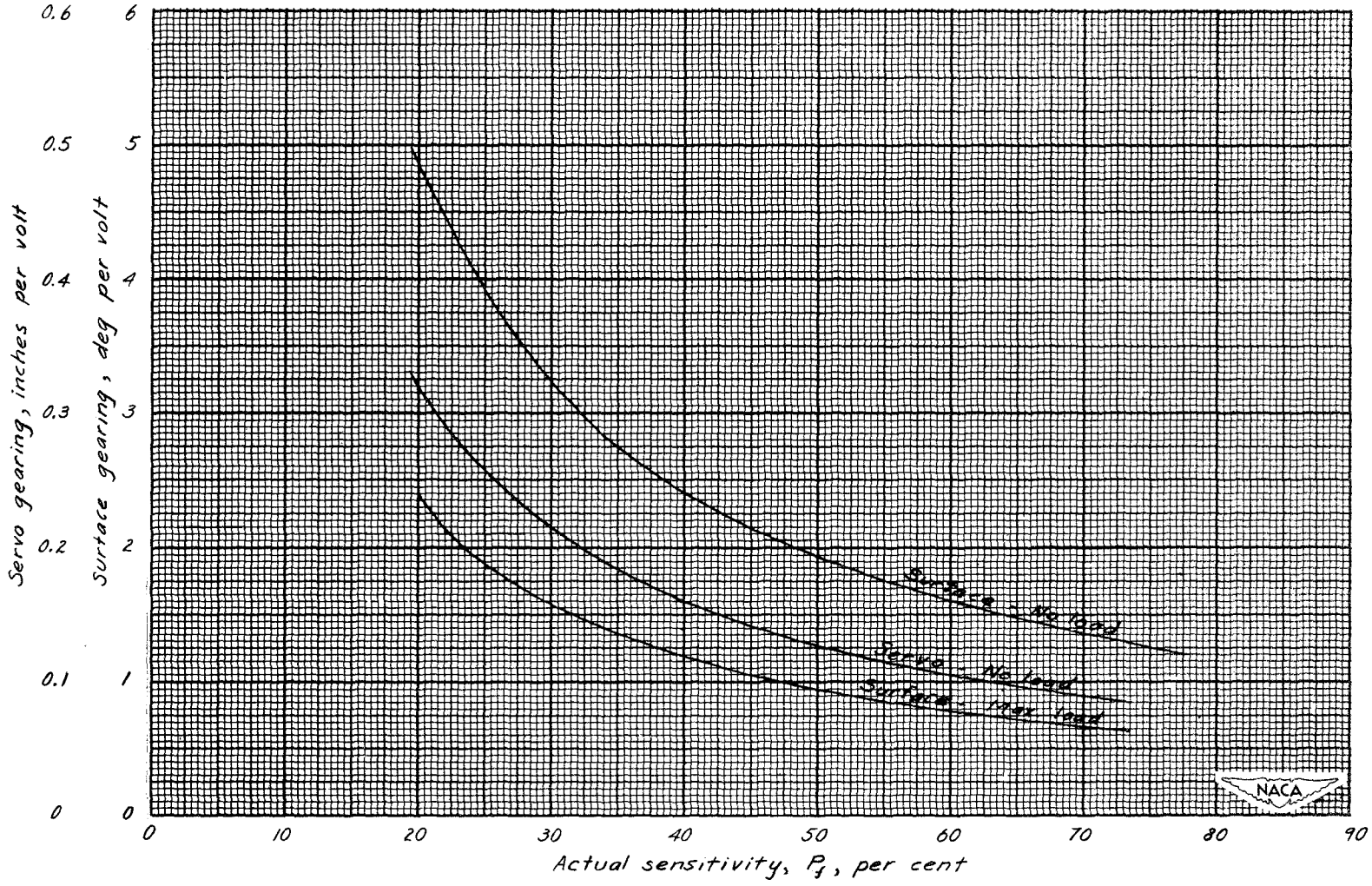

(a) Elevator channel.

Figure 12.– Autopilot gearing characteristics.

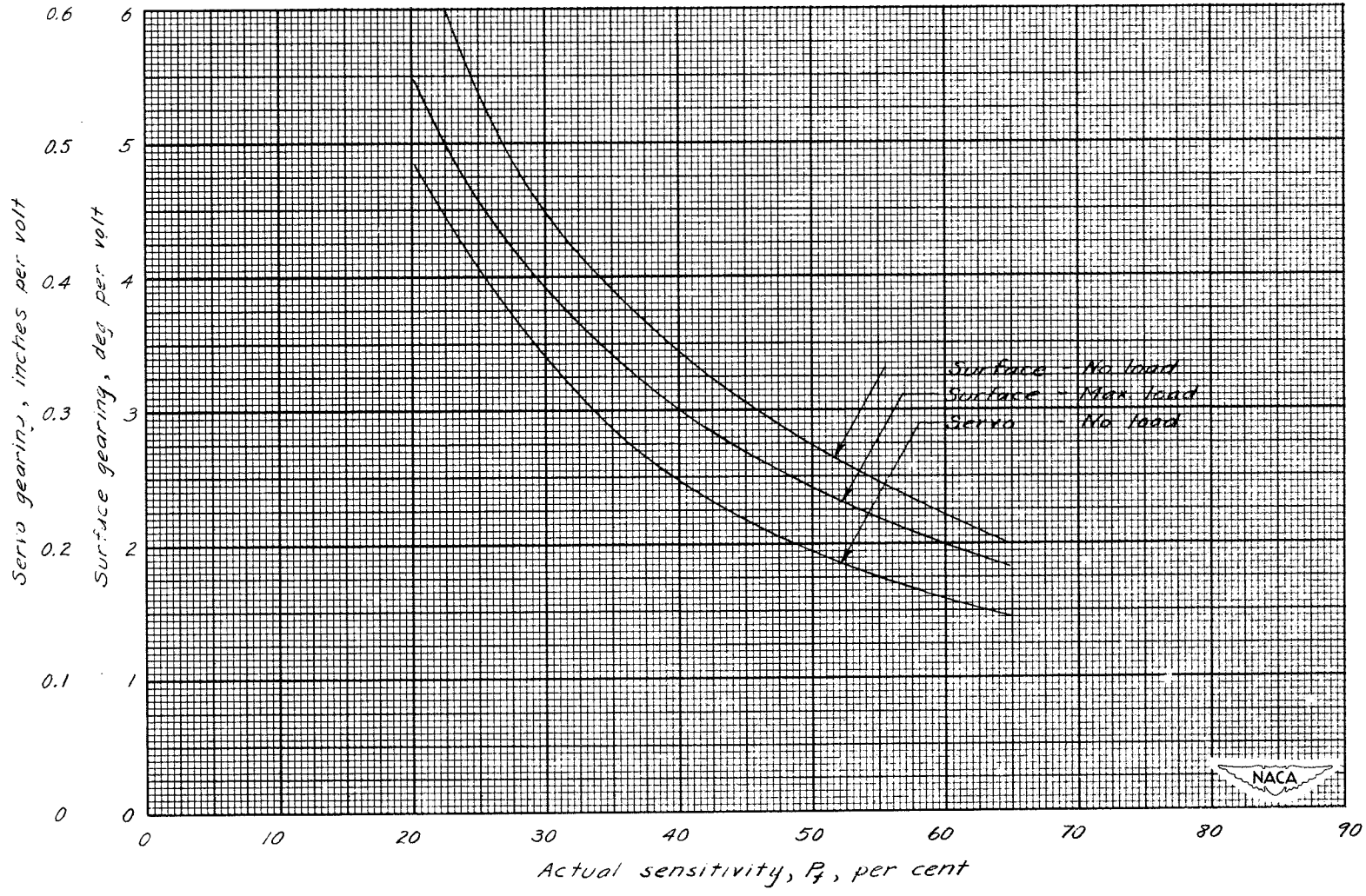

(b) Aileron channel.

Figure 12.- Continued.

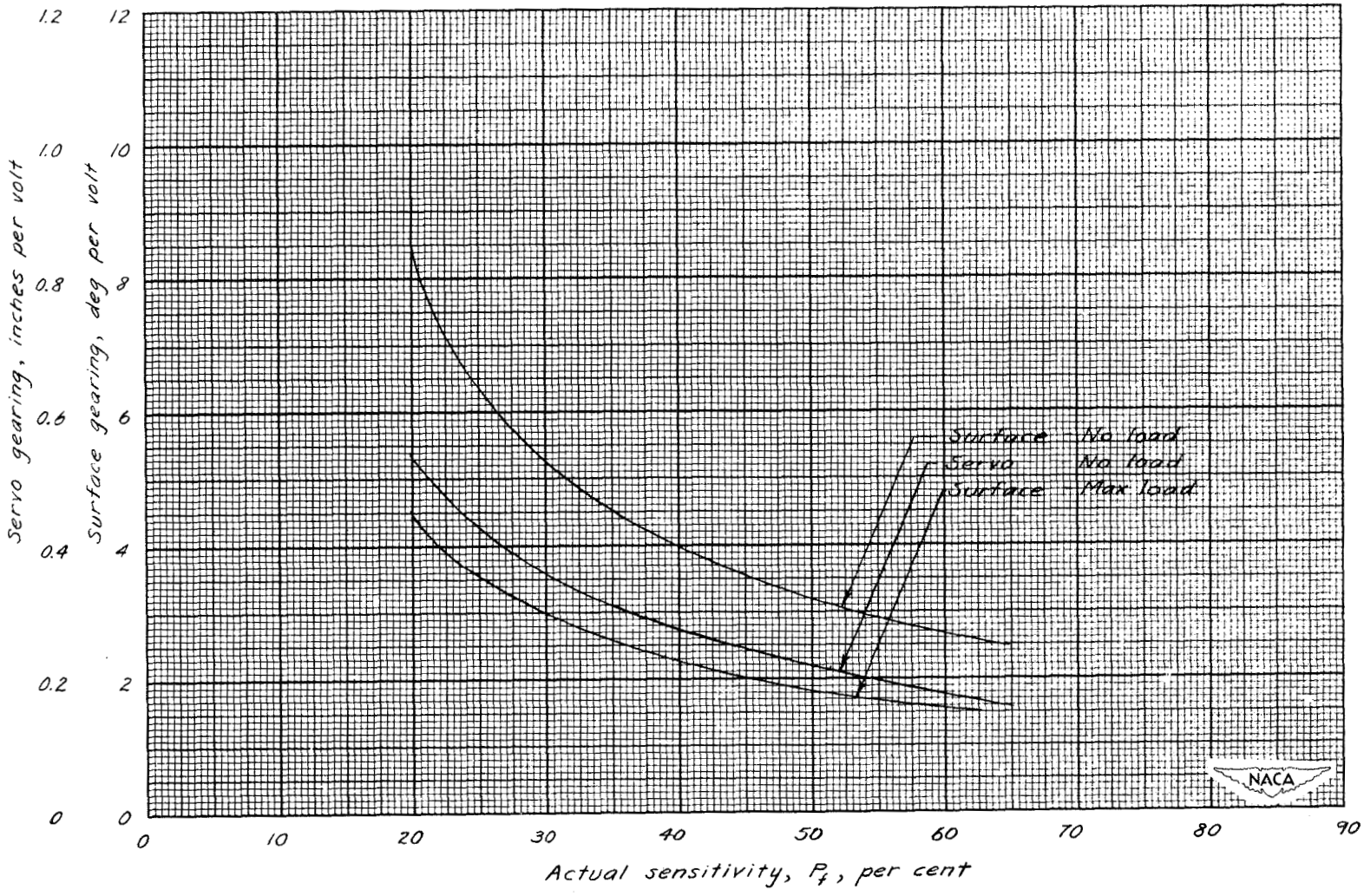

(c) Rudder channel.

Figure 12.- Concluded.

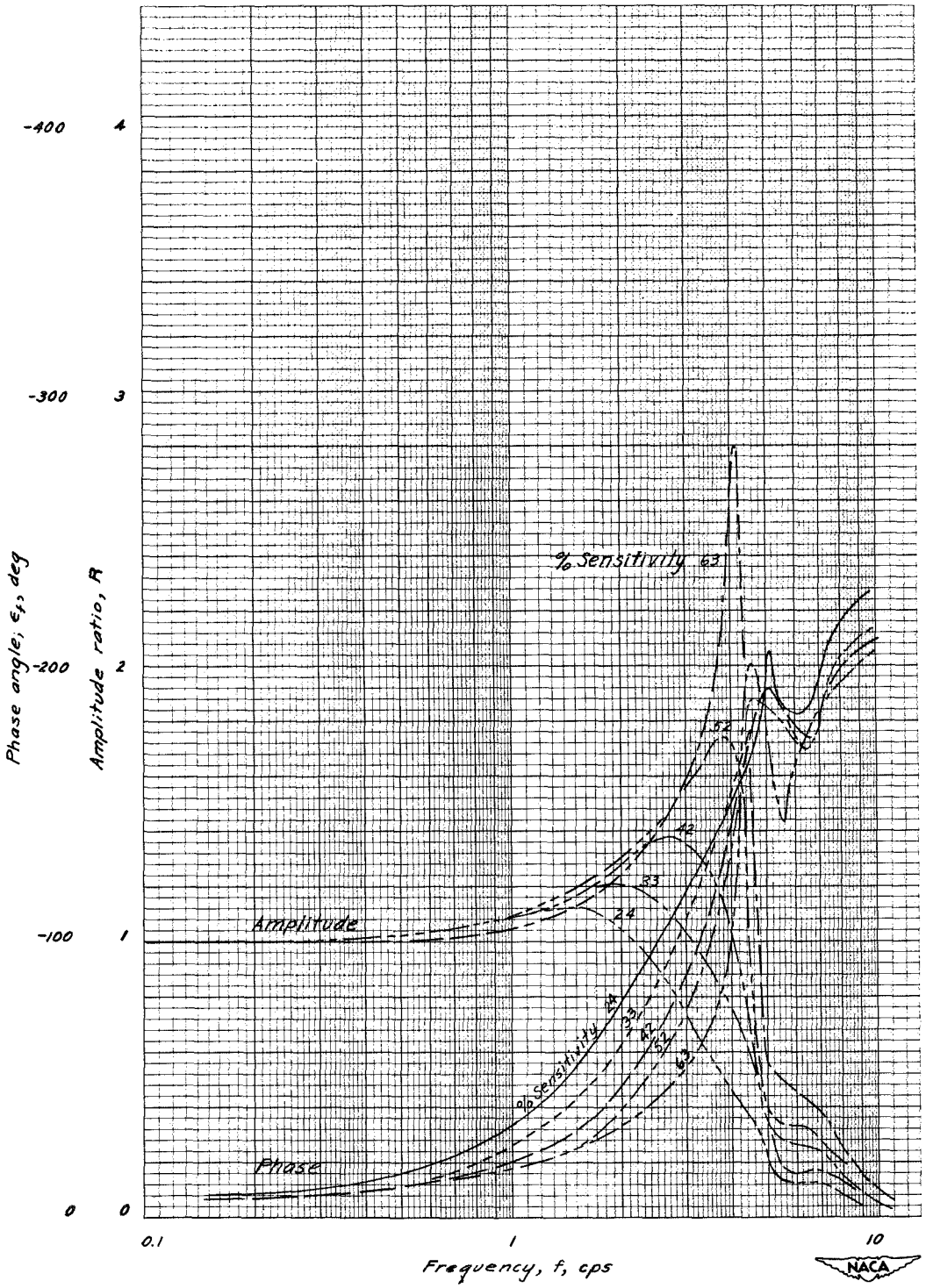

(a) Servo response.

Figure 13.- Effect of sensitivity on elevator-channel frequency response; no load; ±0.115 volt (≈±1/4°) input.

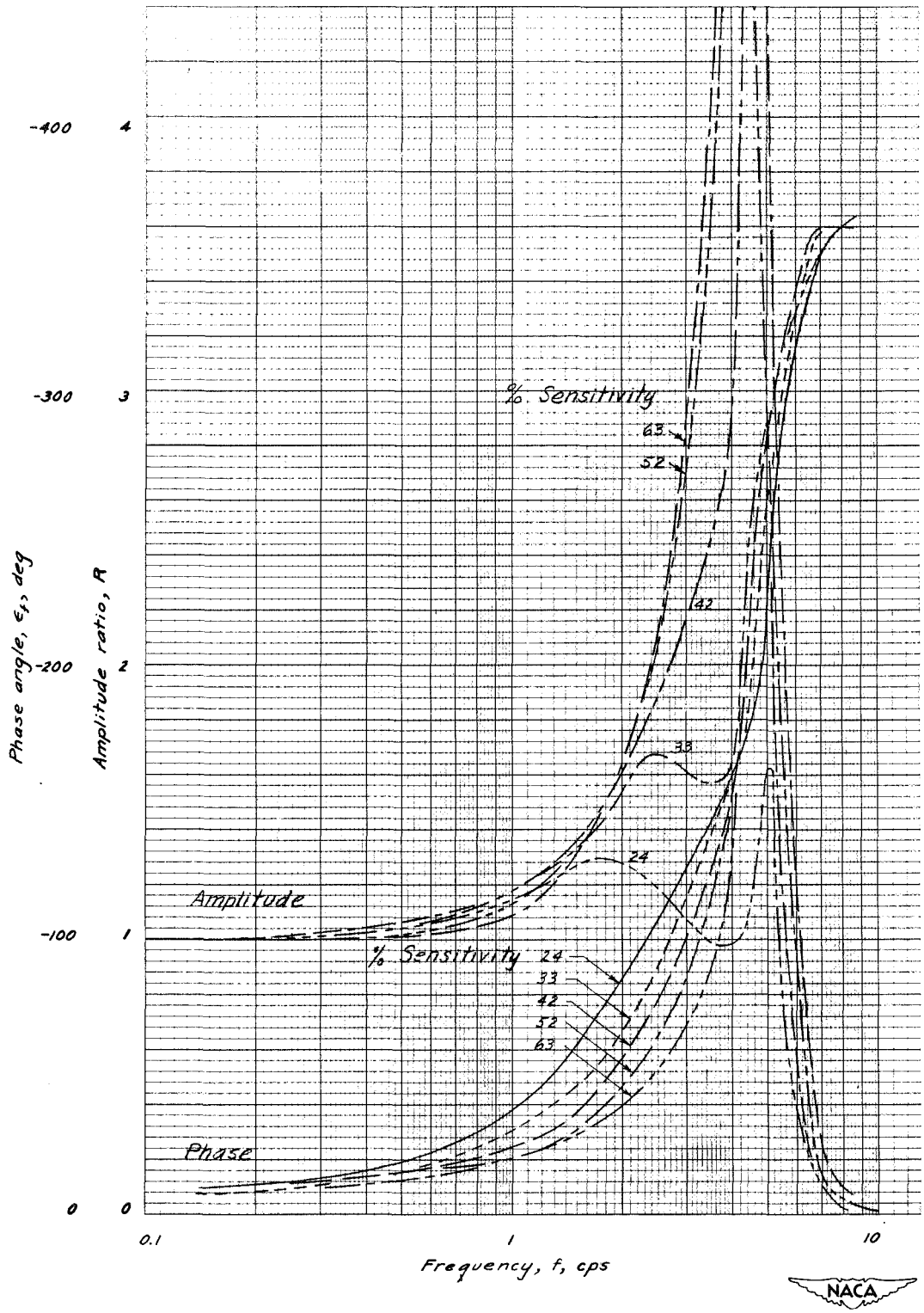

(b) Surface response.

Figure 13.– Concluded.

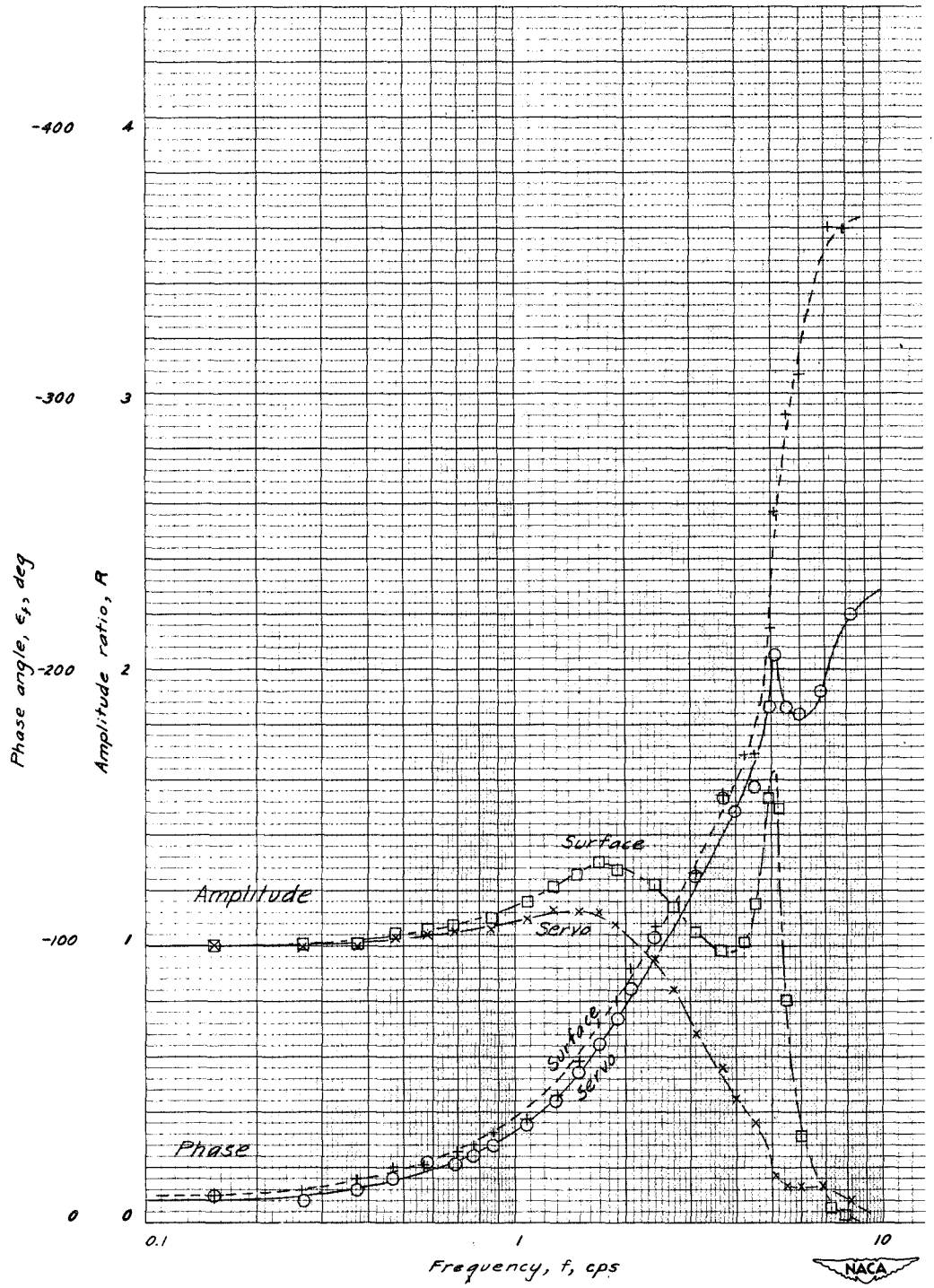

(a) Sensitivity, 24 percent.

Figure 14.– Effect of elevator linkage system on elevator–channel frequency response for various sensitivities; no load; ±0.115 volt ($\approx \pm 1/4^{\circ}$) input.

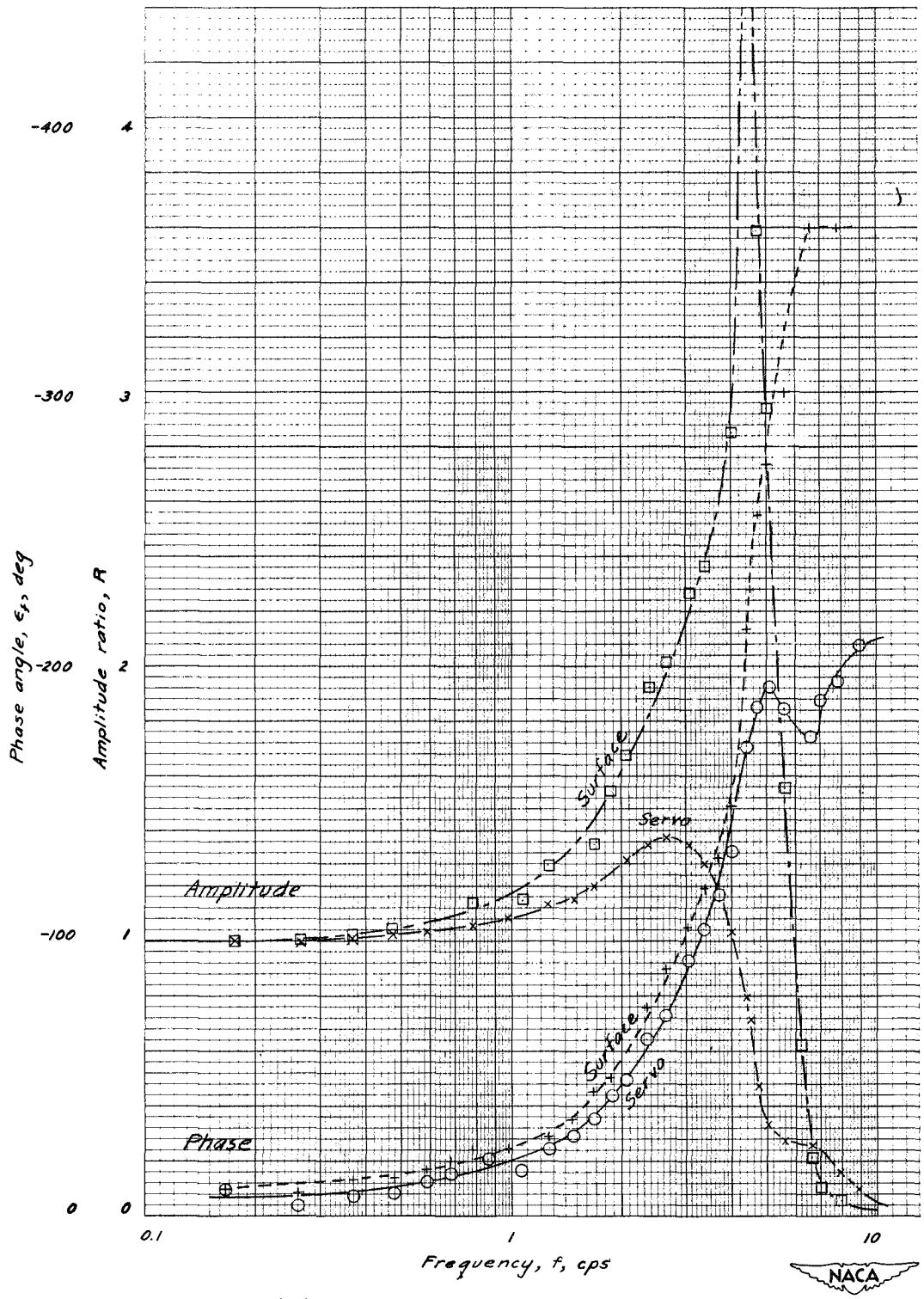

(b) Sensitivity, 42 percent.

Figure 14.- Continued.

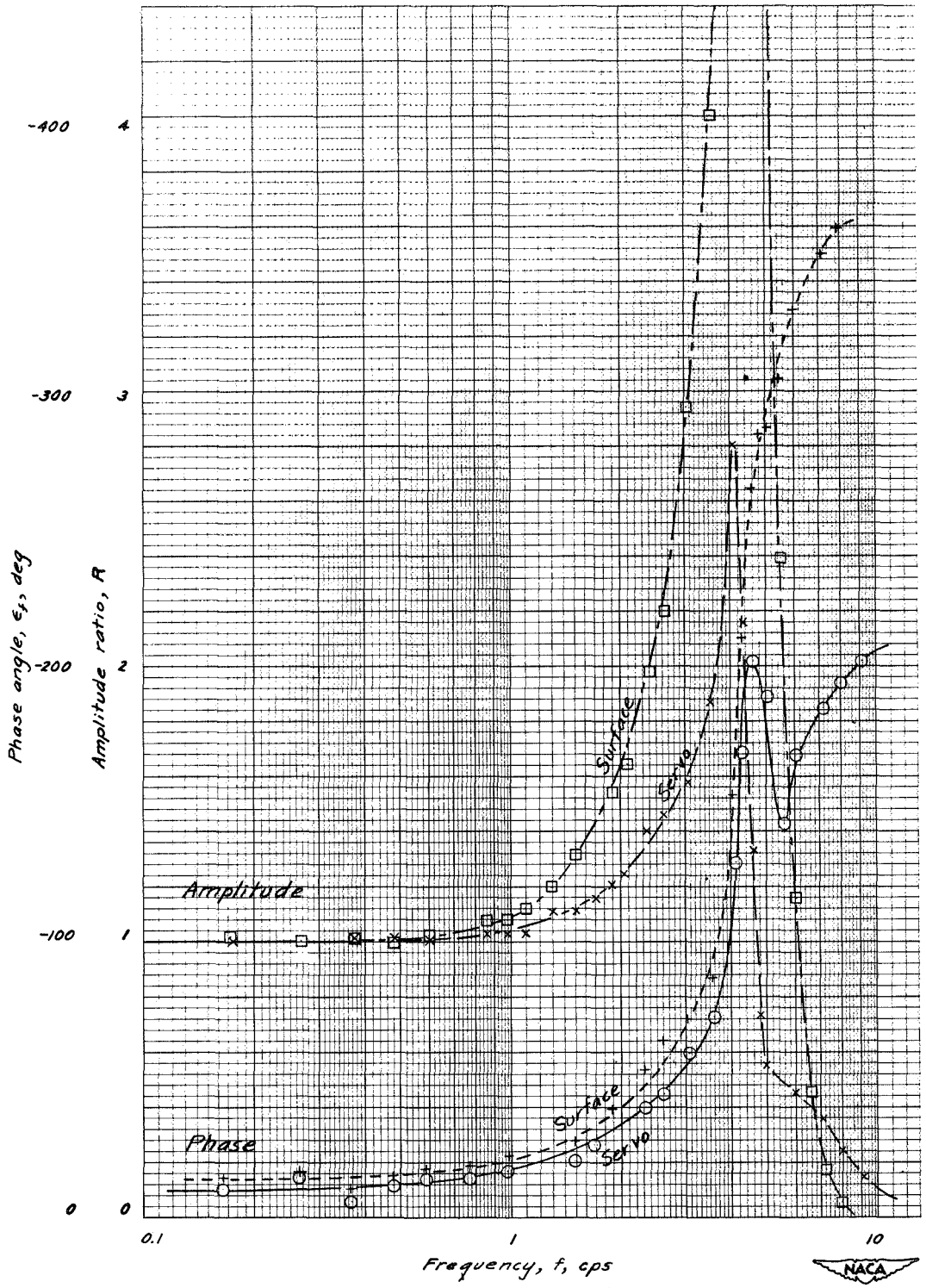

(c) Sensitivity, 63 percent.

Figure 14.- Concluded.

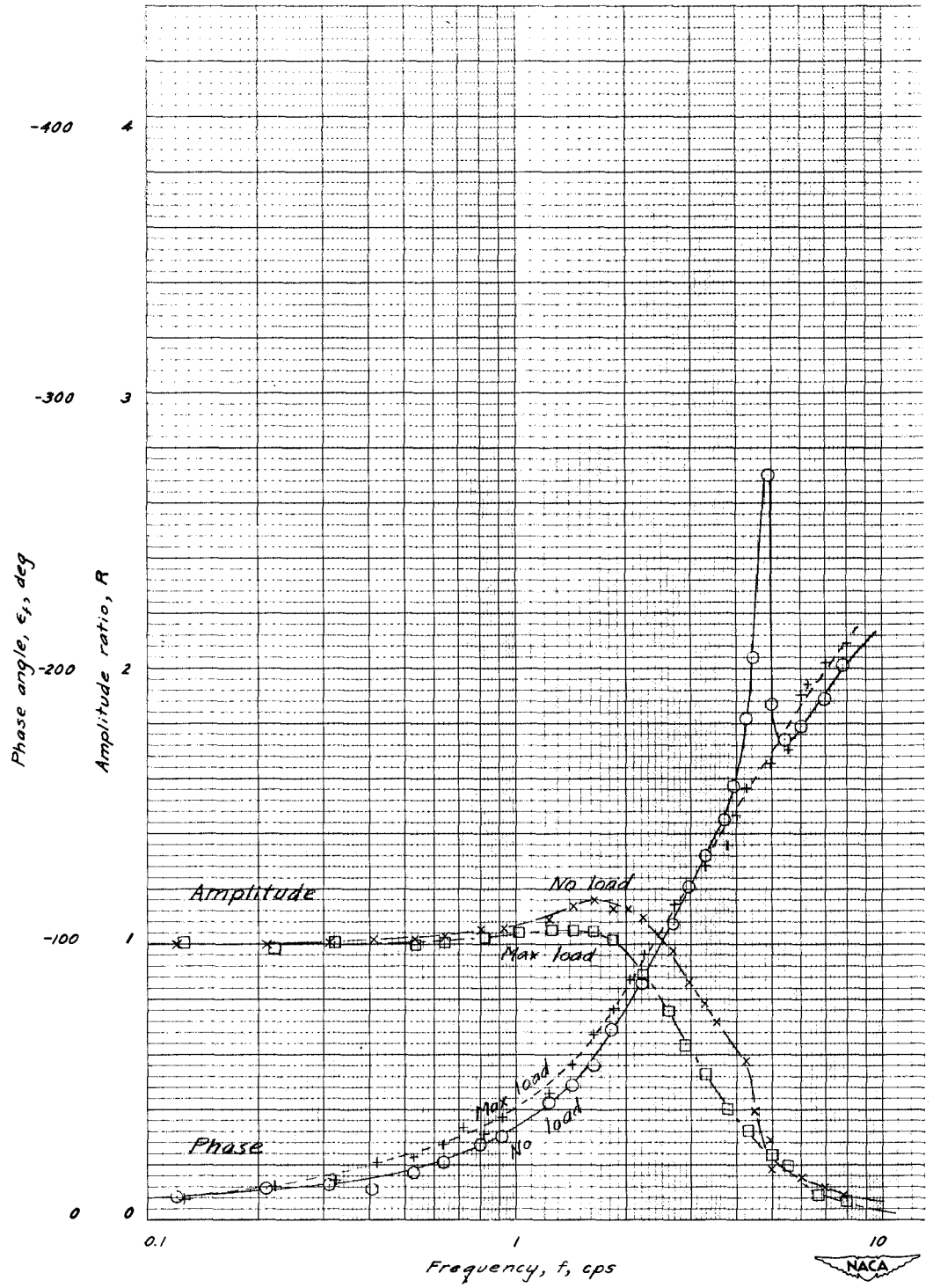

(a) Sensitivity, 24 percent; servo response.

Figure 15.- Effect of load on elevator-channel frequency response; ±0.115 volt (≈±1/4°) input.

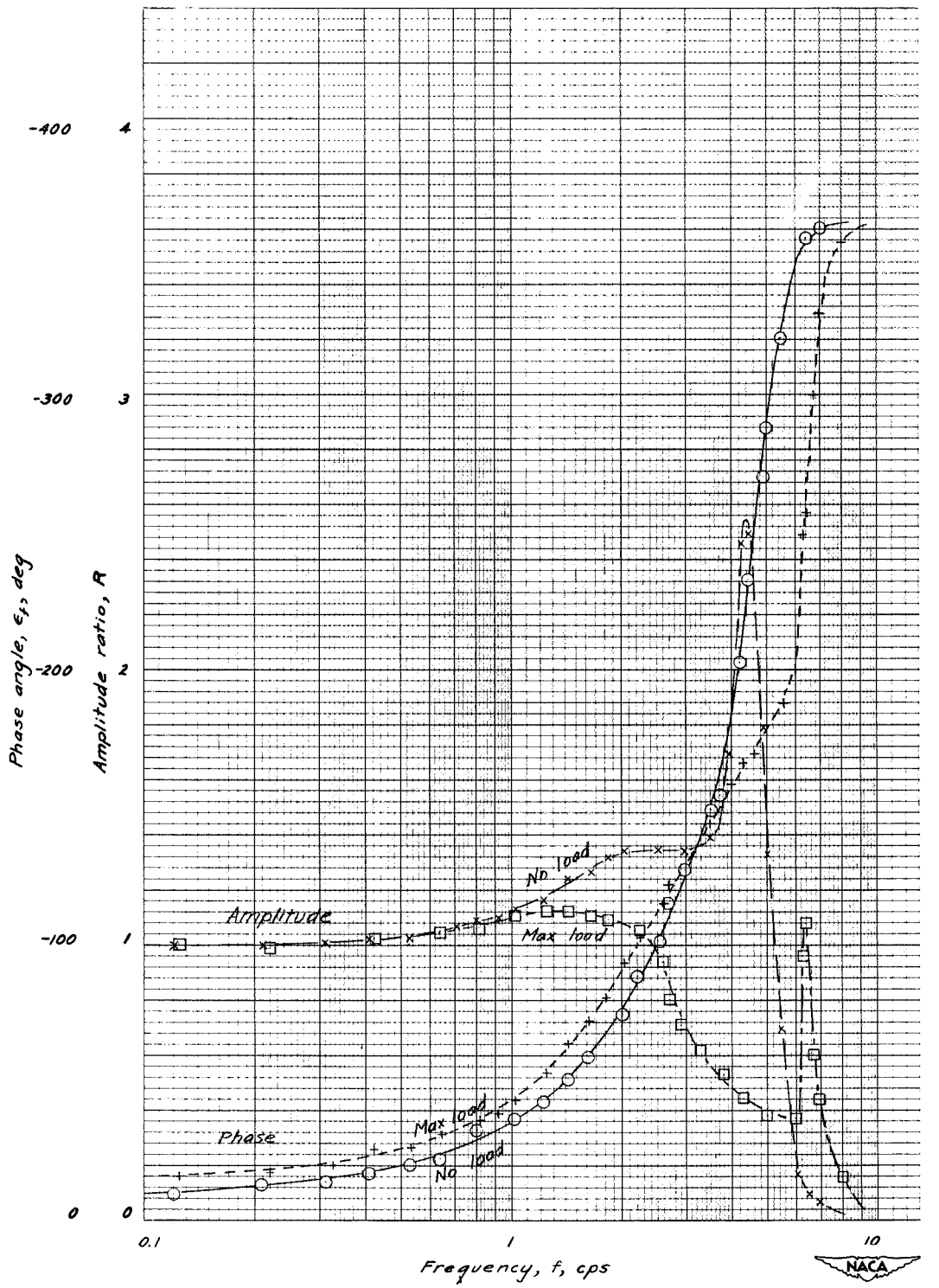

(b) Sensitivity, 24 percent; surface response.

Figure 15.- Continued.

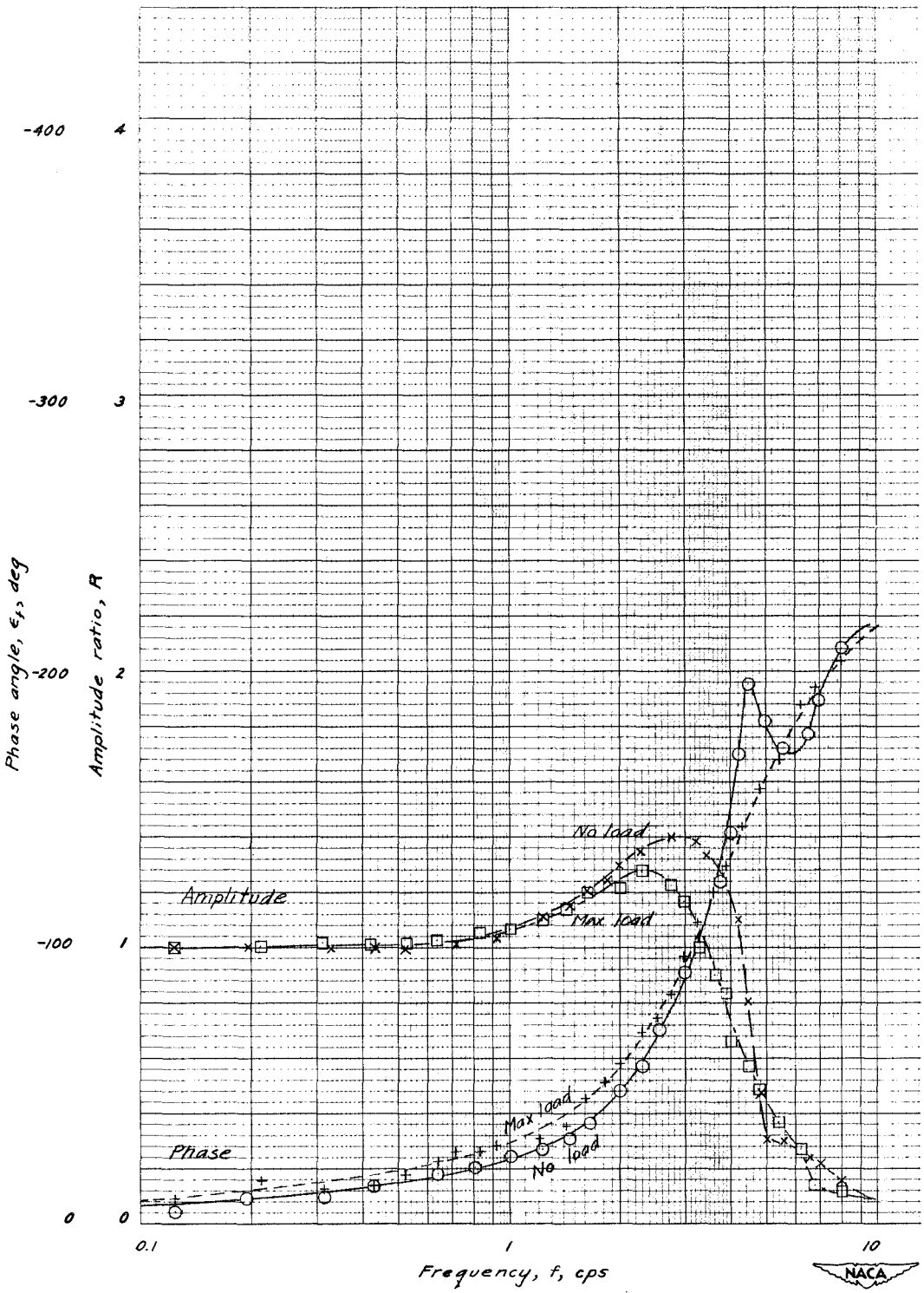

(c) Sensitivity, 42 percent; servo response.

Figure 15.- Continued.

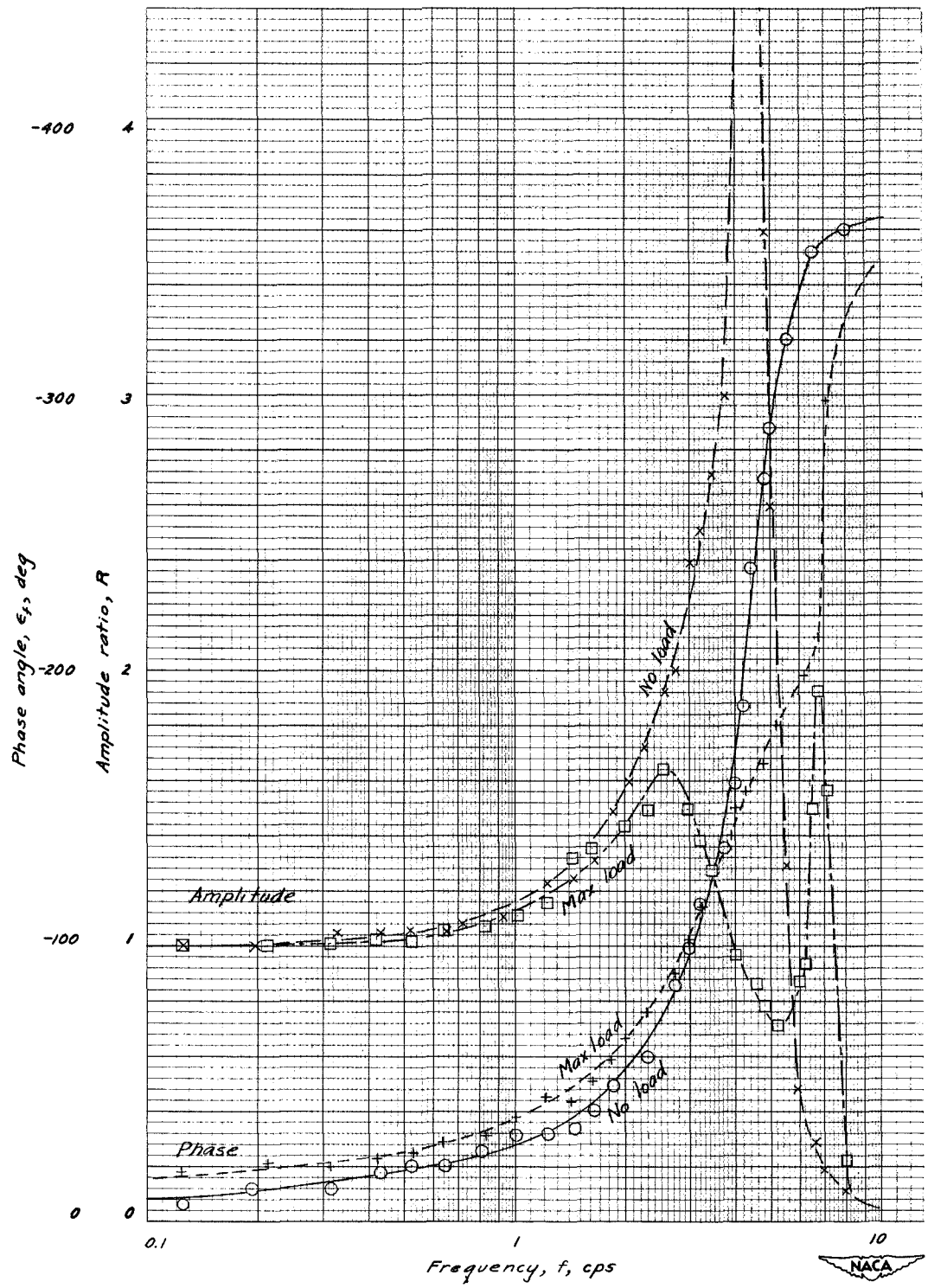

(d) Sensitivity, 42 percent; surface response.

Figure 15.- Concluded.

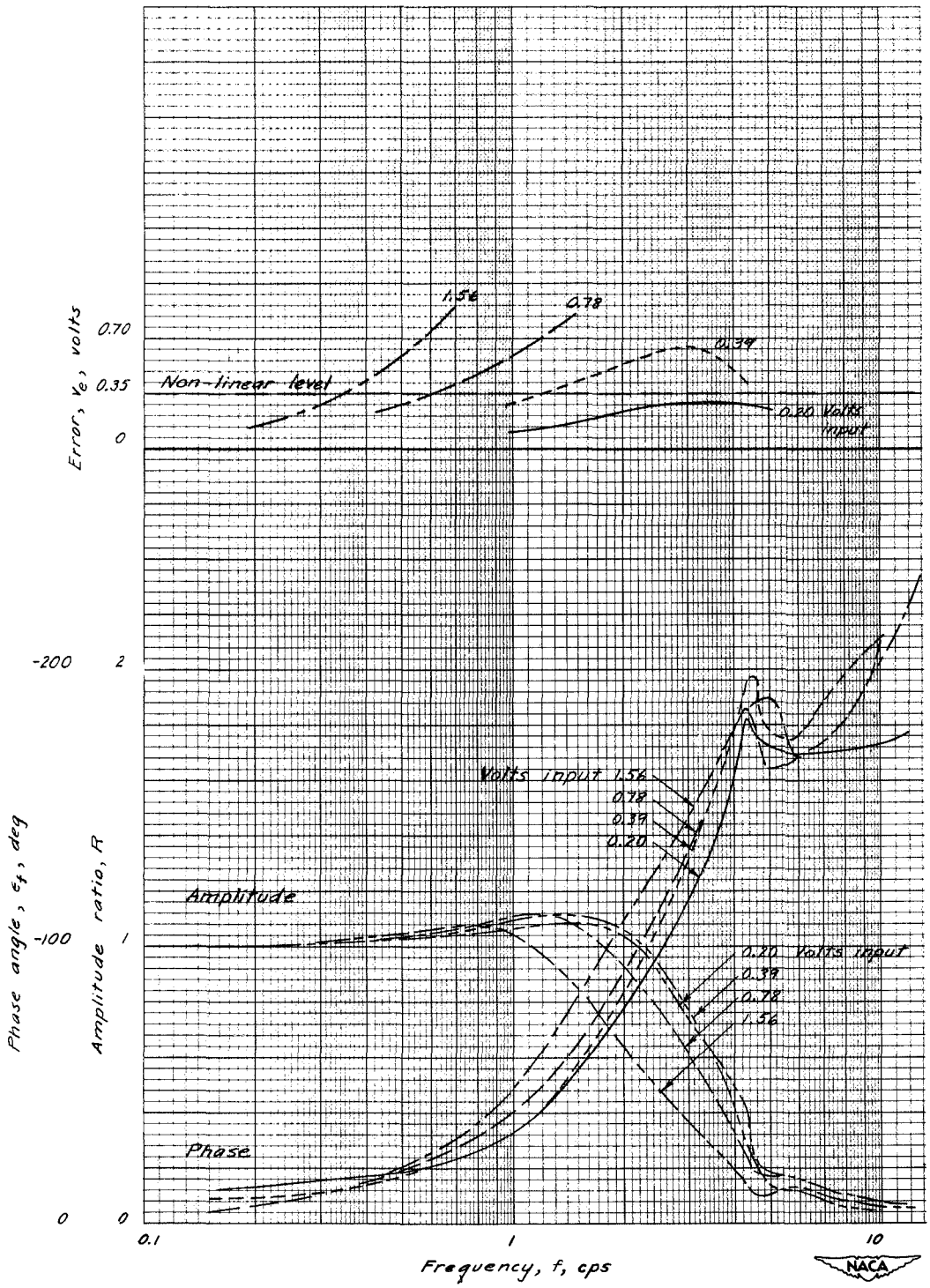

(a) Servo response; no load; sensitivity, 26 percent.

Figure 16.- Effect of input signal amplitude on elevator-channel frequency response.

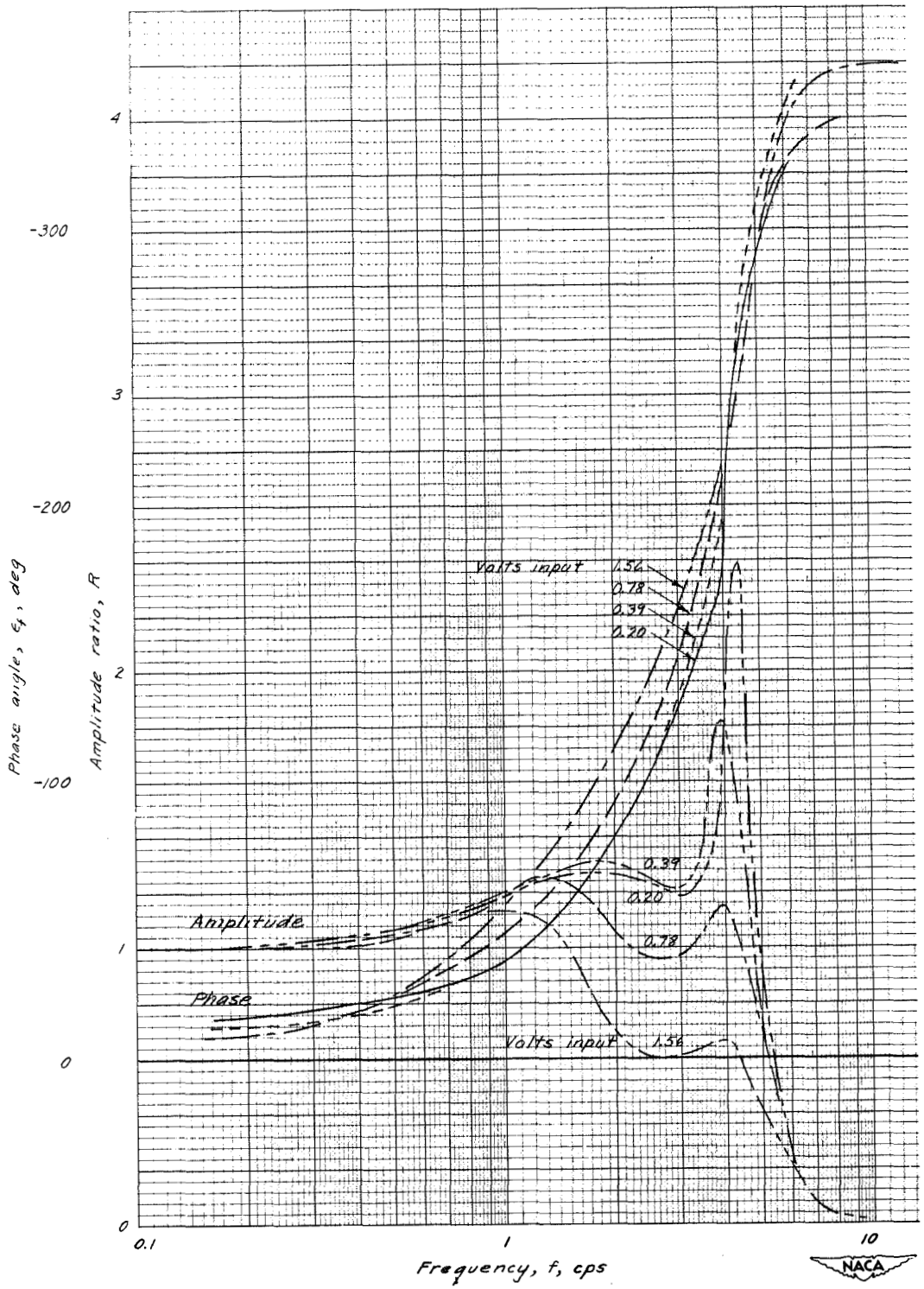

(b) Surface response; no load; sensitivity, 26 percent.

Figure 16.- Continued.

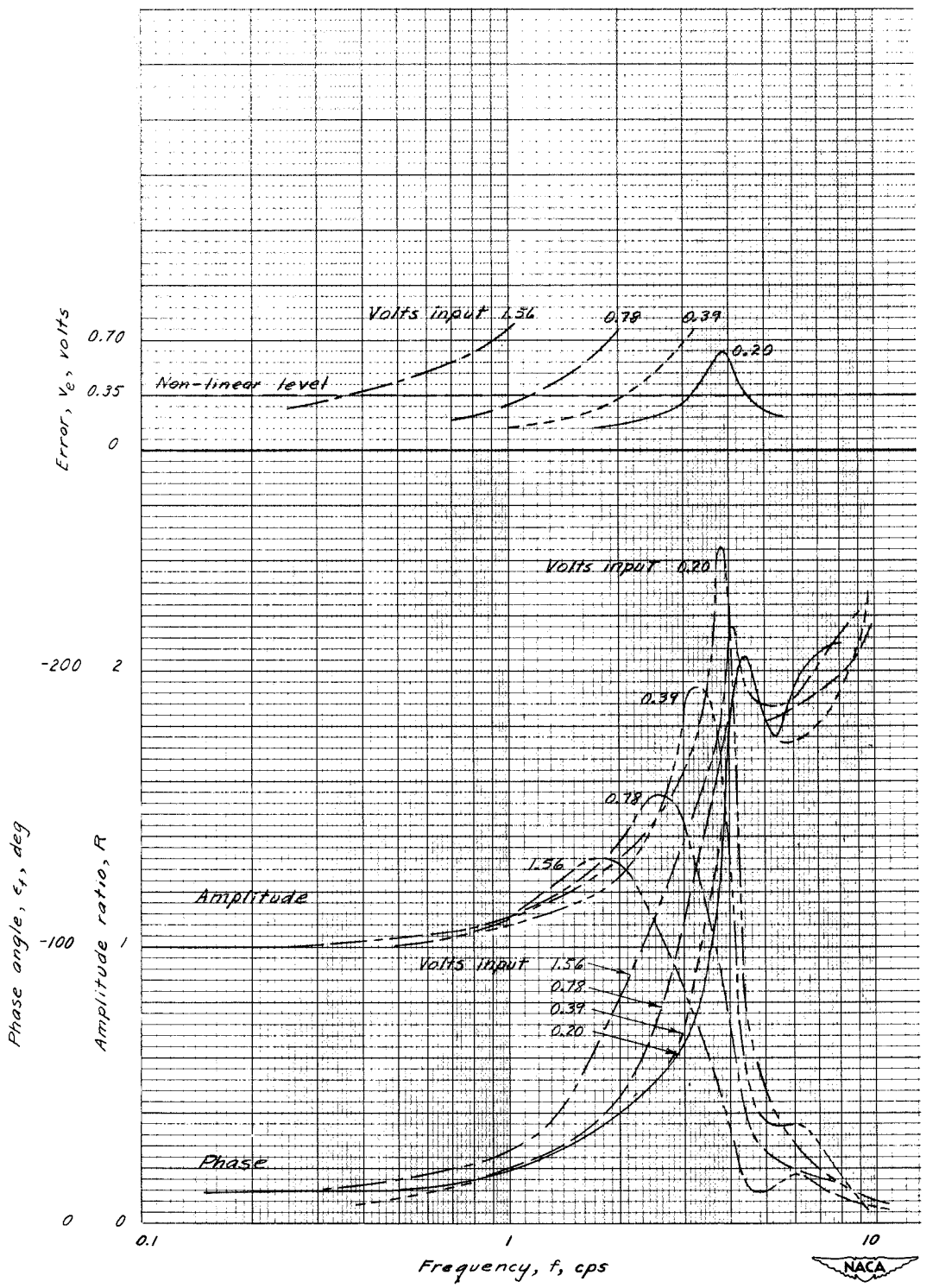

(c) Servo response; no load; sensitivity, 56 percent.

Figure 16.- Continued.

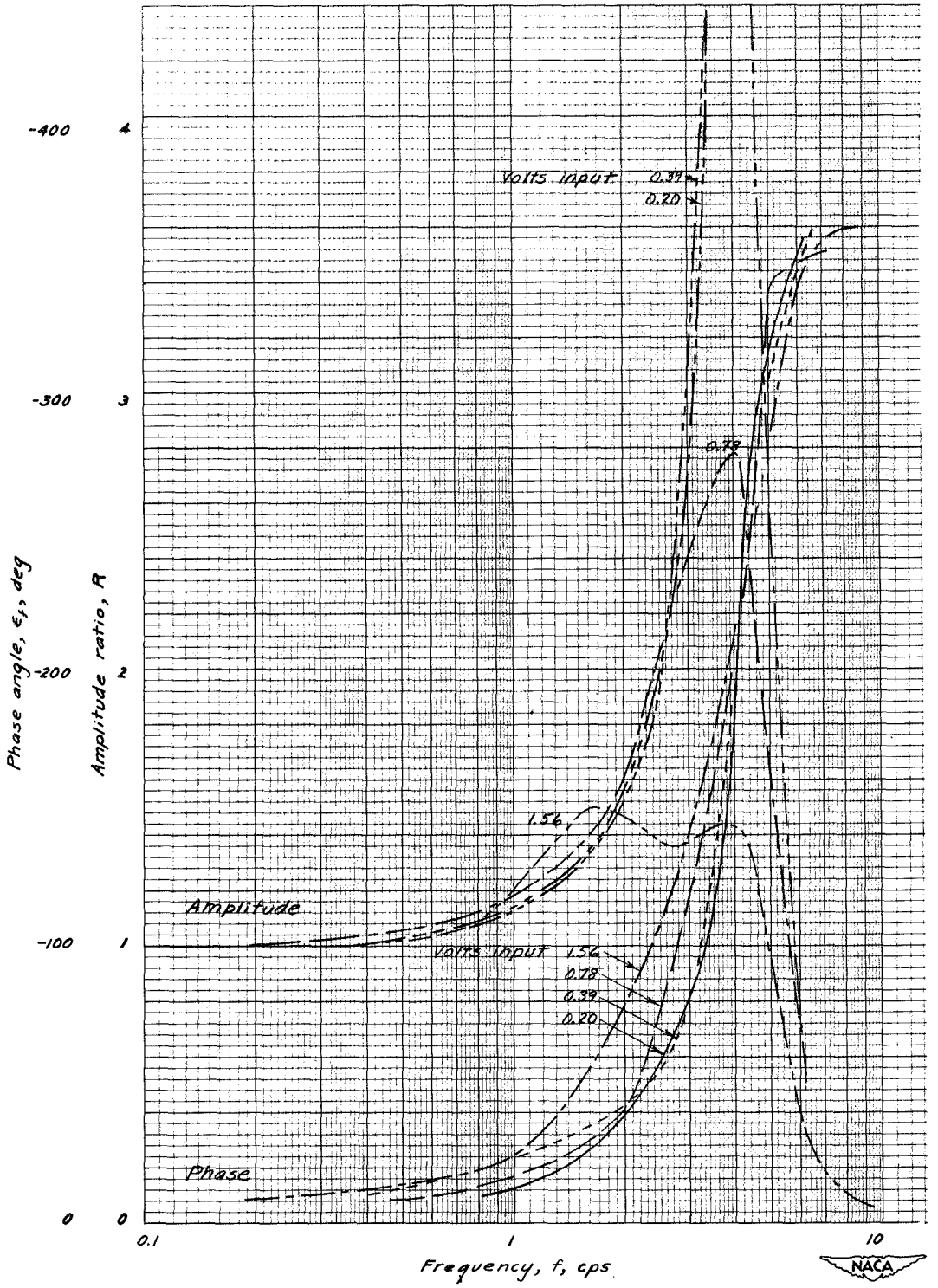

(d) Surface response; no load; sensitivity, 56 percent.

Figure 16.– Continued.

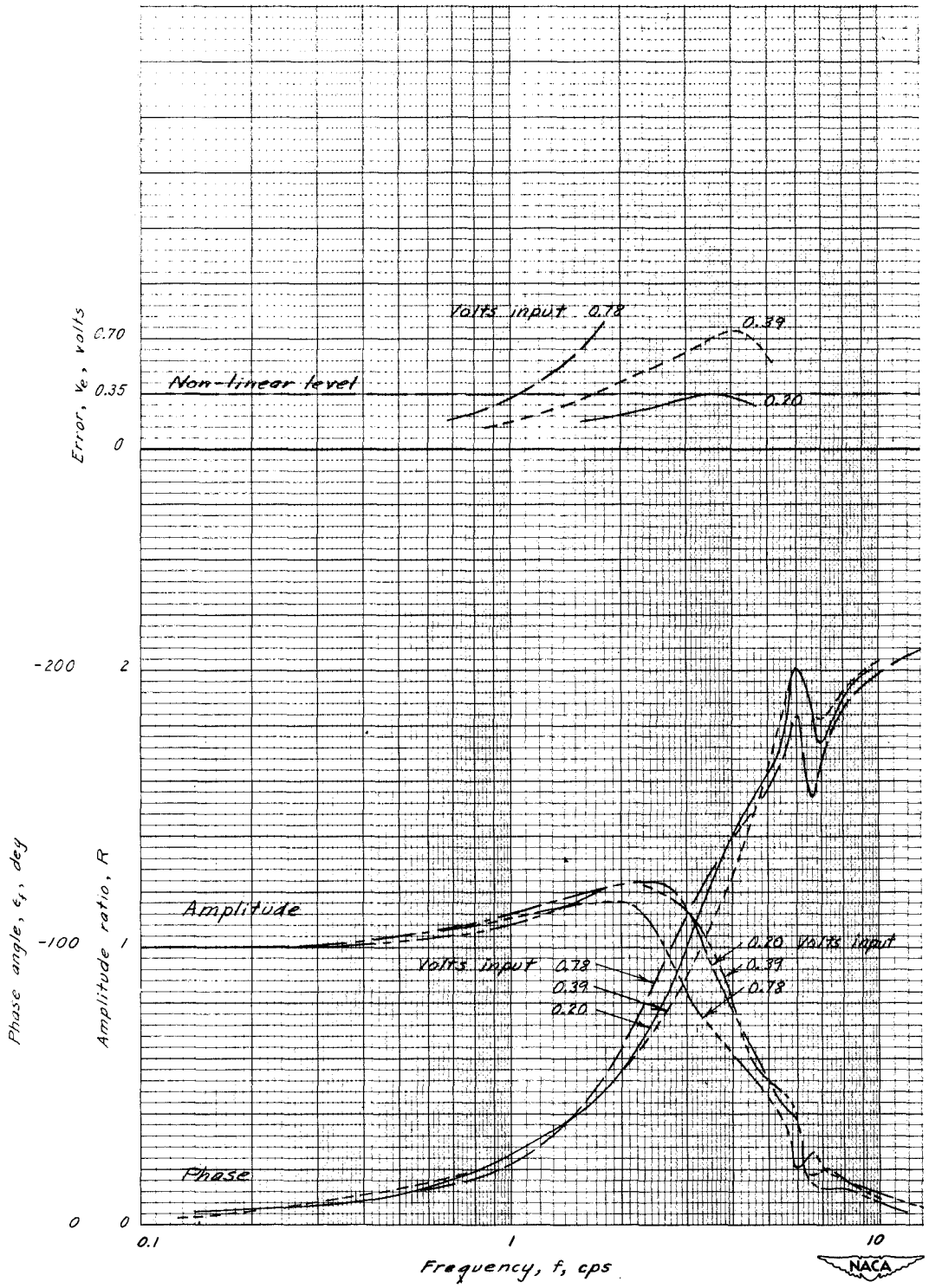

(e) Servo response; maximum load; sensitivity, 41 percent.

Figure 16.- Continued.

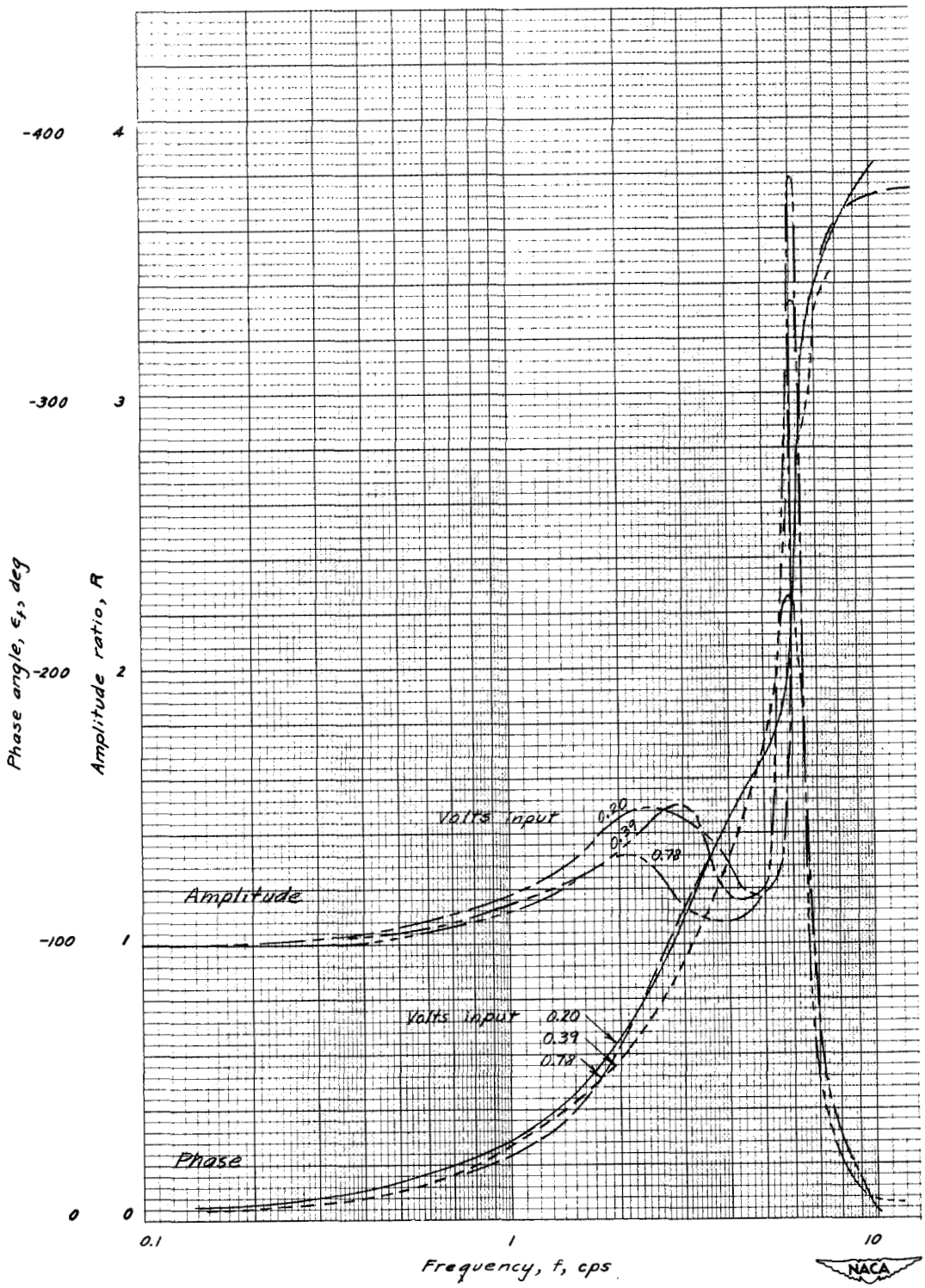

(f) Surface response; maximum load; sensitivity, 41 percent.

Figure 16.– Concluded.

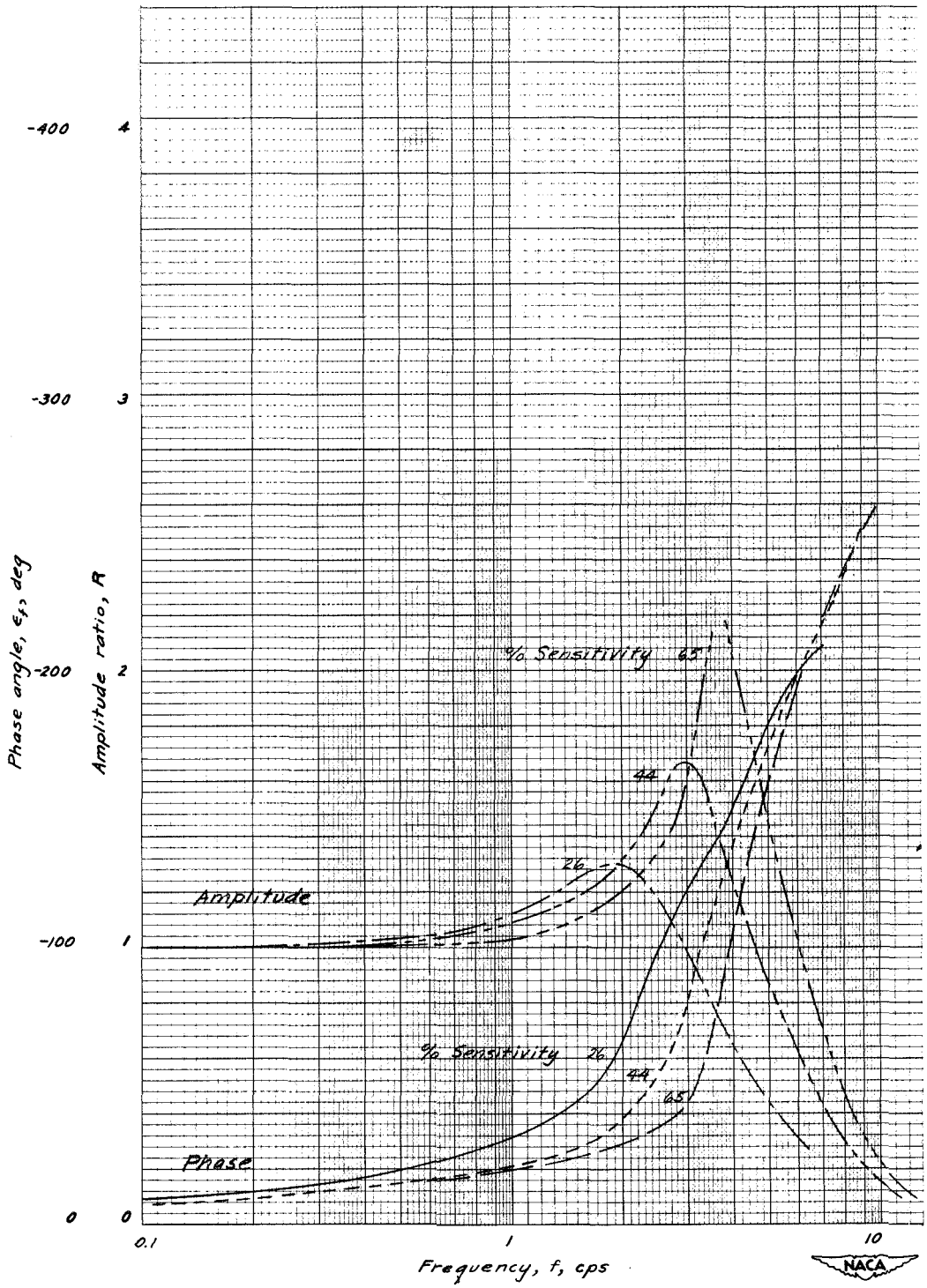

(a) Servo response.

Figure 17.- Effect of sensitivity on aileron-channel frequency response; no load; ±0.275 volt ($\approx \pm 1/2^{\circ}$) input.

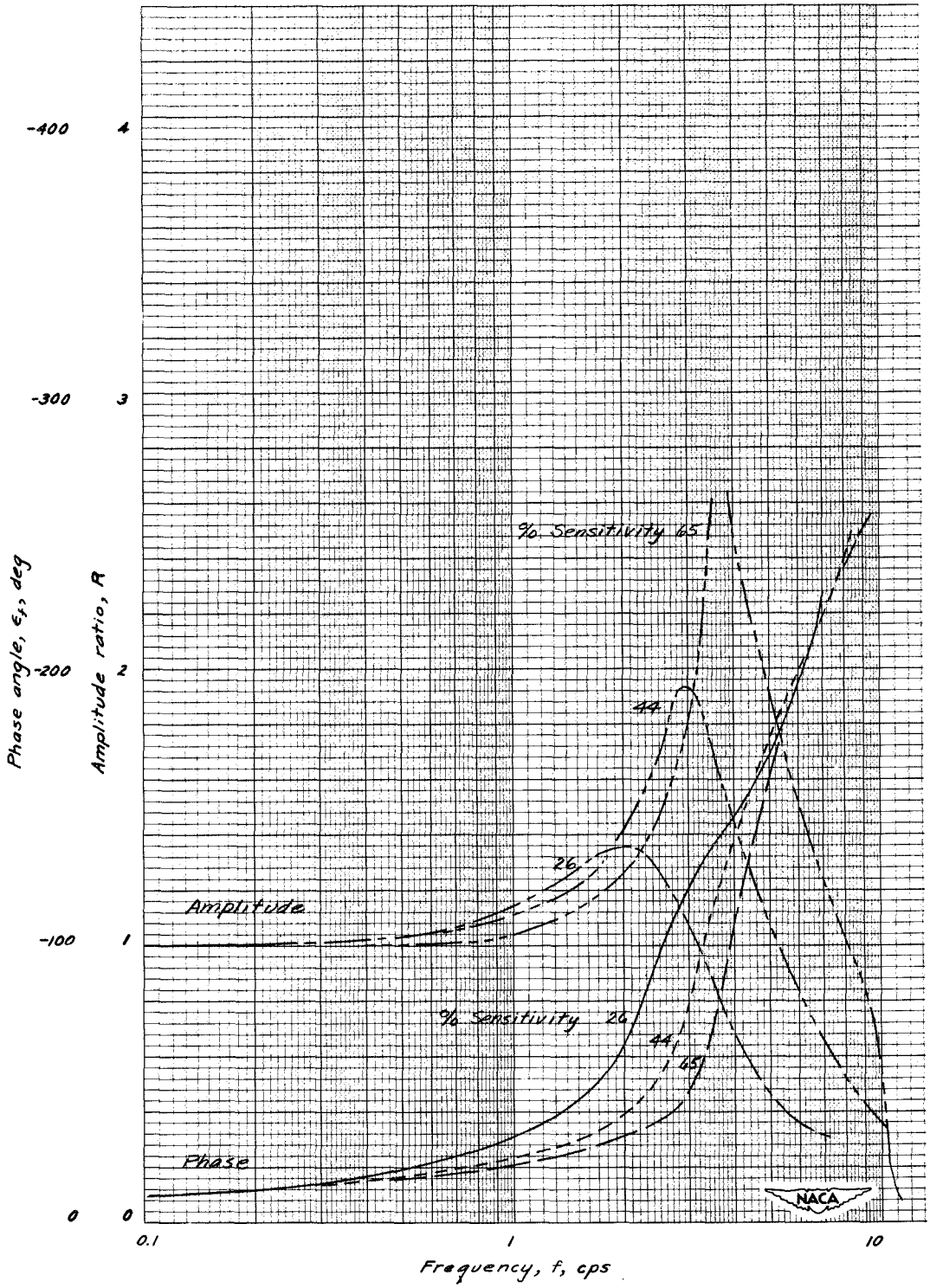

(b) Surface response.

Figure 17.- Concluded.

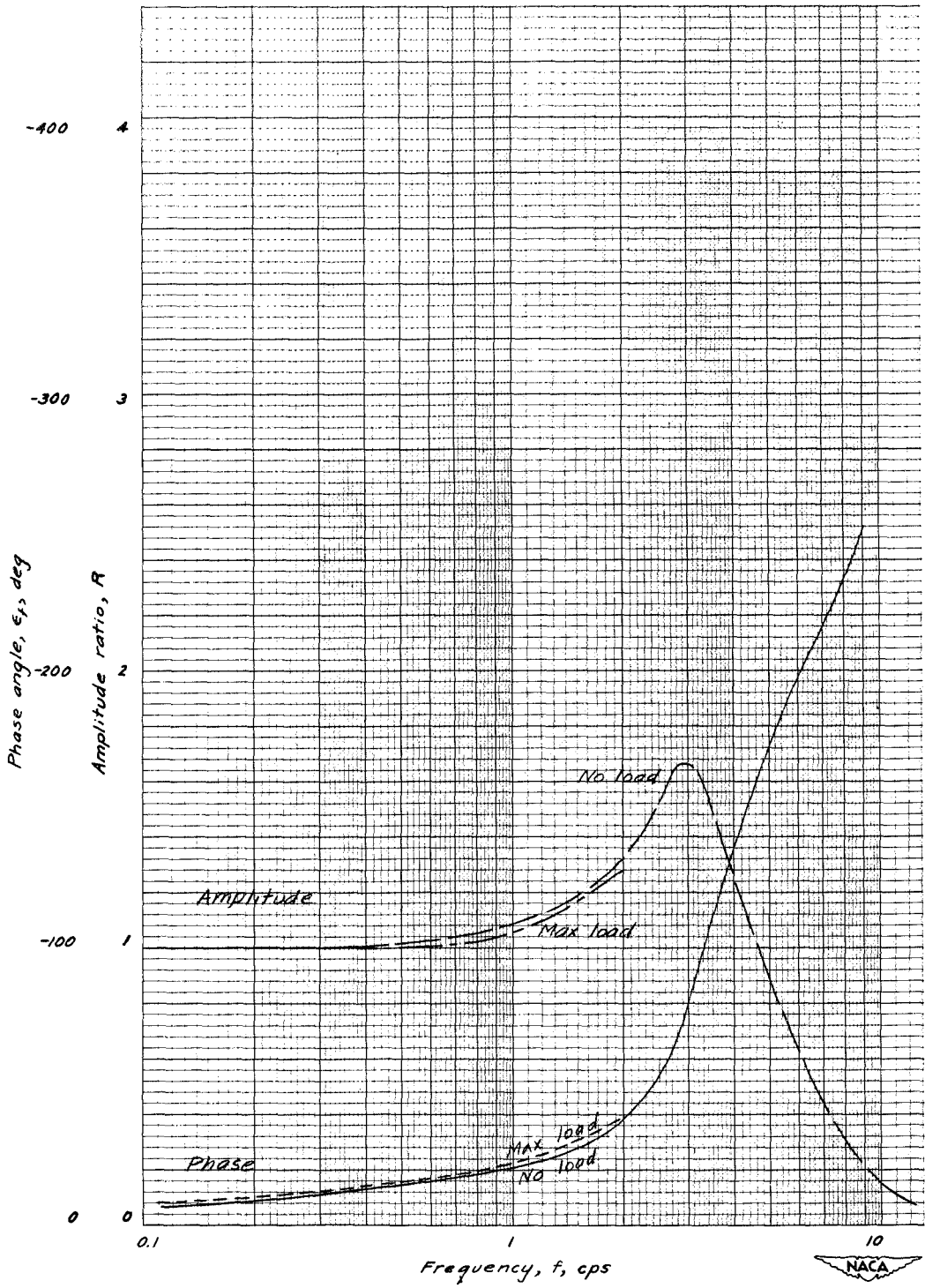

(a) Servo response.

Figure 18.– Effect of load on aileron–channel frequency response; ±0.275 volt (≈±1/2°) input; sensitivity, 44 percent.

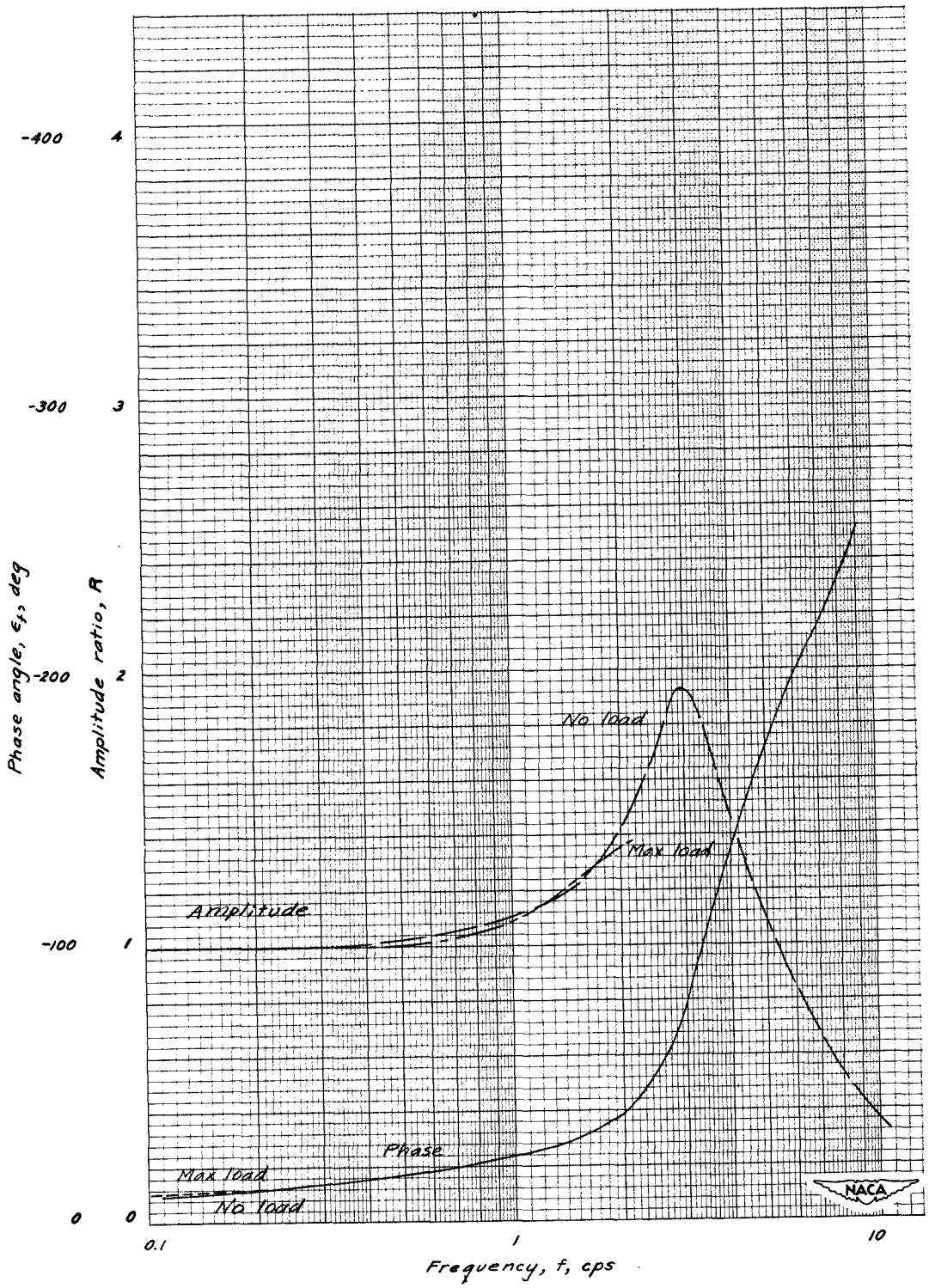

(b) Surface response.

Figure 18.– Concluded.

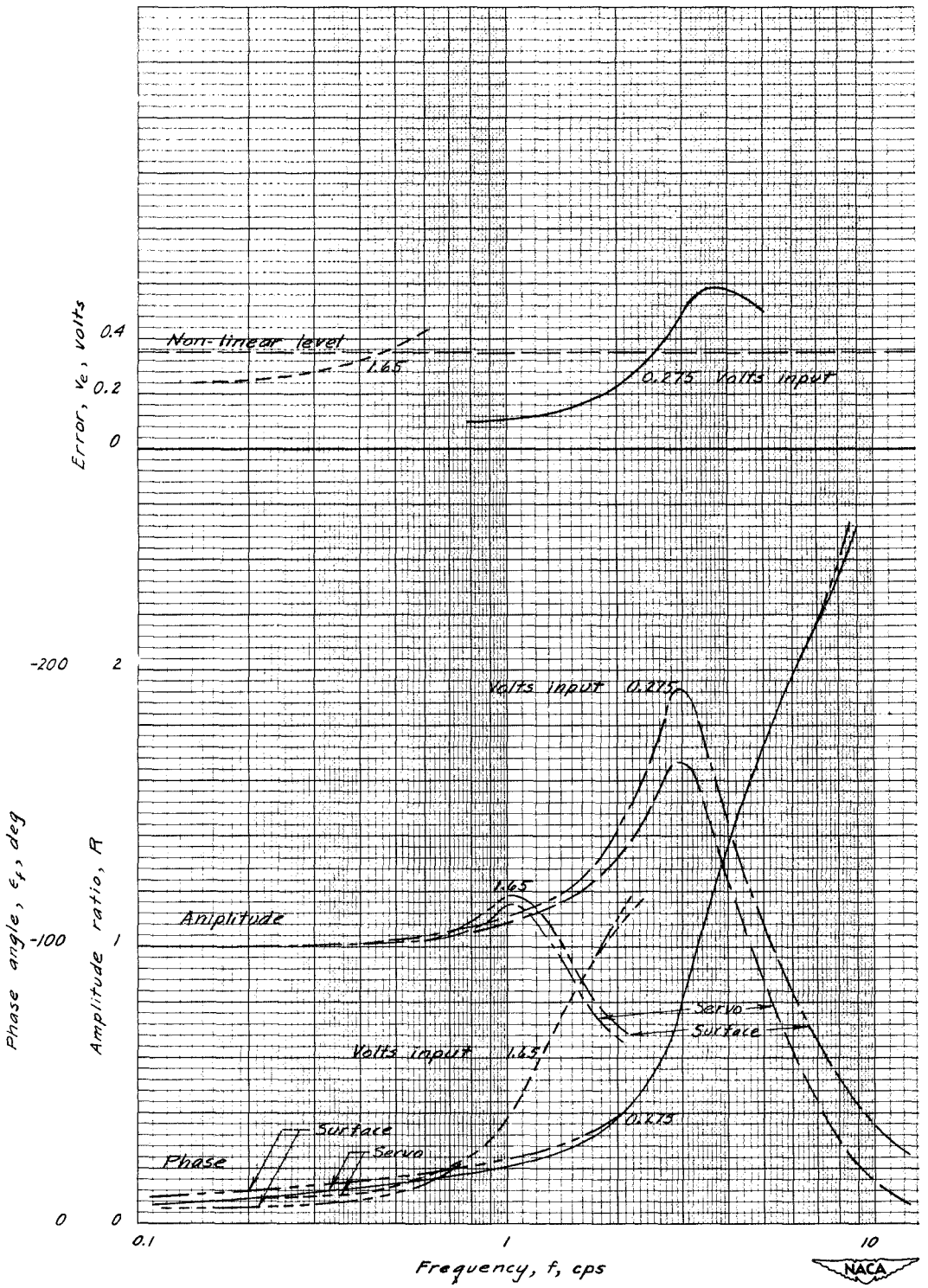

Figure 19.- Effect of input signal amplitude on aileron-channel frequency response; sensitivity, 44 percent; no load.

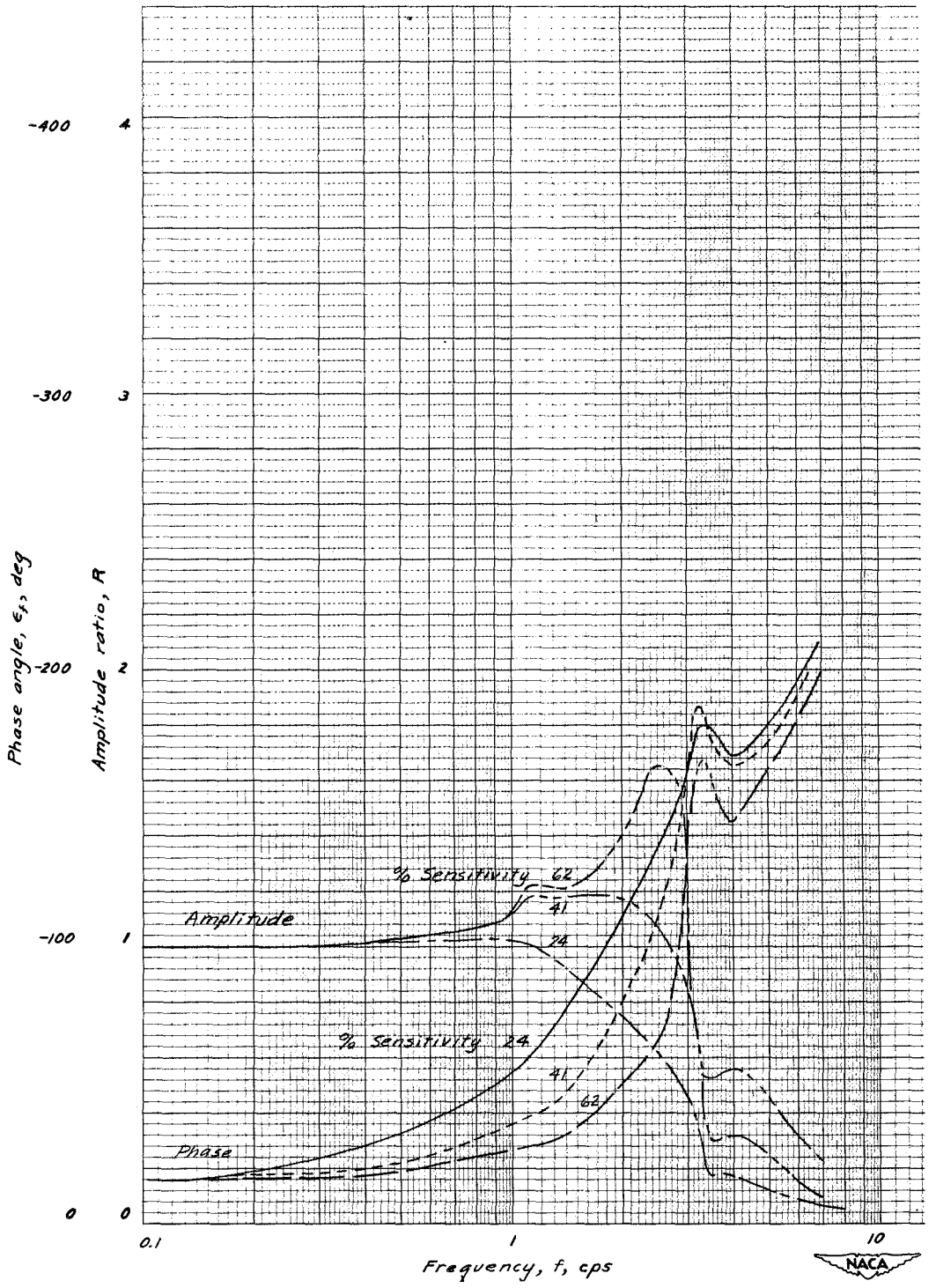

(a) Servo response.

Figure 20.– Effect of sensitivity on rudder–channel frequency response; no load; ±0.25 volt (≈±1/2°) input.

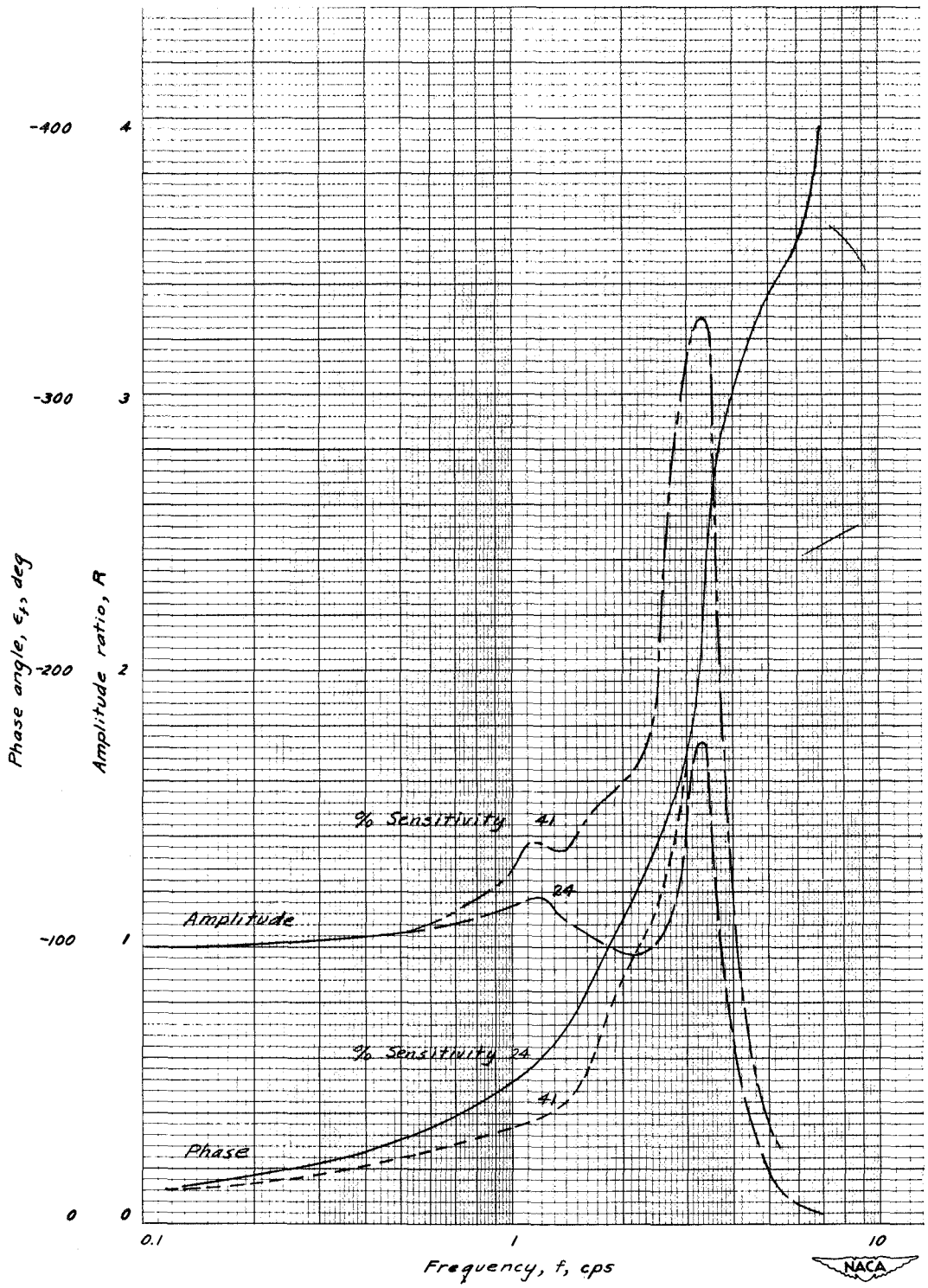

(b) Surface response.

Figure 20.– Concluded.

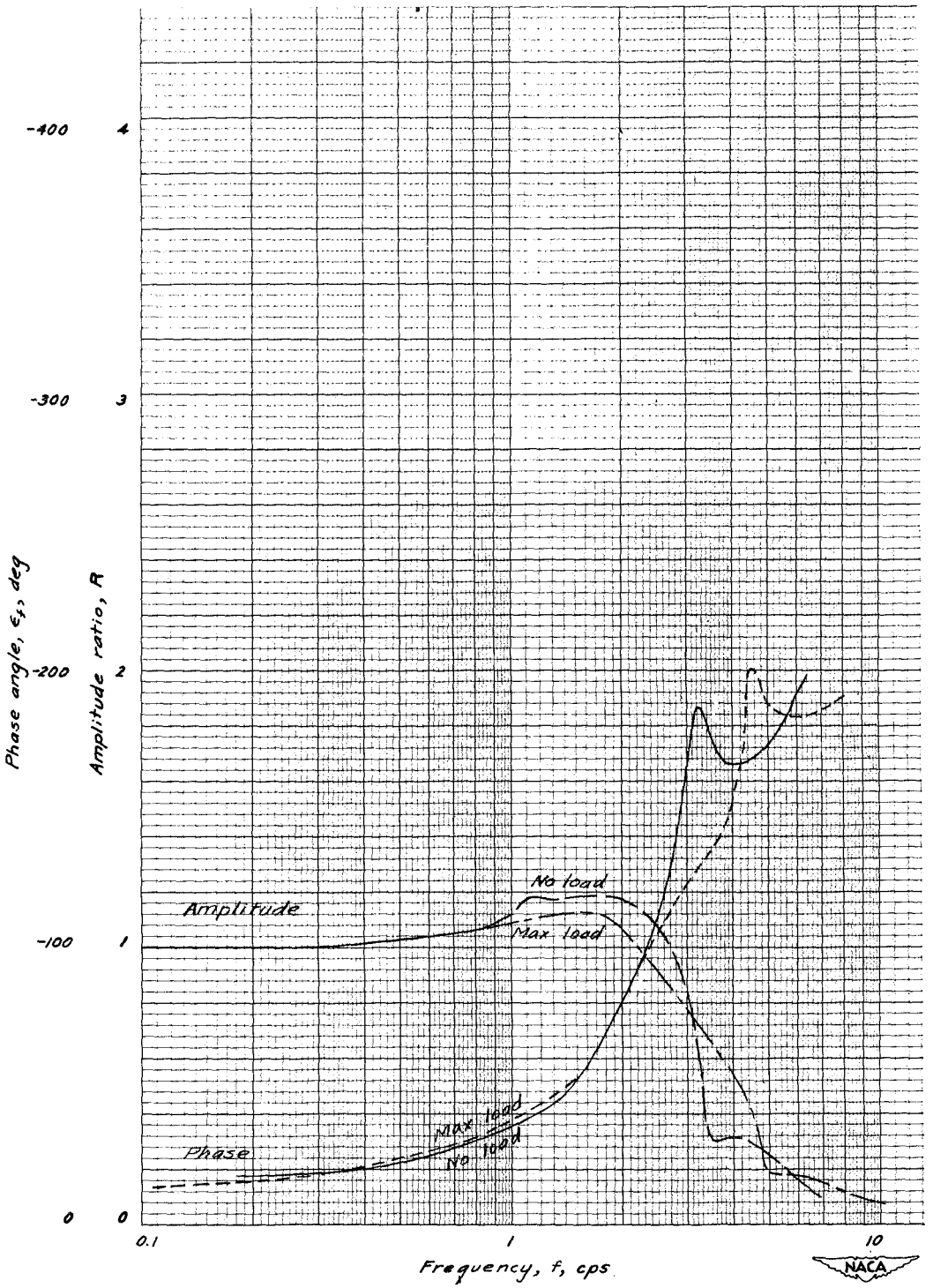

(a) Servo response.

Figure 21.- Effect of load on rudder-channel frequency response; ±0.25 volt (≈±1/2°) input; sensitivity, 41 percent.

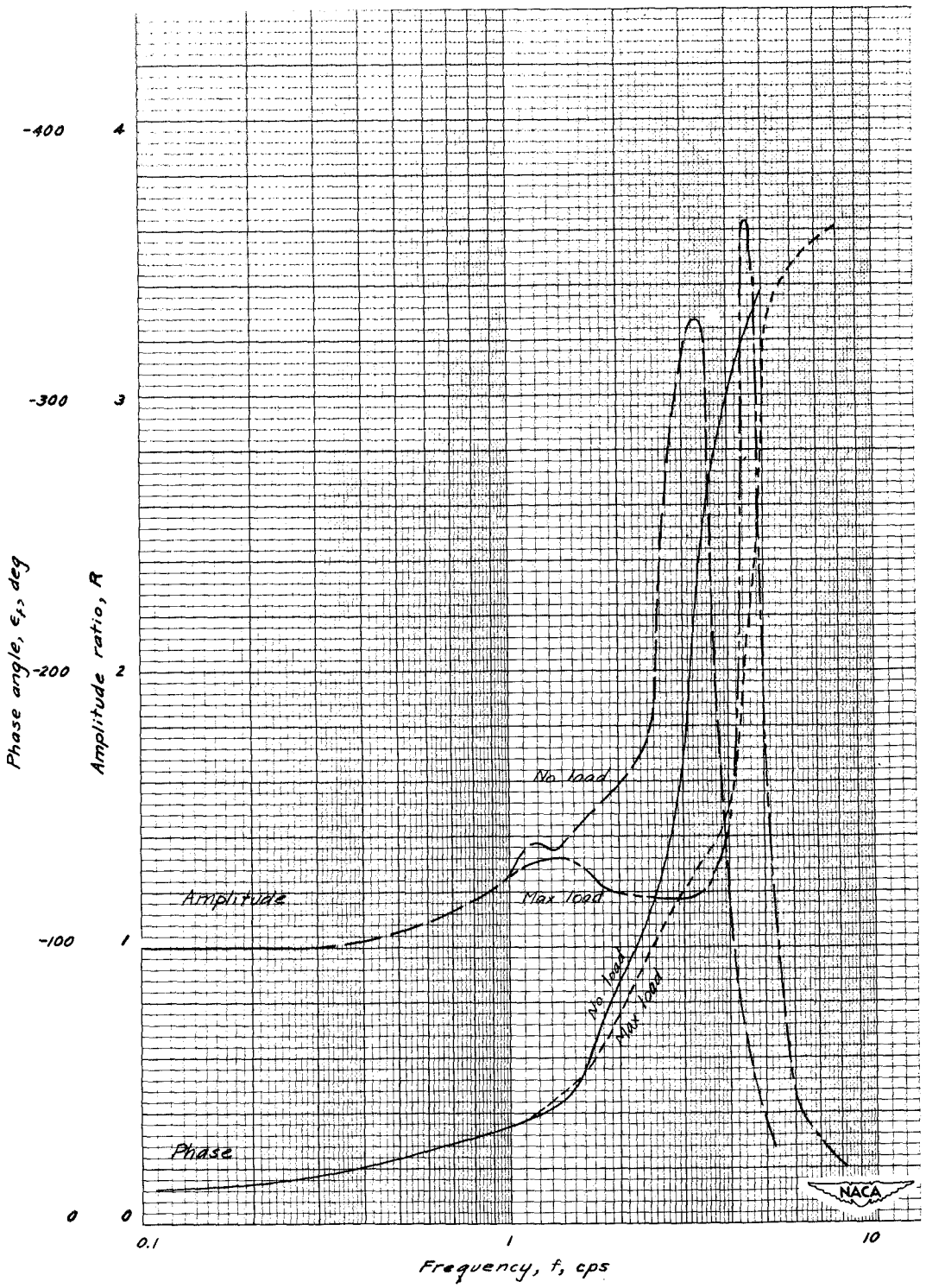

(b) Surface response.

Figure 21.- Concluded.

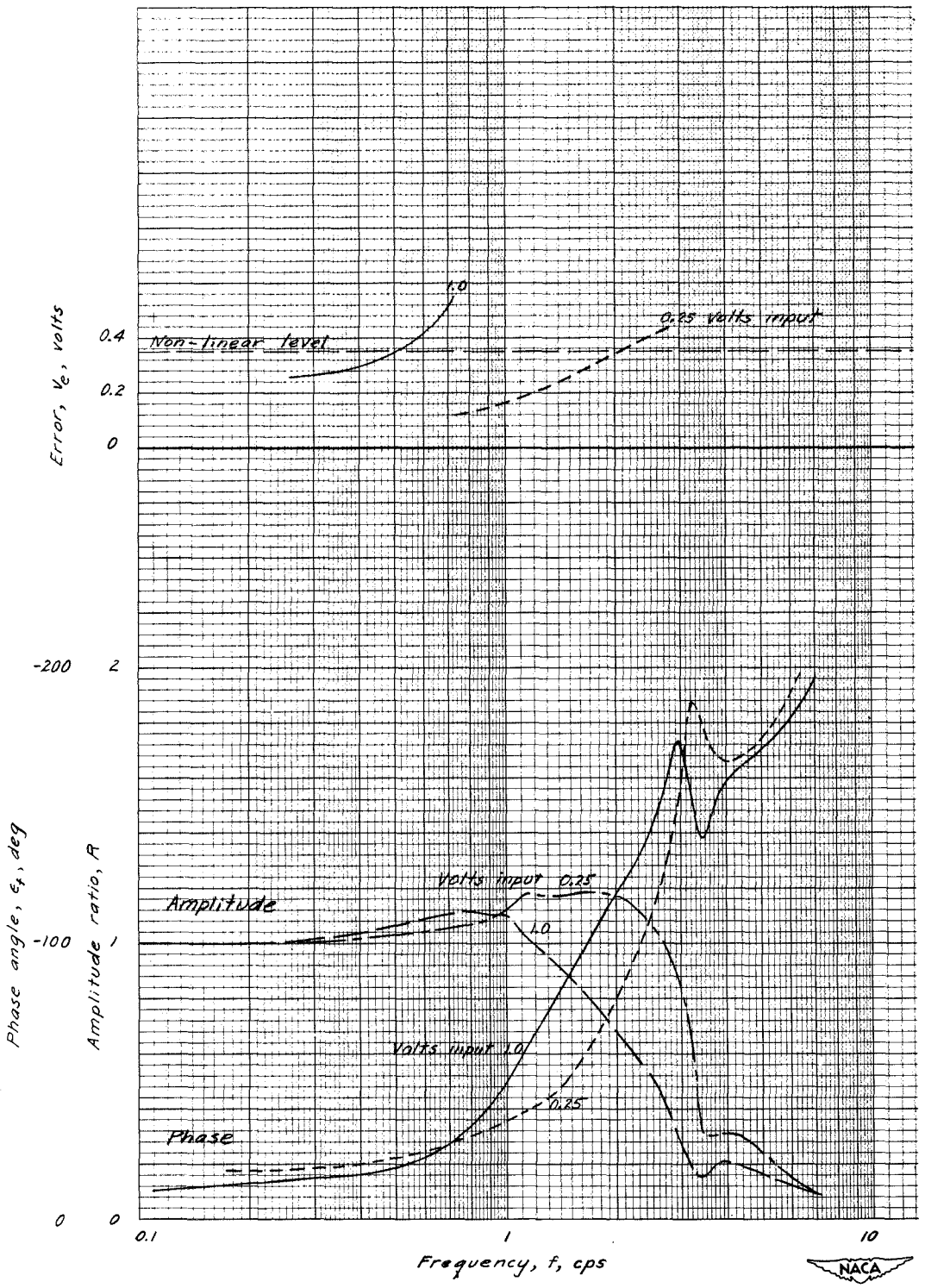

Figure 22.– Effect of input signal amplitude on rudder–channel frequency response; no load; sensitivity, 41 percent.

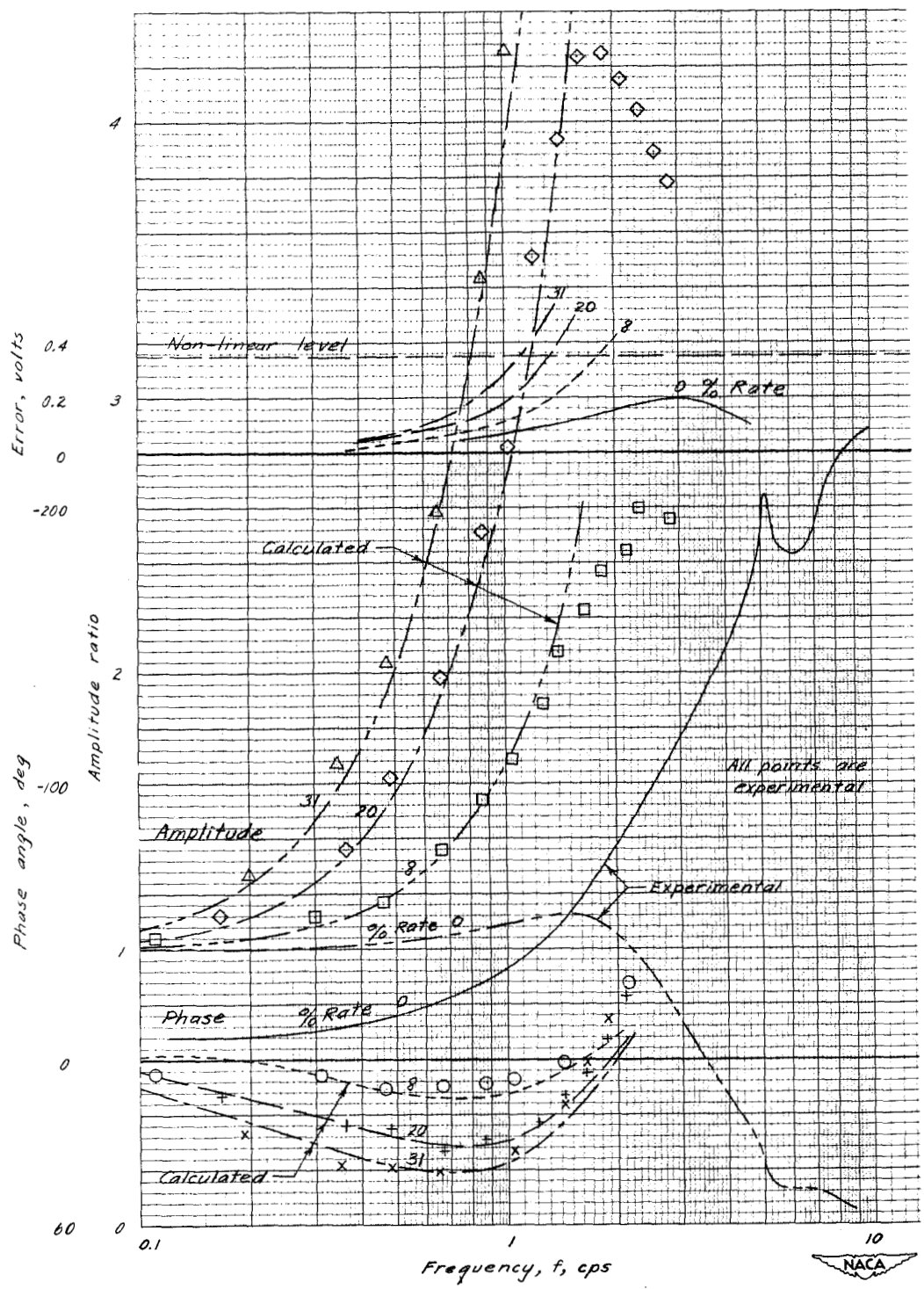

(a) Servo response; experimental and calculated.

Figure 23.- Effect of rate signal on elevator-channel frequency response; ±0.115 volt (≈±1/4°) input; no load; sensitivity, 24 percent.

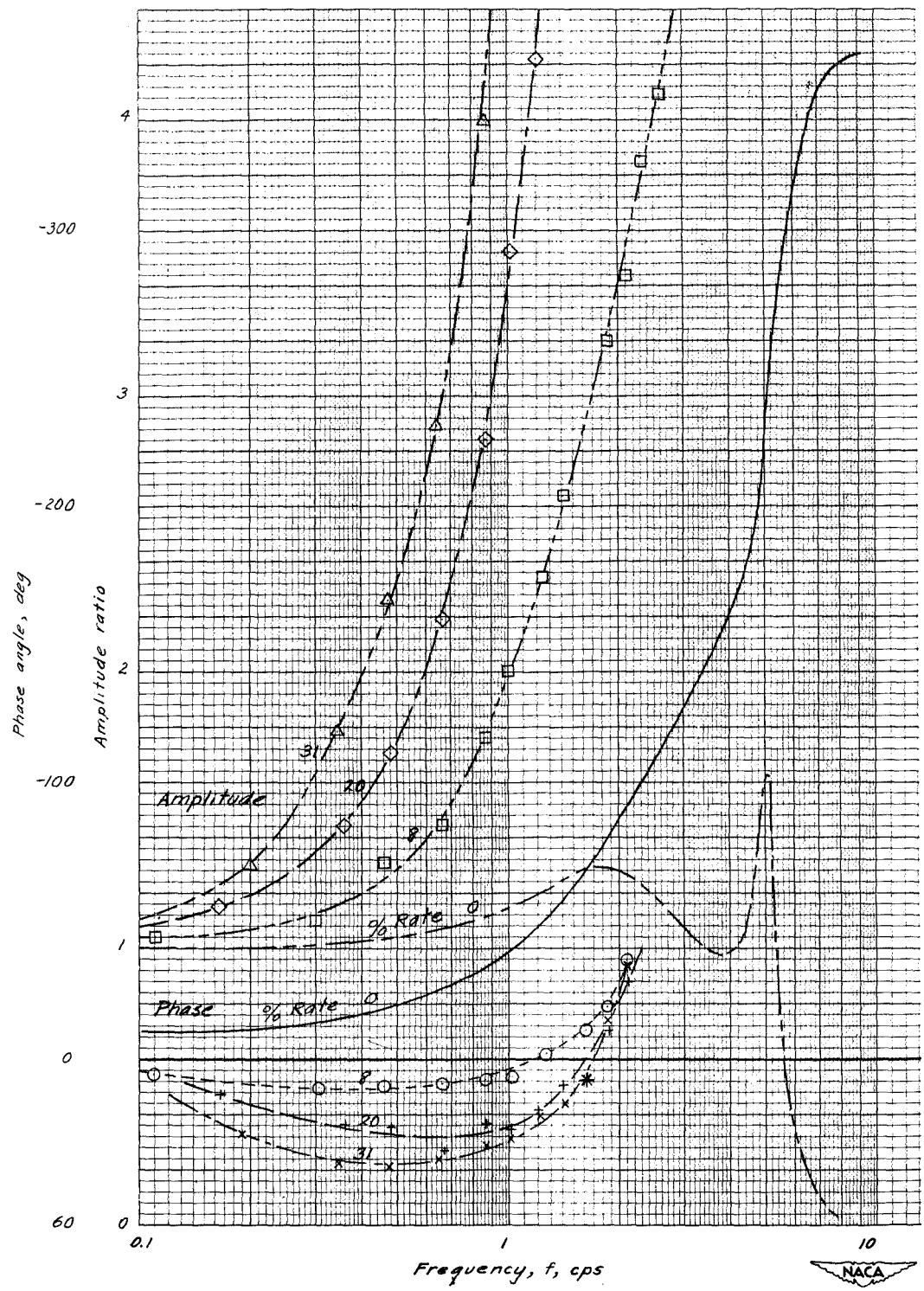

(b) Surface response; experimental only.

Figure 23.- Concluded.

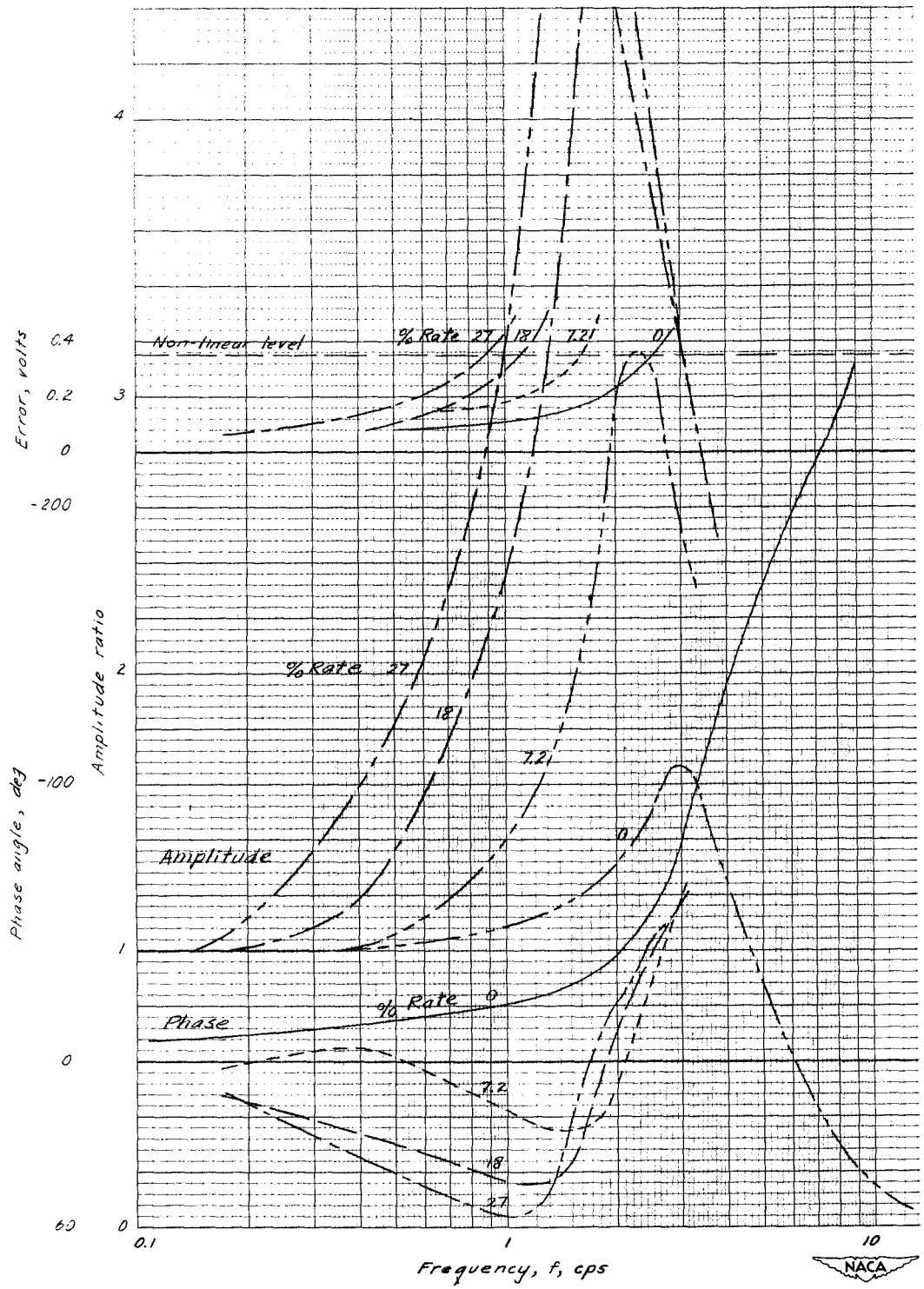

Figure 24.- Effect of rate signal on aileron-channel frequency response; experimental response; ±0.275 volt (≈±1/2°) input; no load; sensitivity, 44 percent.

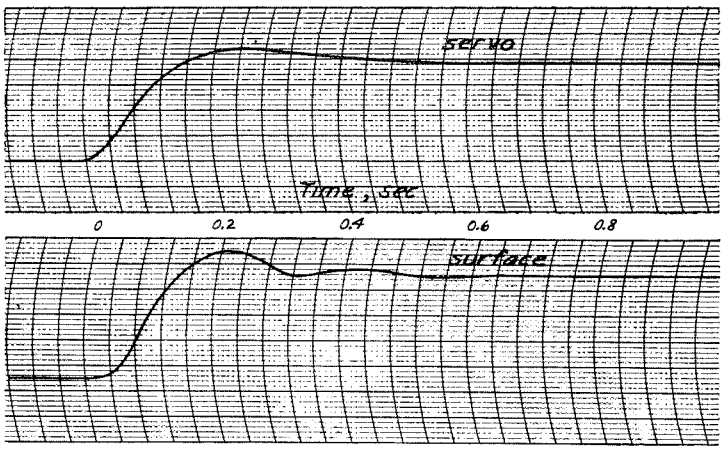

(a) Sensitivity, 24 percent.

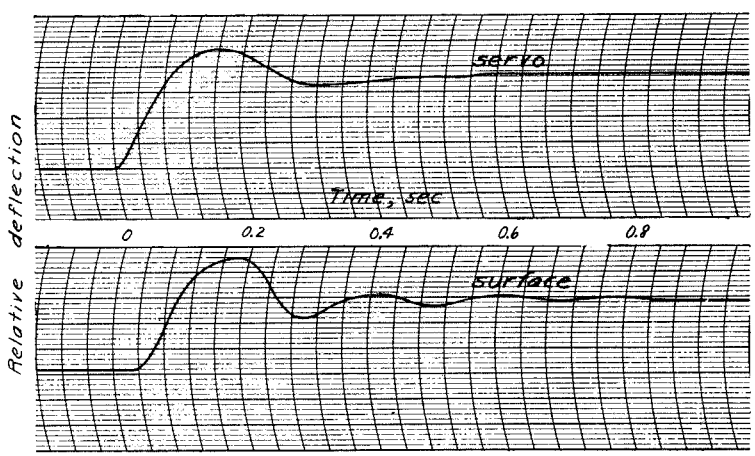

(b) Sensitivity, 42 percent.

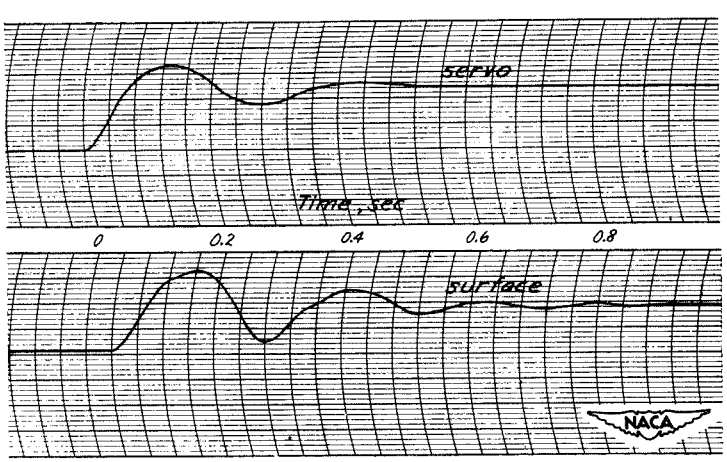

(c) Sensitivity, 63 percent.

Figure 25.- Transient response of elevator channel.

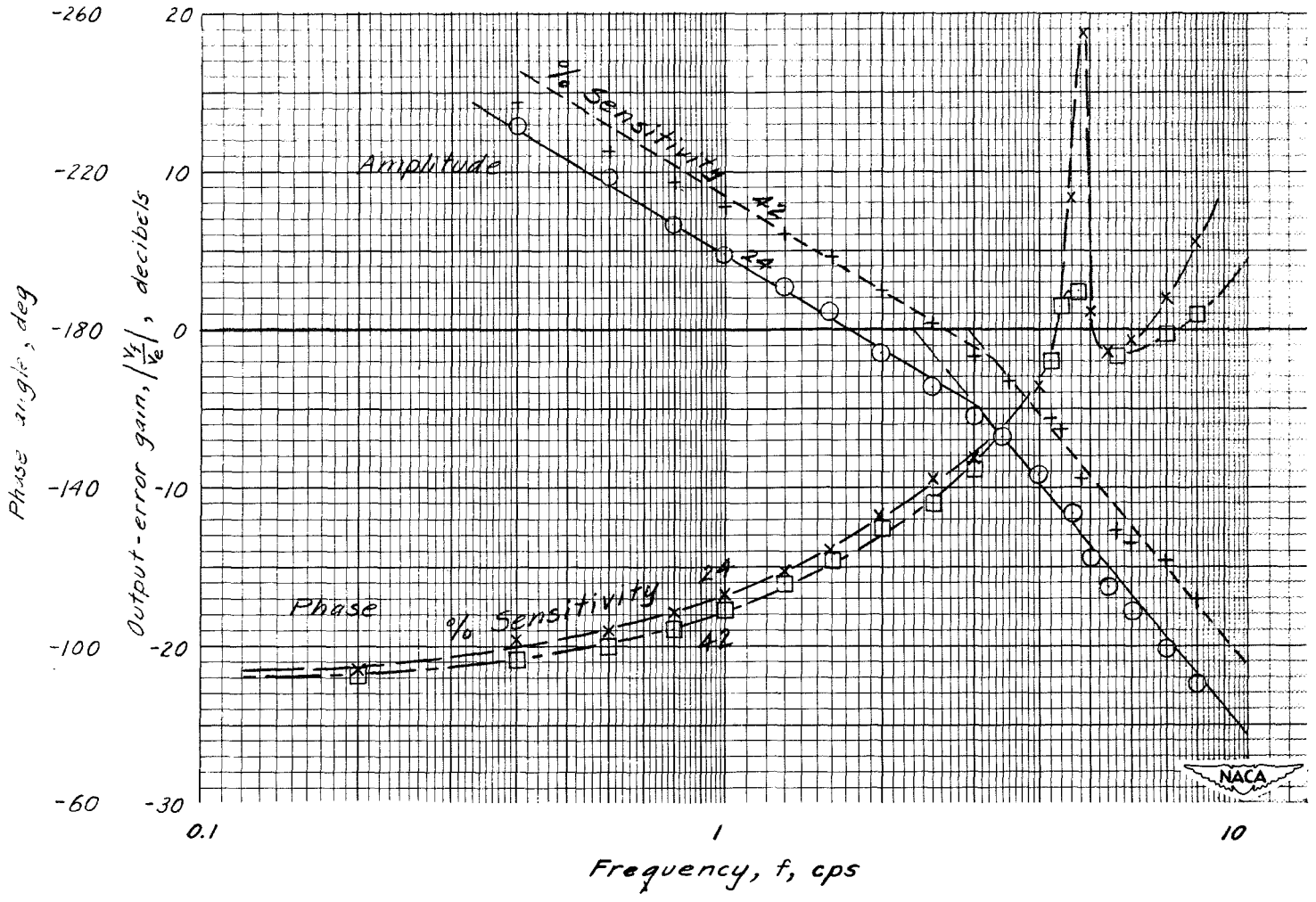

Figure 26.- Open-loop servo frequency response of elevator channel.

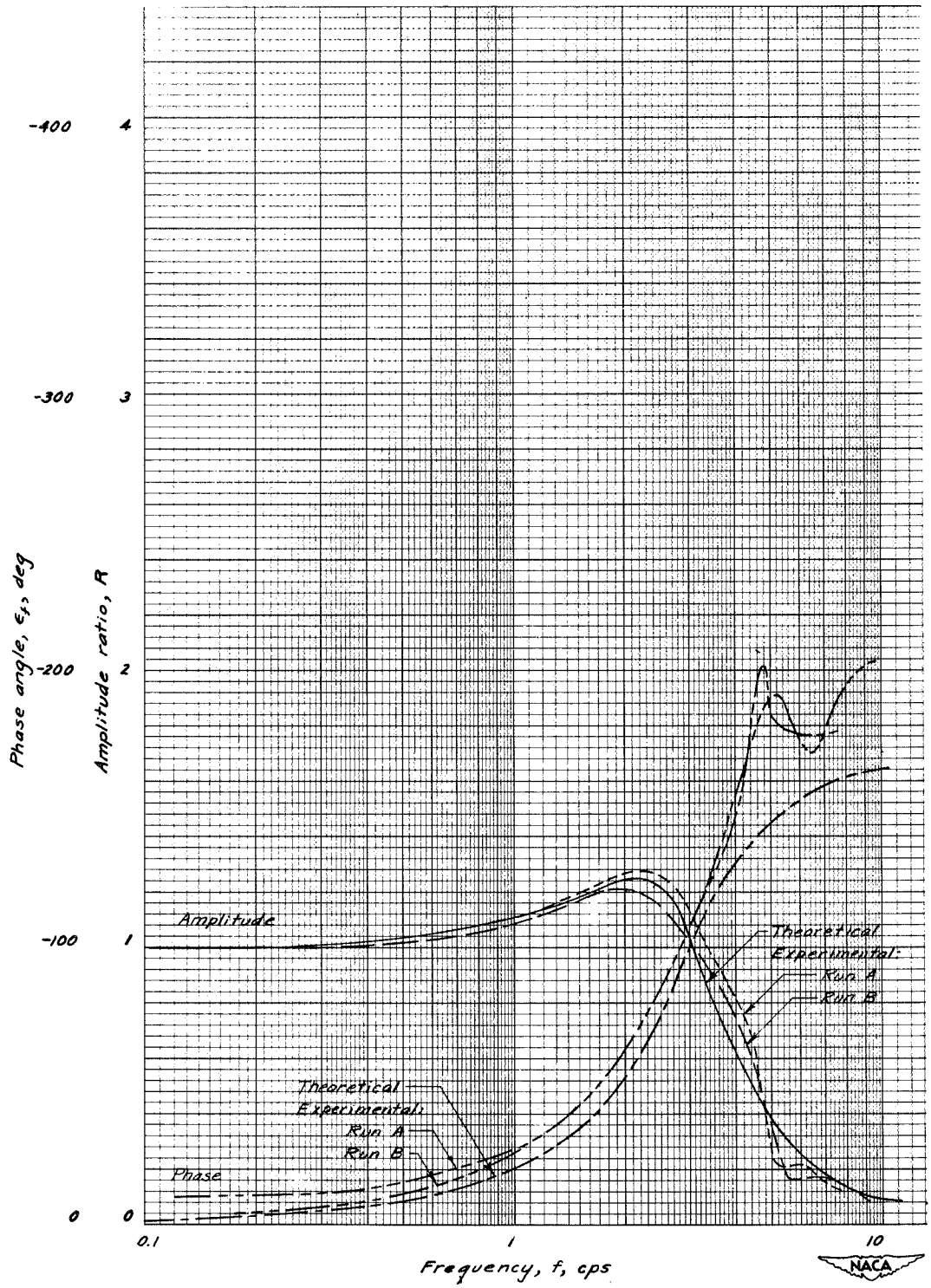

Figure 27.- Comparison of experimental ground tests and theoretical elevator—channel servo frequency response; sensitivity, 33 percent.

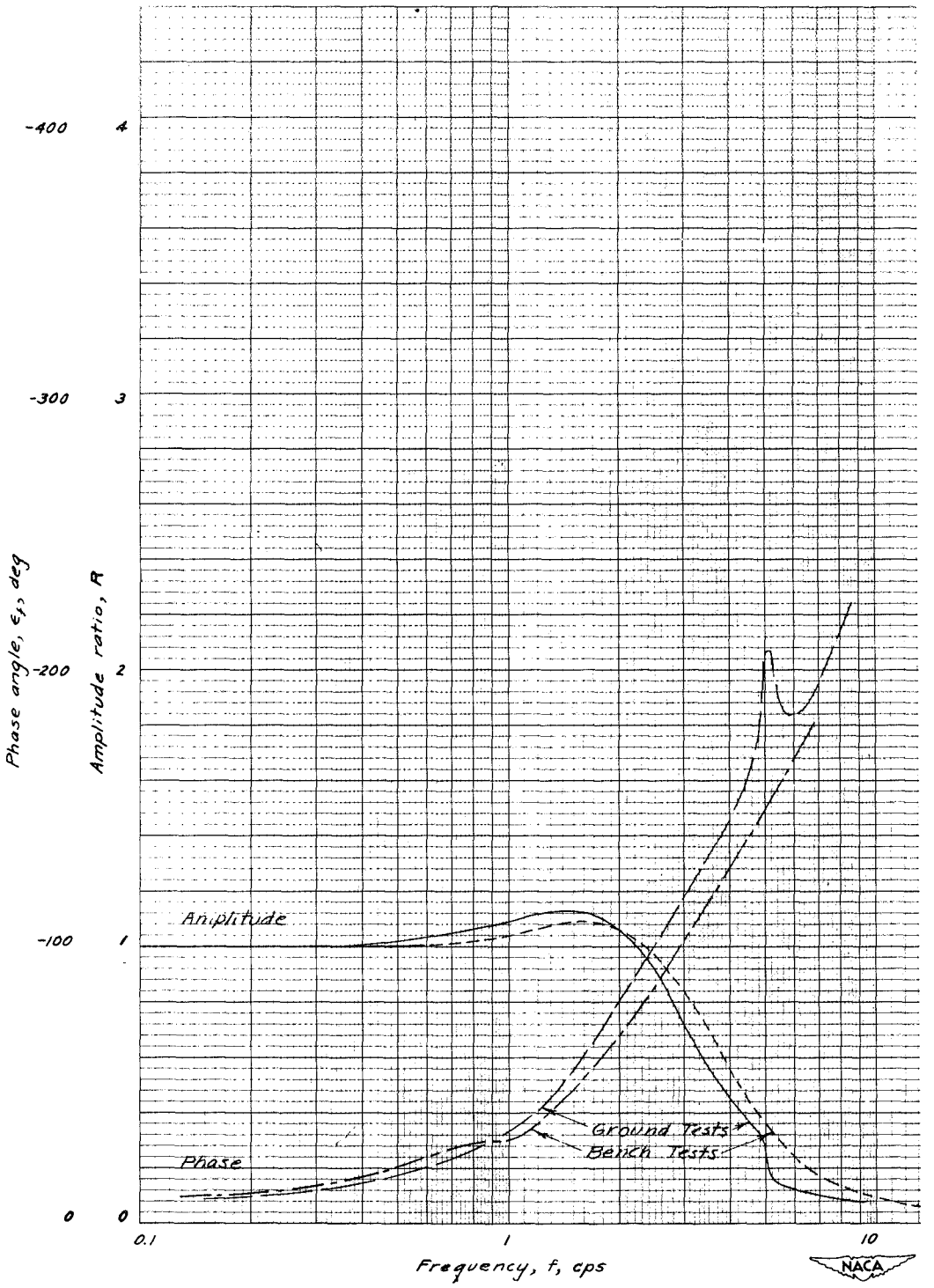

(a) Sensitivity, 24 percent.

Figure 28.- Comparison of bench and ground tests of elevator-channel servo frequency response.

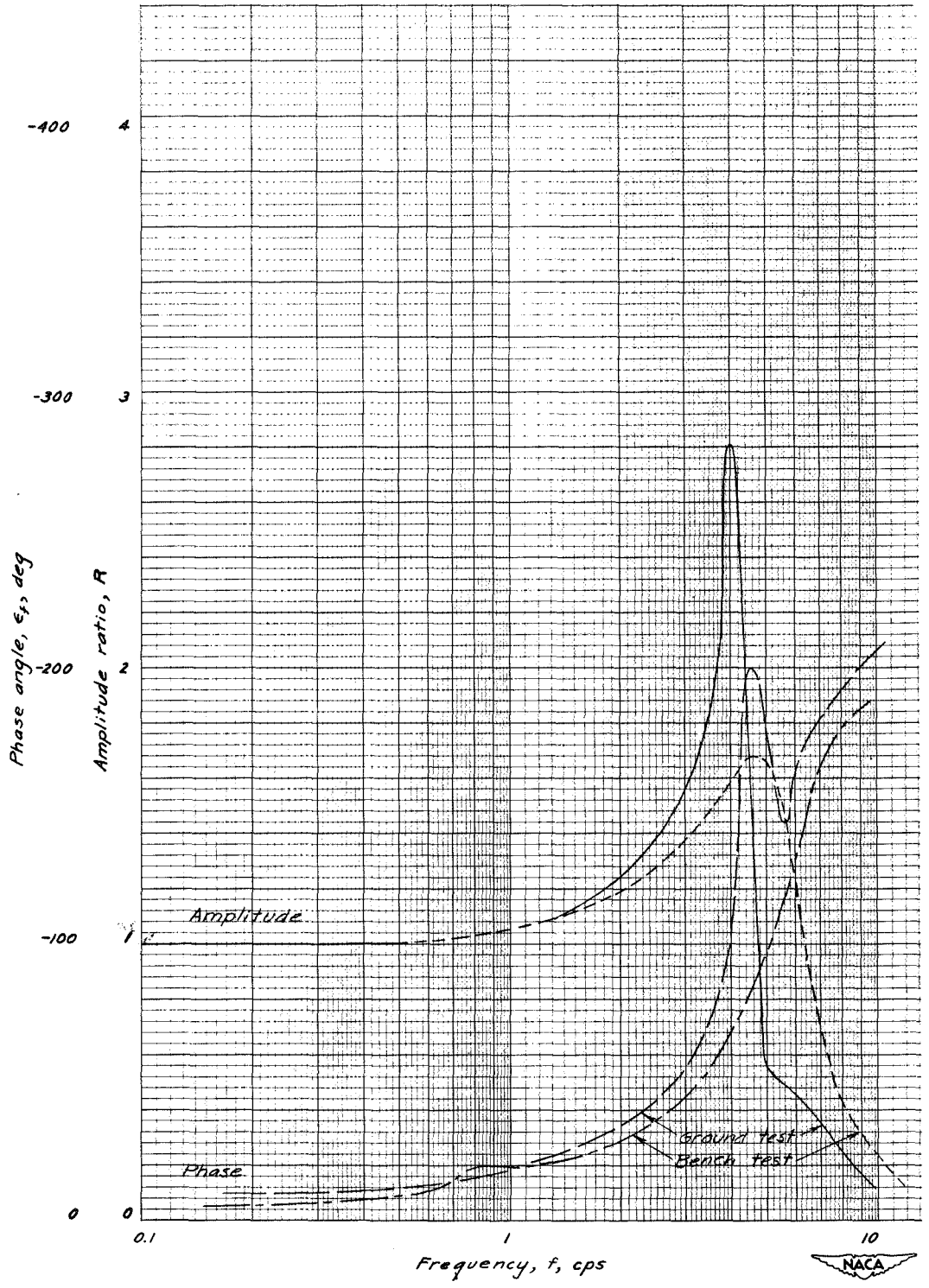

(b) Sensitivity, 63 percent.

Figure 28.- Concluded.

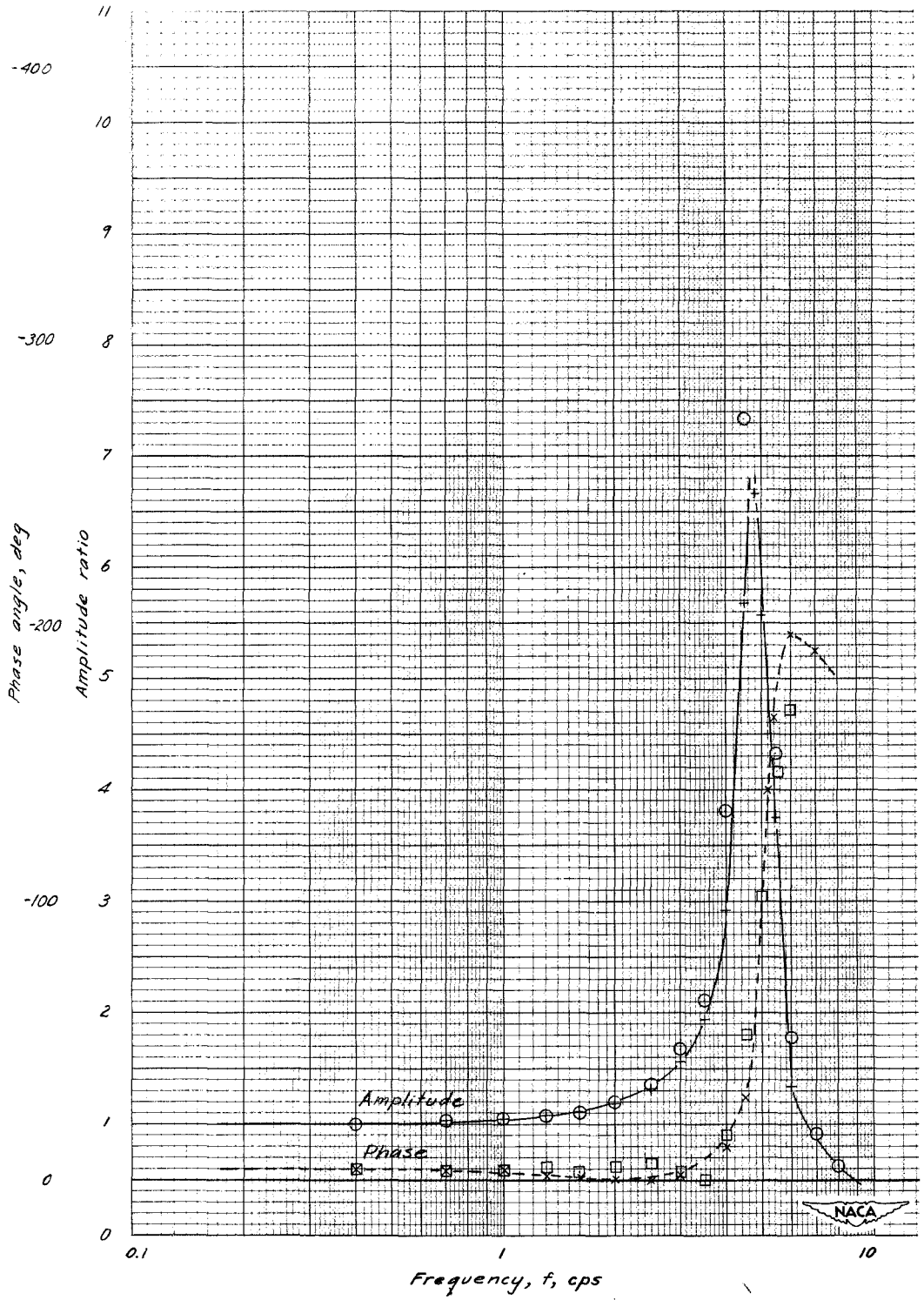

(a) No load.

Figure 29.- Transfer function of elevator control linkage.

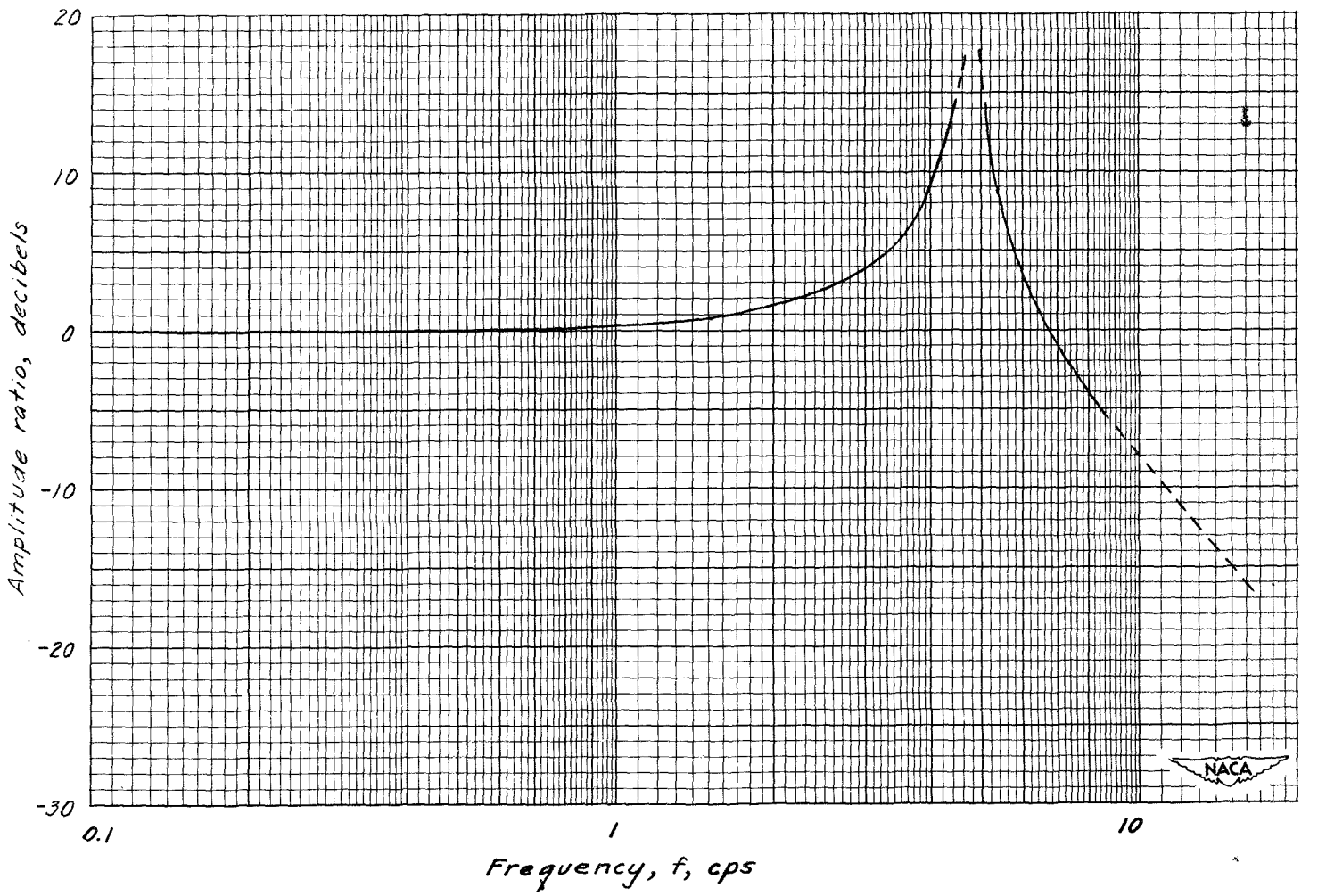

(b) Decibel amplitude ratio; no load.

Figure 29.- Continued.

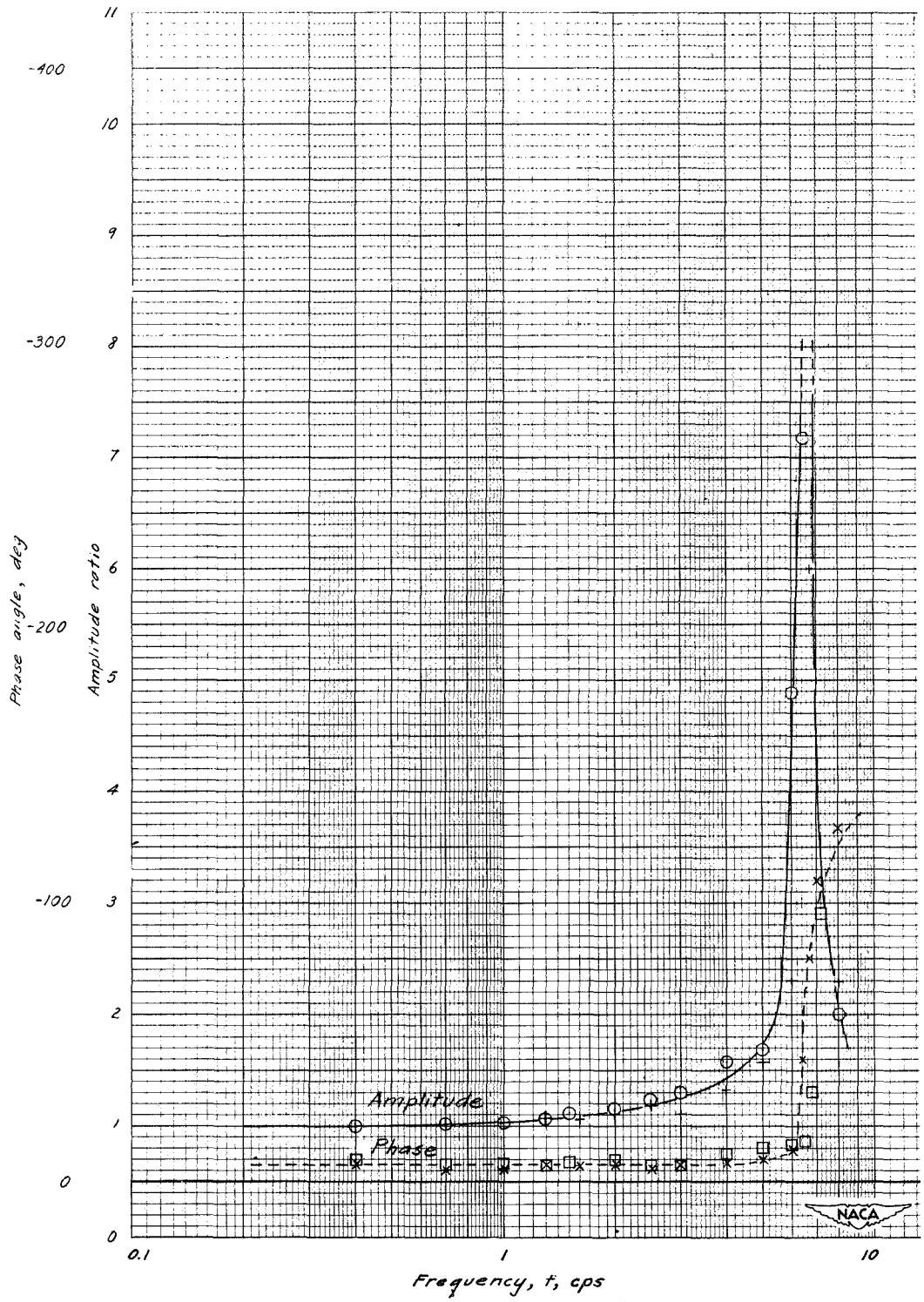

(c) Maximum load.

Figure 29.- Concluded.